

GEOLOGICA ULTRAIECTINA

Medelingen van de
Faculteit Geowetenschappen
Universiteit Utrecht

No. 254

Kinetics of microbial Fe(III) oxyhydroxide
reduction: The role of mineral properties

Steeve Bonneville

Promotor: Prof. Dr. P.S.J Van Cappellen
Department of Earth-Sciences – Geochemistry
Faculty of Geosciences
Utrecht University

Co-promotor Dr. T. Behrends
Department of Earth-Sciences – Geochemistry
Faculty of Geosciences
Utrecht University

Examination committee:

Prof. Dr. E. E. Roden Department of Geology & Geophysics
University Madison-Wisconsin (USA)

Dr. O. Pokrovsky Laboratoire des Mécanismes et Transferts en Géologie
CNRS Université Paul-Sabatier Toulouse (France)

Dr. W. F. M. Röling Department of Molecular Cell Physiology
Free University Amsterdam (The Netherlands)

Prof. Dr. G.J. de Lange Department of Earth-Sciences – Geochemistry
Utrecht University (The Netherlands)

Prof. Dr. J. Middelburg Department of Earth-Sciences – Geochemistry
Utrecht University (The Netherlands)

The research described in this thesis was carried out at the Department of Earth Sciences – Geochemistry, Faculty of Geosciences, Utrecht University, The Netherlands. This thesis was funded by TRIAS (project number 835.80.004 “Redox reactivity and bioavailability of iron oxyhydroxides in the subsurface”).



Kinetics of microbial Fe(III) oxyhydroxide reduction: The role of mineral properties.

(met een samenvatting in het Nederlands)

(résumé en Français)

PROEFSCHRIFT

ter verkrijging van de graad van doctor aan de Universiteit Utrecht University

op gezag van de Rector Magnificus, Prof. Dr. W.H. Gispen,

ingevolge het besluit van het College voor Promoties

in het openbaar te verdedigen op maandag 19 december 2005 des middags te 12:45 uur

door

Steeve Bonneville

geboren op 4 mei 1974 te Fecamp, Frankrijk

“What happen, at the end, is not the inevitable but the unpredictable”

-J. M Keynes

“La science est un jeu dont la règle du jeu consiste à trouver quelle est la règle du
jeu”

-Cavanna, Le saviez-vous?

Table of Contents

Chapter I: General Introduction and Outline of the thesis	9
1.1 Iron(III) oxides	13
1.1.1 <i>Goethite</i>	
1.1.2 <i>Lepidocrocite</i>	
1.1.3 <i>Hematite</i>	
1.1.4 <i>Ferrihydrite</i>	
1.1.5 <i>Dissolution of Fe(III) oxyhydroxides</i>	
1.2. Microbial Fe(III) reduction	18
1.2.1 <i>Fe(III) as the first organic matter oxidant in the Archaeal biosphere?</i>	
1.2.2 <i>Dissimilatory iron reduction in modern sedimentary environments</i>	
1.2.3 <i>Iron reducing microorganisms</i>	
1.2.4 <i>Environmental significance of microbial iron reduction</i>	
1.2.5 <i>Mechanisms of microbial Fe(III) reduction</i>	
1.3. Thesis outline	25
Chapter II: Microbial reduction of iron(III) oxyhydroxides: effects of mineral solubility and availability	33
2.1 Introduction	35
2.2 Materials and methods	36
2.2.1 <i>Fe(III) oxyhydroxides</i>	
2.2.2 <i>Bacteria</i>	
2.2.3 <i>Solubility determinations</i>	
2.2.4 <i>Microbial Fe(III) reductions kinetics</i>	
2.3 Results	39
2.3.1 <i>Fe(III) oxyhydroxide solubilities</i>	
2.3.2 <i>Microbial Fe(III) reduction kinetics</i>	
2.4 Discussions	43
2.4.1 <i>Fe(III) oxyhydroxide solubilities</i>	
2.4.2 <i>Microbial iron reduction kinetics</i>	
2.4.3 <i>Maximum specific reduction rate, v_{max}</i>	
2.4.4 <i>Affinity constant, K_m</i>	
2.5 Conclusions	51
Chapter III: Microbial reduction of Fe(III) oxyhydroxide colloids: a kinetic model	55
3.1 Introduction	57
3.2 Materials and Experimental Methods	58
3.2.1 <i>Fe(III) oxyhydroxides</i>	
3.2.2 <i>Bacteria</i>	
3.2.3 <i>Microbial attachment and reduction of nanohematite</i>	
3.2.4 <i>Detachment experiments</i>	
3.3 Experimental results	61
3.3.1 <i>Nanohematite attachment to <i>S. putrefaciens</i></i>	

3.3.2 <i>Nano hematite reduction by S. putrefaciens</i>	
3.4 Kinetic Model for Microbial Reduction of Fe(III) colloids	63
3.5 Discussion	66
3.5.1 <i>Nano hematite attachment to S. putrefaciens</i>	
3.5.2 <i>Microbial reduction of nano hematite</i>	
3.5.3 <i>Half saturation constants</i>	
3.5.4 <i>Application to other Fe(III) oxyhydroxides</i>	
3.5.5 <i>Bioreduction kinetics and cell density</i>	
3.6 Conclusions	76
Appendix	77
Chapter IV: The role of solubility in microbial Fe(III) oxyhydroxide reduction kinetics	81
4.1 Introduction	83
4.2 Materials and methods	84
4.2.1 <i>Fe(III) oxyhydroxides</i>	
4.2.2 <i>Fe(III) oxyhydroxide dissolution experiments</i>	
4.2.3 <i>Microbial reduction experiments</i>	
4.3 Results	86
4.3.1 <i>Fe(III) oxyhydroxides solubilities</i>	
4.3.2 <i>Dialysis bag method versus pe-pH titrations</i>	
4.3.3 <i>Microbial Fe(III) reduction kinetics</i>	
4.4 Discussion	91
Chapter V: Thermodynamic constraints on microbial Fe(III) oxyhydroxide reduction	97
5.1 Introduction	99
5.2 Materials and methods	100
5.2.1 <i>Fe(III) oxyhydroxides</i>	
5.2.2 <i>Bacteria</i>	
5.2.3 <i>Microbial incubations</i>	
5.2.4 <i>Voltametric measurements of aqueous Fe²⁺</i>	
5.3 Results and Discussion	104
5.3.1 <i>Microbial Fe(III) oxyhydroxide reduction</i>	
5.3.2 <i>Redox measurements and mineral solubilities</i>	
5.3.3 <i>Thermodynamic control of Fe(III) oxyhydroxide reduction?</i>	
5.3.4 <i>The effect of Fe²⁺ on microbial iron reduction</i>	
Chapter VI: Summary	113
English	114
Français	118
Nederlands	122
Dankwoord-Acknowledgements	126
Curriculum vitae	128

Chapter I

Introduction and Outline

Introduction

Iron is the fourth most abundant element in the earth's crust (Reeburgh, 1983) and is an essential redox buffer on Earth (Huston and Logan, 2004; Lecuyer and Ricard, 1999). The cycling of iron influences the various global reservoirs (i.e. atmosphere, oceans, soils, sediments) through chemical and biological processes. In sediments and soils, iron plays a central role in the redox chemistry and biogeochemistry (Stumm and Sulzberger, 1992). In those environments, iron may be present as reactive Fe-bearing solids exhibiting high surface area to volume ratios. Surface-controlled reactions are of great significance in regulating the fate and mass transport of nutrients, metals, metalloids, radionuclides and contaminants (Behrends and Van Cappellen, 2005; Howell, 1994; Payne et al., 1994; Roden and Edmonds, 1997). The large specific surface areas and reactive surface functional groups of Fe(III) (hydr)oxides, iron sulfides and Fe-silicates, and, in some cases, their semi-conducting properties, facilitate a large number of chemical interactions, ranging from specific adsorption reactions to surface catalyzed redox transformations. For instance, iron-rich colloids have been shown to play key roles in the global transport of trace elements from continental watersheds to the sea (Allard et al., 2004; Dia et al., 2000; Pokrovsky and Schott, 2002), in the biogeochemical functioning of oxic-anoxic transitions in the water column and aquatic sediments (Taillefert and Gaillard, 2002), and in migration of contaminants in groundwater systems (Crerar et al., 1981; Schaefer et al., 2003).

Iron is a redox sensitive element, which, at the earth's surface, occurs mainly in two oxidation states: +II and +III. The ability of iron species to become oxidized or reduced links the iron cycle to those of oxygen, carbon and sulfur. At oxic to anoxic transitions, Fe(III) oxyhydroxides reductively dissolve via a number of abiotic and microbial pathways. In particular, they may serve as a terminal electron acceptor for the oxidation of organic matter by heterotrophic bacteria. Microbial oxidation of organic compounds with the reduction of Fe(III) oxyhydroxide is an important process in a variety of subsurface habitats: groundwaters (Chapelle and Lovley, 1992), marine sediments (Canfield et al., 1993; Mark Jensen et al., 2003), freshwater sediments (Lovley and Goodwin, 1988), and the deep subsurface (Lovley and Chapelle, 1995; Lovley et al., 1990). Until a few decades ago, it was generally considered that Fe(III) oxyhydroxide reduction was primarily the result of abiotic reactions (Lovley et al., 1991b). The degradation of organic matter and the removal of dissolved oxygen and nitrate by microor-

ganisms lowers the ambient redox potential and, according to equilibrium thermodynamics, this should shift the Fe(III)-Fe(II) equilibrium in favor of soluble Fe(II) (Halvorson and Starkey, 1927; Hem, 1972). Thus, as microbial metabolism lowers the redox potential, Fe(III) is non-enzymatically converted to Fe(II) in order to maintain (local) equilibrium.

However, no evidence was provided to support local Fe(III)-Fe(II) redox equilibrium, and none of the subsequent studies (Ponnamperuma, 1972; Zehnder, 1988) that have treated Fe(III) reduction as part of a reversible redox equilibrium have demonstrated that Fe(III) can be reduced purely by changes in Eh or pH. In contrast, early studies by Ottow and co-workers consistently indicated that Fe(III) reduction in microbial cultures was the result of direct enzymatic activity (Munch and Ottow, 1980; Ottow, 1968). Evidence gathered during the last decades indicates that microorganisms, widespread in soils, sediments and aquifers, are capable of coupling the oxidation of organic acids, aromatic compounds and some amino acids to the reduction of Fe(III) oxides (Chapelle, 1993; Coates et al., 1995; DiChristina, 1989; DiChristina et al., 1988; Konhauser, 1998; Lonergan et al., 1996; Lovley, 1991). Whereas in marine environments sulfide resulting from sulfate reduction may contribute largely to net Fe(III) reduction (Poulton et al., 2004), there is also indication that dissimilatory iron reduction is an significant process in marine sediments (Canfield et al., 1993; Koretsky et al., 2003; Lowe et al., 2000; Mark Jensen et al., 2003).

Ferric iron oxyhydroxides are ubiquitous, and microbial Fe(III) oxyhydroxide reduction contributes significantly to the degradation of organic matter in a wide spectrum of sedimentary environments. However, compared to other metabolic pathways, only a limited number of research groups have devoted significant efforts to unraveling the ecological, mineralogical and environmental controls on microbial iron reduction. Particularly, there have been few in-depth studies on the role of Fe(III) oxyhydroxide mineralogy on the kinetics of microbial iron reduction. Natural Fe(III) oxyhydroxide are structurally, chemically and morphologically diverse (Perret et al., 2000) and, therefore, they exhibit a large spectrum of reactivities towards microbial reduction. The goal of this thesis is precisely to identify the mineral-related parameters that control microbial Fe(III) oxyhydroxide reduction kinetics. The following sections provide general background information on the mineralogy and properties of iron oxides, and on iron reducing microorganisms and the mechanisms of microbial iron reduction. Finally a brief outline of the thesis is presented.

1.1 Iron(III) oxides

Considering the large amount of research devoted to iron oxides, surprisingly few comprehensive reviews of the state of the art on this class of minerals can be found in the literature. The information summarized below is based on the review of Fricke & Hüttig (1937) and the more recent ones by Cornel and Schwertmann (1991; 1996) and Murray (1979).

There are sixteen ferric iron oxides, oxyhydroxides and hydroxides known to date. In this thesis, these compounds are collectively referred to as Fe(III) oxyhydroxides. This section presents the principal features of the oxyhydroxides goethite and lepidocrocite, the hydroxide ferrihydrite, and the oxide hematite. The formation, structure, crystal size and morphology, plus the specific surface area of the minerals will be briefly addressed. The section ends with a discussion of the principal dissolution mechanisms of Fe(III) oxyhydroxides.

1.1.1 Goethite

Due to its thermodynamic stability, goethite is by far the most common Fe(III) oxyhydroxide mineral in soils. For this reason, soils containing goethite as the principal Fe (III) phase are ubiquitous around the globe and predominate under cool to temperate, humid climates. In warmer regions, goethite is often associated with hematite (section 1.1.3). Beyond its widespread presence in soils, goethite has also recently been proposed to be the dominant authigenic Fe(III) phase in freshwater and marine sediments (van der Zee et al., 2003). There are two recognized pathways by which goethite forms, (i) from the oxidation of Fe(II) released by dissolution of solid Fe(II) compounds (Fe-silicates, -carbonates or -sulfides) or, alternatively, from the reduction of Fe(III) mineral phases, and (ii) via the transformation

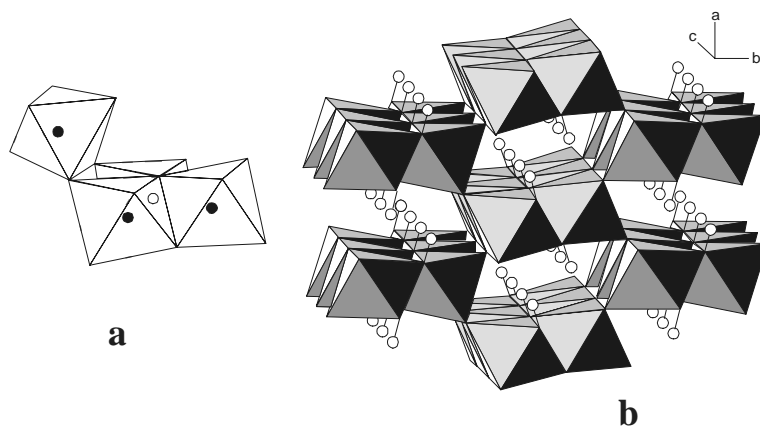
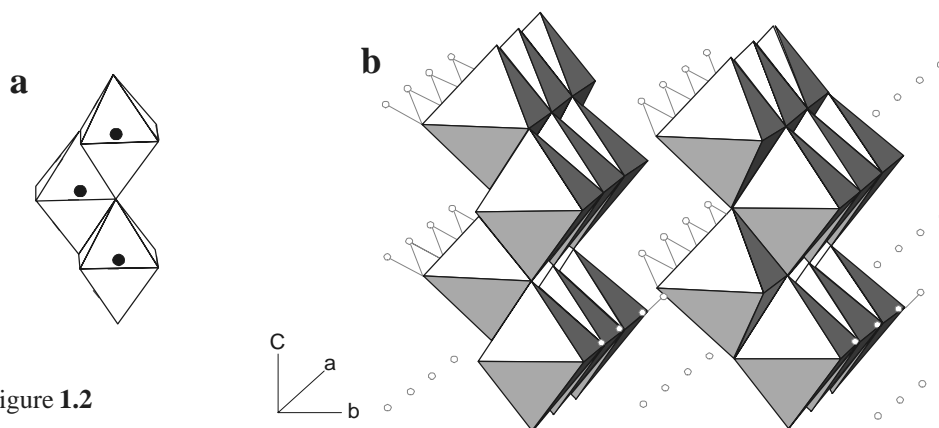


Figure 1.1

In the goethite structure, each Fe(III) ion is surrounded by three O^{2-} and three OH^- resulting in $FeO_3(OH)_3$ octahedra. Double chains of octahedra formed by edge sharing are linked to adjacent double chains by corner sharing (Figure 1.1 a). This arrangement of double chains leads to orthorhombic symmetry. Non-linear hydrogen bonds span diagonally across the empty cation sites in the goethite structure; these bonds help hold together the chains of octahedra (Figure 1.1 b). Although goethite displays a multitude of sizes, there is essentially one basic morphology – acicular or needle shaped. Acicular goethite crystals can range in length from a few tens of nm to several microns. The specific surface area of goethite measured by BET (N_2 adsorption) accordingly exhibits a fairly large range ($8 - 200 \text{ m}^2 \text{ g}^{-1}$).

1.1.2 Lepidocrocite

Lepidocrocite is less widespread than goethite or hematite. However, it has been identified as orange concretions in a variety of soils, under quite different climatic conditions, including temperate climate in the Netherlands (van der Marel, 1951) and England (Brown, 1953), subtropical climate in Natal (South Africa) (Schwertmann and Fitzpatrick, 1977), and tropical climate in Brazil (dos Anjos et al., 1995).



Lepidocrocite is commonly found in environments that alternate seasonally between oxic and anoxic conditions. During the wet season, anaerobic conditions develop and lead to the formation of Fe^{2+} , which oxidizes to lepidocrocite at the contact with oxygen and precipitates locally as concretions. Lepidocrocite is therefore characteristic of the transient presence of Fe^{2+} .

Lepidocrocite is metastable with respect to goethite. As goethite, it consists of double chains of $Fe(O,OH)_6$ octahedra running parallel to the c-axis. Lepidocrocite, however, is a layered

compound, where each double chain shares edges with adjacent double chains. The chain is displaced by half, with respect to its neighbors (Figure 1.2 a), thus forming corrugated sheets of octahedra. These sheets are held together solely by hydrogen bonds (Figure 1.2 b). The basic morphologies of lepidocrocite are lath-like, tabular, diamond-shaped or rectangular, depending of the crystallization conditions. The specific surface areas of lepidocrocite range from 15-260 m² g⁻¹. Shape and specific surface area are apparently strongly dependent on the pH conditions during formation.

1.1.3 Hematite

Although it has a similar thermodynamic stability as goethite, hematite is mostly restricted to soils of subtropical and tropical regions (Tardy and Nahon, 1985). Hematite is very often found in association with goethite. Hence, the ratio hematite/(hematite+goethite) is used to characterize soils as either hematitic (red soils at lower latitudes) or goethitic (brown soils at higher latitudes). In nature, the formation of hematite requires the presence of ferrihydrite, which is formed during the wet and relatively cool winter months, and later transformed by dehydration reaction in hematite during the dry and warm summer months (Schwertmann et al., 1999; Torrent and Cabedo, 1986).

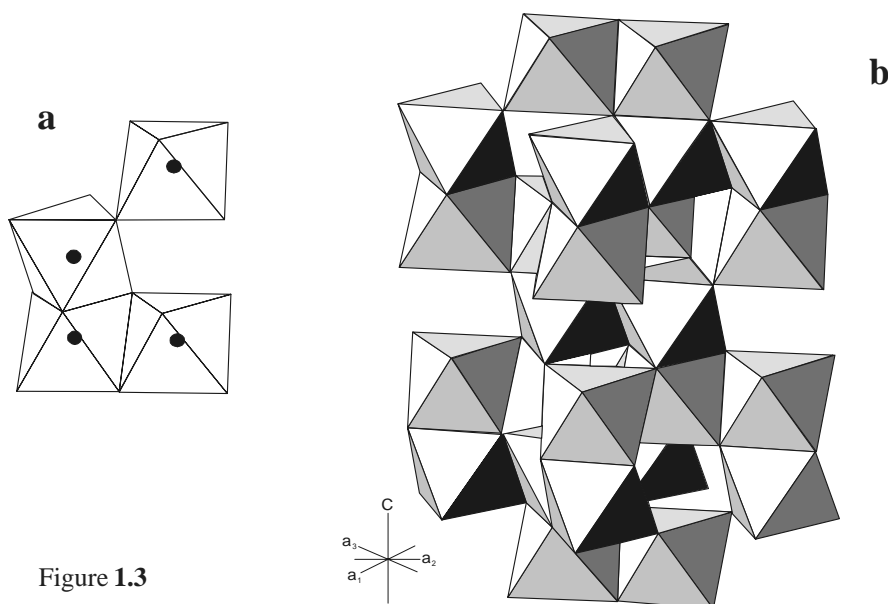


Figure 1.3

Hematite consists of layers of $\text{Fe}(\text{O})_6$ octahedra that are connected by edge- and face-sharing stacked perpendicular to the *c* direction (Figure 1.3 a). The absence of hydrogen bonds results in a compact structure, responsible for the high density and crystallinity of hematite (Figure 1.3 b). The most common habits for hematite crystals are rhombohedral, platy and rounded. Morphologies of hematite include plates, discs, rods, spindles, cubes, ellipsoids and spheres. Synthesized hematites have usually high surface areas, ranging from 10-90 $\text{m}^2 \text{g}^{-1}$ depending on particle size and shape. In nature, however, much lower surface area hematite ($< 1 \text{m}^2 \text{g}^{-1}$) can be found, for instance in ore deposits. Hematite, but also goethite and lepidocrocite, are well-known semiconductors. Although they have a rather low conductivity of electrons compared to most industrial semiconductor materials (Lindgren et al., 2002), the semiconducting properties may be critical in electron transfer reactions involved in microbial Fe(III) oxyhydroxide reduction (Rosso et al., 2003).

1.1.4 Ferrihydrite

Due to its metastable nature, ferrihydrite is usually of ephemeral occurrence. It is found in relatively young soils (Lilienfein et al., 2003), iron-rich spring deposits (Bau et al., 1998), and in marine hydrothermal systems (Kennedy et al., 2004) or podsols (McBride et al., 1983). Both a high rate of Fe(II) oxidation (compared to lepidocrocite formation) and the presence of organic compounds (humic acids) promote ferrihydrite formation. Oxidation can also be assisted by microorganisms, such as *Lepthotrix* or *Galionella* (Casanova et al., 1999). As a result of fast Fe(II) oxidation kinetics and the presence of organic compounds that prevent the formation of crystalline Fe(III) phases, ferrihydrite exhibits a poorly ordered structure. Two end-member structures are referred to as 2-lines and 6-lines ferrihydrite, based on their X-Ray diffraction patterns.

Structural studies carried out on 6-lines material, reveal a defective hematite-type structure (Chukhrov et al., 1973; Jansen et al., 2002), whereas 2-lines ferrihydrite consists of local, coherently scattered regions formed by four planar $\text{Fe}(\text{O},\text{OH})_6$ octahedra (Feitknecht et al., 1973). The low degree of crystallinity of ferrihydrite is linked both to the presence of vacant Fe sites in the structure and to replacement of some oxygens by H_2O and OH . Ferrihydrite usually forms very small particles a few nm across and more or less spherical in shape. Consequently, surface areas of ferrihydrite determined by a wide range of methods are very high, between 150 and 700 $\text{m}^2 \text{g}^{-1}$.

1.1.5 Dissolution of Fe(III) oxyhydroxides

As a mineral group, Fe(III) oxyhydroxides are characterized by low to very low solubilities. For iron to cycle through the ecosystem (biota, water and soil), mobilization of iron (i.e. dissolution) must take place. Several dissolution mechanisms of Fe(III) oxyhydroxides can be distinguished: (i) dissolution promoted by surface protonation, (ii) ligand promoted dissolution, and, (iii) reductive dissolution.

The detailed mechanism for proton-promoted dissolution has been summarized by Stumm and Sulzberger (1992). The reaction pathway involves the chemisorption of protons at the surface of the Fe(III) oxyhydroxide, thereby weakening the Fe-O bonds by polarization and, in doing so, promoting the detachment of Fe from the bulk Fe(III) phase. The rate of dissolution by protonation is highly dependent on pH conditions. In nature, this dissolution mechanism is particularly relevant in acidic environments, for instance, in acid mine drainage or acidic lakes.

Proton-promoted dissolution can be further enhanced by organic acids (e.g., oxalic and citric acid) or anions (Cl⁻) which also adsorb to the Fe(III) oxyhydroxide surface (Chang and Matijevic, 1983; Stumm et al., 1985). In soils, the action of organic ligands is often combined to that of siderophores, which form very stable Fe(III) complexes (Roemheld, 1991). This is an important mechanism occurring in the rhizosphere, as it allows biota satisfy their iron needs under aerobic conditions (Watteau and Berthelin, 1990).

In the absence of oxygen, reductive dissolution is by far the most prominent dissolution mechanism (Cornell and Schwertmann, 1996). Microbial Fe(III) oxyhydroxide reduction is thought to be responsible for a large part of the Fe(III) reduction in terrestrial environments. However, a range of reductants, including methane and sulfide, may also reduce the Fe(III) oxyhydroxides abiotically (Canfield and Berner, 1987; Miura et al., 1992). The chemical reduction kinetics of Fe(III) oxyhydroxides by sulfide in particular have been extensively studied (Dos Santos Afonso and Stumm, 1992; Poulton, 2003; Poulton et al., 2004). A similar body of knowledge on rate mechanisms, rate expressions and kinetic parameters for microbial Fe(III) oxyhydroxide reduction is only now starting to emerge.

1.2 Microbial Fe(III) reduction

The following section provides a brief overview of the relevance of microbial Fe(III) reduction in past and present day environments. More details concerning this subject can be found in, among others: Lovley (1991; 1993; 2000), Lovley and Lloyd (2000), Finneran and Lovley (2003) and Straub (2001).

1.2.1 Fe(III) as the first organic matter oxidant in the Archaean biosphere?

Microbial Fe(III) reduction may have been the first globally important mechanism of biological oxidation of organic matter to carbon dioxide. Under the anaerobic conditions of the first 2 billion years of the Earth's history, abundant dissolved Fe(II), but little dissolved sulfur, oxygen or nitrate, were present (Walker, 1987). However, as oxygenic photosynthesis emerged, possibly as early as 3 billion year ago (Des Marais, 2000; Xiong et al., 2000), Fe(II) was oxidized to Fe(III) by locally produced O₂. Hence, Fe(II) could have been the ultimate electron acceptor for photosynthesis (Cloud, 1973). Some studies suggest that Fe(II) may also have been oxidized by phototrophic Fe(II) oxidizing bacteria, however their contribution to Fe(II) oxidation during the Archaean is still under debate (Fortin and Langley, 2005; Straub et al., 2004).

Thus, during the Archaean, relatively large amounts of organic matter and Fe(III) oxides may have been co-produced. Well-known are the huge accumulations of sedimentary iron as Banded Iron Formations (BIFs). The two ingredients for dissimilatory iron reduction were therefore present, and the organic matter could have been oxidized to CO₂ using Fe(III) minerals as terminal electron acceptor (Baur, 1985; Perry, 1973; Walker, 1984). In other words, the Archaean biogeosphere could have been characterized by an intense cycling of iron, in which Fe(II) served as electron donor for primary production and Fe(III) oxyhydroxides as electron acceptor for organic matter oxidation (Walker, 1987). Early earth conditions may have favored the emergence of dissimilatory Fe(III) reduction, prior to the evolution of other respiratory processes, such as sulfate and nitrate reduction or aerobic respiration (Baur, 1985; Obuekwe et al., 1987).

1.2.2 Dissimilatory iron reduction in modern sedimentary environments

Dissimilatory Fe(III) reduction remains a significant process for organic matter oxidation in modern sedimentary environments. However, a range of other electron acceptors for organic matter oxidation is available, including O₂, NO₃⁻, Mn oxides and SO₄²⁻. In sedimentary environments, particularly when sediment mixing and the input of organic matter are sufficiently low, the various organic matter

pathways are separated in space and define a sequence of electron acceptor reduction dictated by the energy yields for the microbial populations. In this sequence of terminal electron acceptors, Fe(III) oxyhydroxides are generally reduced after Mn(IV, III) oxides and before sulfate (Froelich et al., 1979).

A number of studies have suggested that microbial iron reduction in soils and sediments is a relatively minor respiratory process (Addy et al., 1976; Kelly, 1982; Verdouw and Dekkers, 1980). However, this conclusion is mainly based on low levels of pore water Fe(II). Dissolved Fe(II) concentrations, however, may greatly underestimate the extent of Fe(III) oxyhydroxide reduction, as the Fe(II) that is produced during Fe(III) oxyhydroxide reduction may to a large degree adsorb on mineral surfaces (Howeler and Bouldin, 1971; Hyacinthe et al., 2005; Lovley and Phillips, 1988a; Roden and Urrutia, 2002). In addition, Fe(II) readily forms various Fe(II) minerals, such as vivianite (Berner, 1981; Cornwell, 1987), siderite (Berner, 1981), magnetite (Hansel et al., 2003), and it may absorb into organic matter (Hilton et al., 1986; Van Breemen, 1988).

Ideally, rates of microbial iron reduction should be measured directly. *In situ* measurements, however, are complicated by the fact that Fe(III) reduction may be restricted to a narrow band of few centimeter or less in sediments (Aller et al., 1986; Ellis-Evans and Lemon, 1989; Hamilton-Taylor and Morris, 1985; Hyacinthe and Van Cappellen, 2004; Stauffer and Armstrong, 1986; Trefry and Presley, 1982). Furthermore, traditional sediment incubation methods may not readily distinguish between microbial and abiotic reduction processes. In analogy with sulfate reduction and denitrification, isotopic tracer methods have been proposed for *in situ* Fe(III) reduction rate determination (Lovley and Phillips, 1986a). However, a recent study has shown the occurrence of rapid isotope exchanges between aqueous and solid-state iron, which interferes with the use of isotopic methods for Fe(III) reduction rate determinations (Pedersen et al., 2005). The direct measurement of *in situ* Fe(III) oxyhydroxide reduction rates is definitely a challenge for further research.

1.2.3 Iron reducing microorganisms

1.2.3.1 Fermentative Fe(III) reducers

Fermentative bacteria were the first microorganisms shown to reduce Fe(III) oxyhydroxides while growing under anaerobic conditions. In early studies, Runov (1926) noted Fe(III) oxyhydroxide reduction in pure cultures of *Escherichia coli*, *Clostridium pasteurianum* and *Lactobacillus lactis*. Further studies found that a wide variety of fermentative microorganisms

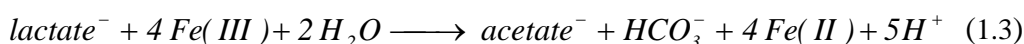
were able to reduce Fe(III) oxyhydroxides during anaerobic growth (Bromfield, 1954; Hammann and Ottow, 1974; Jones et al., 1983; Jones et al., 1984). However, fermentative Fe(III) oxyhydroxide reducing bacteria transfer less than 5% of the reducing equivalents from their metabolized substrates to Fe(III) oxyhydroxides (Lovley, 1987; Lovley and Phillips, 1988b). Therefore, it would appear that Fe(III) reduction is only a minor pathway for the electron flow in the fermentative microorganisms.

1.2.3.2 Organic acid-oxidizing Fe(III) reducers

Geobacter metallireducens GS-15 was the first bacteria shown to completely oxidize organic compounds to carbon dioxide with Fe(III) as sole electron acceptor (Lovley and Phillips, 1988b). *Geobacter metallireducens* is a strictly anaerobic gram-negative rod, which in the absence of oxygen oxidizes acetate with the concurrent reduction of Fe(III) to Fe(II), according to the reaction:



The observed temperature dependence, pH optimum, as well as the requirement for direct contact between bacteria and the Fe(III) oxide mineral, indicate that the reduction of Fe(III) in this process corresponds to a direct enzymatic reduction (Lovley and Phillips, 1988b). Enzymatic Fe(III) reduction was subsequently confirmed by the identification of membrane-bound Fe(III) reductases in *Shewanella putrefaciens* (Beliaev and Saffarini, 1998). The latter organism is another well-known organic acid-oxidizer, isolated from a corroded pipe system carrying crude oil (DiChristina et al., 1988; Obuekwe et al., 1981). This microorganism can oxidize formate completely into carbon dioxide, and lactate partially into acetate, via the reactions:



S. putrefaciens is a facultative anaerobe and also is able to reduce a variety of other electron acceptors including nitrate, nitrite, tetrathionate, glycine, fumarate, thiosulfate, sulfite, chromate and U(VI) (Lovley et al., 1991a). Although relatively few microorganisms capable of obtaining energy for growth from coupling oxidation of organic acids to the reduction of Fe(III) have been isolated (Straub et al., 2001), they are nevertheless widespread. Culture enrichments and molecularprobe studies have shown that these organisms inhabit a variety of fresh- and brackish-water sediments (Kappler et al., 2004; Lovley and Phillips, 1986b), marine sediments (Lowe et

al., 2000; Mark Jensen et al., 2003), soils (Qi et al., 2004; Roden and Zachara, 1996; Röling et al., 2001) and deeper subsurface environments (Lovley et al., 1990).

1.2.4 Environmental significance of microbial iron reduction

1.2.4.1 Degradation of aromatic compounds

Aromatic compounds are important constituents of natural organic matter, but also constitute some of the most common anthropogenic contaminants. Aromatic hydrocarbons, for example, are a major source of groundwater pollution. Microbial iron reduction may, in some cases, provide a pathway for the degradation of aromatic contaminants in groundwater (Lovley, 1995; Röling et al., 2001). For instance, *Geobacter metallireducens* GS-15 can completely oxidize common contaminants, such as toluene, phenol, *p*-cresol, benzoate, benzylalcohol, benzaldehyde, *p*-hydroxybenzoate, *p*-hydroxybenzylalcohol and *p*-hydroxybenzaldehyde, to CO₂ (Lovley et al., 1989; Lovley and Lonergan, 1990). Purified enrichment cultures have further been shown to metabolize other aromatic compounds, including syringic acid, ferulic acid, nicotinic acid, *o*-phthalic acid, *m*-cresol, tyrosine, phenylacetate and a variety of mono- and dihydroxybenzoates. More recently, microorganisms closely related to the Fe(III) reducer *Geothrix fermentans* and the aerobe *Variovorax paradoxus* have been shown to oxidize compounds as recalcitrant as benzene and xylenes (Lovley, 1997b; Rooney-Varga et al., 1999).

1.2.4.2 Products of microbial Fe(III) reduction

The reduction of Fe(III) oxyhydroxides to dissolved Fe(II) is an important biogeochemical process in all anaerobic sedimentary systems. It is also a major water quality issue: when high Fe(II)-containing groundwater is pumped to the surface, oxidative precipitation of Fe(III) oxyhydroxides may clog wells and plumbing. The colloidal Fe(III) oxyhydroxides may further discolor clothes and impair the taste of drinking water (Vuorinen et al., 1986). Microbial Fe(III) reduction also results in the generation of Fe(II) containing minerals in sedimentary environments, including magnetite (Fe(II)Fe(III)₂O₄), siderite (FeCO₃) and vivianite (Fe₃PO₄·8H₂O). Magnetite is not an obligatory end-product of dissimilatory Fe(III) reduction, and Fe(III) reducing bacteria do not direct the synthesis of magnetite via enzymatic catalyzed reactions (Bell et al., 1987). Rather, magnetite formation during Fe(III) dissimilatory reduction is an abiotic process, and can be rationalized on the basis of thermodynamic equilibria (Bell et al., 1987; Lovley, 1990).

The metabolism of Fe(III) reducing bacteria may provide localized conditions of high Fe(II) and alkalinity at the cell-Fe(III) oxide interface, thereby promoting magnetite formation. Magnetite production during Fe(III) reduction is distinct from assimilatory production of magnetite in magnetotactic bacteria, where intracellular chains of single domain magnetite are formed (Blakemore, 1982; Frankel and Blakemore, 1989). In contrast, magnetite produced during dissimilatory iron reduction is extracellular. The metabolism of *Geobacter sp.* typically produces, on a per cell basis, 5000-fold more magnetite than magnetotactic bacteria (Lovley et al., 1987; Sparks et al., 1990). Magnetite formation during dissimilatory iron reduction may possibly explain the extensive deposition of magnetite in banded iron formations (Baur, 1985; Lovley, 1990; Lovley et al., 1987; Walker, 1984).

1.2.4.3 Trace elements

Microbial reduction of Fe(III) plays an important role in the fate and transport of trace metals and nutrients, particularly phosphate, in groundwaters. Fe(III) oxyhydroxides strongly bind phosphate under oxidizing conditions (Mortimer, 1941). With the development of anaerobic conditions, Fe(II) and phosphate are simultaneously released into the surrounding water (Hyacinthe and Van Cappellen, 2004; Mortimer, 1941). As phosphate is frequently the limiting nutrient in freshwater environments, microbial iron reduction may ultimately be the cause of algal blooms and eutrophication (Mesnage et al., 2002).

A wide variety of toxic trace metals adsorb and coprecipitate with Fe(III) oxyhydroxides (Francis and Dodge, 1990; Lovley, 1987; Luoma and Davis, 1983; Means et al., 1978; Pokrovsky and Schott, 2002; Roden and Edmonds, 1997). As a result of microbial Fe(III) oxyhydroxides reduction, these trace metals may be released into interstitial waters of aquatic sediments (Balistrieri and Murray, 1986; Cornwell, 1986; Kadko et al., 1987), anoxic bottom waters (Todd et al., 1988), or groundwater (Bourg et al., 1989). This remobilization of heavy metals is a potential hazard to ecosystems and drinking-water supplies. For instance in Bangladesh, microbial Fe(III) oxyhydroxide reduction may contribute substantially to the mobilization of As(III) and As(V), causing a large-scale contamination of the aquifers (Appelo et al., 2002). However, Fe(III) reduction can also lead to the immobilization of certain trace elements. For instance, the reduction of soluble U(VI) to insoluble U(IV) by Fe(II) produced by Fe(III) reduction is an important mean for the immobilization of dissolved uranium from aquatic environments (Anderson et al., 1989; Behrends and Van Cappellen, 2005; Roden and Scheibe, 2005; Swarzenski et al., 1999).

1.2.5 Mechanisms of microbial Fe(III) reduction

1.2.5.1 Fe(III) reductases?

From studies on *S. putrefaciens* and *S. oneidensis* it has become evident that *c*-type cytochromes play a major role in iron respiration, possibly as terminal Fe(III) reductases (Myers and Myers, 1997b; Myers and Myers, 2003; Myers and Myers, 2004). These cytochromes are located mainly in the periplasmic space, or associated with the outer membrane of the cell (Myers and Myers, 2004). In *S. oneidensis* MR-1, more than 50% of the total ferric reductase activity was observed in the outer membrane. The outer membrane protein MtrB has been proposed to be a key component of ferric reductases in *S. oneidensis* MR-1 (Beliaev and Saffarini, 1998; Beliaev et al., 2001). Inactivation of the *mtrB* gene resulted in the loss of Fe(III) reducing capability. Other proteins have also been proposed to be involved in Fe(III) reductases: MtrC (outer membrane), CymA and MtrA (periplasmic space) (Myers and Myers, 1997a; Myers and Myers, 2000). A 150-kDa outer membrane protein from *S. oneidensis* has been suggested to interact directly with the Fe(III) oxyhydroxide surface and facilitate the electron transfer (Lower et al., 2001).

Another recently discovered means of transferring electrons from the cell to the surface of a Fe(III) oxyhydroxide involves the pili of the iron reducing bacterium *Geobacter sulfurreducens* (Reguera et al., 2005). Microtopographic analyses using atomic force microscopy (AFM) indicate that these pili are highly conductive. However, a role of pili in iron reduction has so far not been demonstrated for other iron reducing bacteria, including *S. putrefaciens*. It would thus appear that the nature of the iron-reducing factors may vary from one bacterial species to another. However, for all iron reducing bacteria studied, the iron reducing enzymatic factors are closely associated with the outer membrane. Whereas this may be a rather unusual location for respiratory enzymes, it is, however, perfectly suited in the case of a solid-phase terminal electron acceptor.

1.2.5.2 Cell-mineral electron transfer

The following strategies for the utilization of an insoluble Fe(III) oxyhydroxide have been proposed: (i) direct contact between the cell and the Fe(III) oxyhydroxide mineral, (ii) transfer of electrons from the microorganism to a reduced soluble compound (the electron shuttle) in the surrounding solution, with subsequent reaction of the electron shuttle with the Fe(III) oxyhydroxide, (iii) production of a Fe(III) chelator by the organism, which mobilizes Fe(III) from the mineral and subsequently delivers the complexed Fe(III) to the organism. The last

mechanism may be a common strategy adopted by plants and fungi to assimilate trace amounts of iron (see section 1.1.5). However, it seems rather unlikely that iron-reducing bacteria would rely heavily on the random fate of dissolved chelated Fe(III) for their energy generation. The use of electron shuttles to mediate the reduction of Fe(III) oxyhydroxide is a more promising option. In this case, the bacteria reduce common soluble compounds, in particular humic acids, which in turn are regenerated by abiotically reducing Fe(III) oxyhydroxide (Kappler et al., 2004; Nevin and Lovley, 2002). In this manner, a small amount of electron shuttle can undergo multiple reduction-oxidation cycles and catalyze Fe(III) reduction.

Nevertheless, direct contact between bacteria and Fe(III) oxyhydroxides is considered to be the prevalent strategy for the enzymatic reduction of the minerals (Arnold et al., 1988; Lovley and Phillips, 1988b; Munch and Ottow, 1983). The requirement of direct cell-mineral contact for microbial Fe(III) oxyhydroxide, however, has not been unambiguously proven. When a semi-permeable membrane separates iron reducing bacteria from the Fe(III) oxyhydroxide, no reduction takes place (Arnold et al., 1988; Munch, 1983). This observation has been used as evidence that iron-reducing bacteria do not release Fe(III) chelators or electron shuttles themselves. However, positive control experiments performed subsequently, with chelators or electron shuttle compounds present in the medium, show no reduction as well when Fe(III) oxyhydroxides are separated from the iron reducing bacteria by a semi-permeable membrane (Lovley, 1997a). Therefore, more definitive experiments are needed to determine whether physical contact is a pre-requisite for microbial Fe(III) oxyhydroxide reduction in the absence of electron shuttles and Fe(III) chelators.

In nature, iron-reducing microbial communities probably take variously advantage of the different strategies described above to carry out dissimilatory Fe(III) reduction. Compared to the large array of situations that can be encountered in nature, we investigate, in this thesis, a highly simplified biogeochemical system, with *Shewanella putrefaciens* as model iron-reducing microorganism added to pure, synthetic Fe(III) oxyhydroxides. By design, we work with experimental systems to which no electron shuttles or Fe(III) chelators are added.

1.3 Thesis outline

This thesis focuses on the kinetic controls of microbial Fe(III) oxyhydroxide reduction. The thesis research is part of the TRIAS project “Redox Reactivity and Bioavailability of Iron Oxyhydroxides in the Subsurface”, funded by the Netherlands Organization of Scientific Research (NWO). The project aims at the establishment of quantitative relationships between the bioavailability of Fe(III) oxyhydroxides and their mineralogical, physical and chemical properties.

Among others, dissimilatory Fe(III) reduction kinetics depends on the bioavailability of organic matter and Fe(III) oxyhydroxides, as well as on the biomass and community structure of the iron reducing population. A logical starting point of our research is to derive an empirical kinetic description of the dissimilatory iron reduction, under a set of simplified conditions. Hence, batch incubations with a pure culture of *Shewanella putrefaciens* are carried out with pure Fe(III) oxyhydroxides in the presence of excess organic substrate (lactate). The effects of the initial concentrations of various Fe(III) oxyhydroxides on the iron reduction kinetics are addressed in **Chapter II**.

In **Chapter III** the role of cell-mineral attachment on the rate of dissimilatory reduction of Fe(III) oxyhydroxides by *S. putrefaciens* is investigated, and a kinetic model for microbial reduction of Fe(III) is developed. In **Chapter IV**, the effect of Fe(III) oxyhydroxide solubility on the microbial reduction kinetics is investigated, based on the precise determination of the thermodynamic stabilities of the minerals. Finally, **Chapter V** looks into the possible inhibitory role of Fe²⁺ produced as a result of the reductive dissolution of Fe(III) oxyhydroxides on the iron reducing activity of the bacteria. A summary of the principal findings of this thesis can be found in **Chapter VI**.

References

- Addy S. K., Presley B. J., and Ewing M. (1976) Distribution of manganese, iron and other trace elements in a core from the northwest Atlantic. *J. Sed. Petrol.* **46**, 813-818.
- Allard T., Menguy N., Salomon J., Calligaro T., Weber T., Calas G., and Benedetti M. F. (2004) Revealing forms of iron in river-borne material from major tropical rivers of the Amazon Basin (Brazil). *Geochim. Cosmochim. Acta* **67**, 3079-3094.
- Aller R. C., Mackin J. E., and Cox R. T., Jr. (1986) Diagenesis of iron and sulfur in Amazon inner shelf muds: apparent dominance of iron reduction and implications for the genesis of ironstones. *Cont. Shelf Res.* **6**, 263-289.
- Anderson R. F., LeHuray A. P., Fleisher M. Q., and Murray J. W. (1989) Uranium deposition in Saanich Inlet sediments, Vancouver Island. *Geochim. Cosmochim. Acta* **53**, 2205-2213.
- Appelo C. A. J., Van Der Weiden M. J. J., Tournassat C., and Charlet L. (2002) Surface Complexation of Ferrous Iron and Carbonate on Ferrihydrite and the Mobilization of Arsenic. *Environ. Sci. Technol.* **36**, 3096-3103.
- Arnold R. G., DiChristina T. J., and Hoffmann M. R. (1988) Reductive dissolution of iron(III) oxides by *Pseudomonas* sp. 200. *Biotechnol. Bioeng.* **32**, 1081-1096.
- Balistrieri L. S. and Murray J. W. (1986) The surface chemistry of sediments from the Panama Basin: The influence of manganese oxides on metal adsorption. *Geochim. Cosmochim. Acta* **50**, 2235-2243.
- Bau M., Usui A., Pracejus B., Mita N., Kanai Y., Irber W., and Dulski P. (1998) Geochemistry of low-temperature water-rock interaction: evidence from natural waters, andesite, and iron-oxyhydroxide precipitates at Nishiki-numa iron-spring, Hokkaido, Japan. *Chem. Geol.* **151**, 293-307.
- Baur M. E. (1985) Millimeter-scale variations of stable isotope abundances in carbonates from banded iron-formations in the Hamersley Group of Western Australia. *Econ. Geol.* **80**, 270-282.
- Behrends T. and Van Cappellen P. (2005) Competition between enzymatic and abiotic reduction of uranium(VI) under iron reducing conditions. *Chem. Geol.* **220**, 315-327.
- Beliaev A. S. and Saffarini D. A. (1998) *Shewanella putrefaciens* mtrB encodes an outer membrane protein required for Fe(III) and Mn(IV) reduction. *J. Bacteriol.* **180**, 6292-6297.
- Beliaev A. S., Saffarini D. A., McLaughlin J. L., and Hunnicutt D. (2001) MtrC, an outer membrane decahaem c cytochrome required for metal reduction in *Shewanella putrefaciens* MR-1. *Mol. Microbiol.* **39**, 722-730.
- Bell P. E., Mills A. L., and Herman J. S. (1987) Biogeochemical conditions favoring magnetite formation during anaerobic iron reduction. *Appl. Environ. Microbiol.* **53**, 2610-2616.
- Berner R. A. (1981) Authigenic mineral formation resulting from organic matter decomposition in modern sediments. *Fortschr. Miner.* **59**, 117-135.
- Blakemore R. P. (1982) Magnetotactic bacteria. *Annu. Rev. Microbiol.* **36**, 217-238.
- Bourg A. C. M., Darmendrail D., and Ricour J. (1989) Geochemical filtration of riverband and migration of heavy metals between the Deule River and the Ansereuilles alluvion-chalk aquifer (Nord, France). *Geoderma* **44**, 229-244.
- Bowell R. J. (1994) Sorption of arsenic by iron oxides and oxyhydroxides in soils. *Applied Geochemistry* **9**, 279-286.
- Bromfield S. M. (1954) The reduction of ferric compounds by soil bacteria oxide by bacteria. *J. Gen. Microbiol.* **11**, 1-6.
- Brown G. (1953) The occurrence of lepidocrocite in British soils. *J. Soil Sci.* **4**, 220-228.
- Canfield D. E. and Berner R. A. (1987) Dissolution and pyritization of magnetite in anoxic marine sediments. *Geochim. Cosmochim. Acta* **51**, 645-659.
- Canfield D. E., Thamdrup B., and Hansen J. W. (1993) The anaerobic degradation of organic matter in Danish coastal sediments: iron reduction, manganese reduction, and sulfate reduction. *Geochim. Cosmochim. Acta* **57**, 3867-83.
- Casanova J., Bodenan F., Negrel P., and Azaroual M. (1999) Microbial control on the precipitation of modern ferrihydrite and carbonate deposits from the Cezallier hydrothermal springs (Massif Central, France). *Sedimentary Geology* **126**, 125-145.
- Chang H. C. and Matijevic E. (1983) Interactions of metal hydrous oxides with chelating agents. IV. Dissolution of hematite. *J. Colloid Interface Sci.* **92**, 479-488.
- Chapelle F. H. (1993) *Ground-water Microbiology and Geochemistry*. Wiley & Sons.
- Chapelle F. H. and Lovley D. R. (1992) Competitive exclusion of sulfate reduction by iron(III)-reducing bacteria: a mechanism for producing discrete zones of high-iron ground water. *Ground Water* **30**, 29-36.
- Chukhrov F. V., Zvyagin B. B., Gorshkov A. I., Ermilova L. P., and Balashova V. V. (1973) Ferrihydrite. *Izvest.*

Akad. Nauk. SSSR, Ser. Geol. **4**, 23-33

- Cloud P. (1973) Paleocological significance of the banded iron formation. *Econ. Geol.* **68**, 1135-1143.
- Coates J. D., Lonergan D. J., Philips E. J. P., Jenter H., and Lovley D. R. (1995) *Desulfuromonas palmitatis* sp. nov., a marine dissimilatory Fe(III) reducer that can oxidize long-chain fatty acids. *Arch. Microbiol.* **164**, 406-413.
- Cornell R. M., Schneider W., and Giovanoli R. (1991) Preparation and characterization of colloidal α -iron oxide hydroxide (FeOOH) with a narrow size distribution. *J. Chem. Soc. Faraday Trans.* **87**, 869-873.
- Cornell R. M. and Schwertmann U. (1996) *The Iron Oxides: Structure, Properties, Reactions, Occurrence and Uses*. VCH.
- Cornwell J. C. (1986) Diagenetic trace-metal profiles in Arctic lake sediments. *Environ. Sci. Technol.* **20**, 299-302.
- Cornwell J. C. (1987) Phosphorus cycling in arctic lake sediment: adsorption and authigenic minerals. *Arch. Hydrobiol.* **109**, 161-179.
- Crerar D. A., Means J. L., Yuretic R. F., Borcsik M. P., Amster J. L., Hastings D. W., Knox G. W., Lyon K. E., and Quiett R. F. (1981) Hydrogeochemistry of the New Jersey Coastal Plain. 2. Transport and deposition of iron, aluminum, dissolved organic matter, and selected trace elements in stream, ground- and estuary water. *Chem. Geol.* **33**, 23-44.
- Des Marais D. J. (2000) When Did Photosynthesis Emerge on Earth? *Science* **289**, 1703-1705.
- Dia A., Gruau G., Olivie-Lauquet G., Riou C., Molenat J., and Curmi P. (2000) The distribution of rare earth elements in groundwaters: assessing the role of source-rock composition, redox changes and colloidal particles. *Geochim. Cosmochim. Acta* **64**, 4131-4151.
- DiChristina T. J. (1989) Dissimilative iron(III) reduction by *Alteromonas putrefaciens* strain 200. 192 pp.
- DiChristina T. J., Arnold R. G., Lidstrom M. E., and Hoffmann M. R. (1988) Dissimilative iron reduction by the marine eubacterium *Alteromonas putrefaciens* strain 200. *Water Sci. Technol.* **20**, 69-79.
- dos Anjos L. H. C., Franzmeier D. P., and Schulze D. G. (1995) Formation of soils with plinthite on the toposequence in Maranhao State, Brazil. *Geoderma* **64**, 257-279.
- Dos Santos Afonso M. and Stumm W. (1992) Reductive Dissolution of Iron(III) (Hydr)oxides by Hydrogen Sulfide. *Langmuir* **8**, 1671-1675.
- Ellis-Evans J. C. and Lemon E. C. G. (1989) Some aspects of iron cycling in maritime Antarctic lakes. *Hydrobiologia* **172**, 149-164.
- Feitknecht W., Giovanoli R., Michaelis W., and Mueller M. (1973) Hydrolysis of iron (III) salt solutions. I. Hydrolysis of iron(III) chloride solutions. *Helv. Chim. Acta* **56**, 2847-2856.
- Finneran K. T. and Lovley D. R. (2003) Anaerobic in situ bioremediation. In *MTBE Remediation Handbook* (ed. E. E. Moyer and P. T. Kosteki). Amherst Scientific Publishers.
- Fortin D. and Langley S. (2005) Formation and occurrence of biogenic iron-rich minerals. *Earth-Sci. Rev.* **72**, 1-19.
- Francis A. J. and Dodge C. J. (1990) Anaerobic microbial remobilization of toxic metals coprecipitated with iron oxide. *Environ. Sci. Technol.* **24**, 373-378.
- Frankel R. B. and Blakemore R. P. (1989) Magnetite and magnetotaxis in microorganisms. *Bioelectromagnetics* **10**, 223-237.
- Fricke R. and Hüttig G. F. (1937) Hydroxide und Oxyhydrate. In *Handbuch der allgemeinen Chemie* (ed. P. Walden), pp. 640. Akademische Verlagsgesellschaft m. b. H.
- Froelich P. N., Klinkhammer G. P., Bender M. L., Luedtke N. A., Heath G. R., Cullen D., Dauphin P., Hammond D., Hartman B., and Maynard V. (1979) Early oxidation of organic matter in pelagic sediments of the eastern equatorial Atlantic: suboxic diagenesis. *Geochim. Cosmochim. Acta* **43**, 1075-1090.
- Halvorson H. O. and Starkey R. I. (1927) Studies on the transformations of iron in nature. I. Theoretical considerations. *J. Phys. Chem.* **31**, 626-631.
- Hamilton-Taylor J. and Morris E. B. (1985) The dynamics of iron and manganese in the surface sediments of a seasonally anoxic lake. *Archiv. Hydrobiol.* **72**, 135-165.
- Hammann R. and Ottow J. C. G. (1974) Reductive dissolution of iron(III) oxide by Saccharolytic clostridia and *Bacillus polymyxa* under anaerobic conditions. *Z. fuer Pflanzenernaehr. Bodenkd.* **137**, 108-115.
- Hansel C. M., Benner S. G., Neiss J., Dohnalkova A., Kukkadapu R. K., and Fendorf M. (2003) Secondary mineralization pathways induced by dissimilatory iron reduction of efrrihydrite under advective flow. *Geochim. Cosmochim. Acta* **67**, 2977-2992.
- Hem J. D. (1972) Chemical factors that influence the availability of iron and manganese in aqueous systems. *Geol. Soc. Am. Bull.* **83**, 443-450.
- Hilton J., Long G. J., Chapman J. S., and Lishman J. P. (1986) Iron mineralogy in sediments. A Moessbauer study. *Geochim. Cosmochim. Acta* **50**, 2147-2151.
- Howeler R. H. and Bouldin D. R. (1971) Diffusion and consumption of oxygen in submerged soils. *Soil Sci. Soc.*

- Am. Proc.* **35**, 202-208.
- Huston D. L. and Logan G. A. (2004) Barite, BIFs, and bugs: evidence for the evolution of the Earth's early hydrosphere. *Earth Planet. Sci. Lett.* **220**, 41-55.
- Hyacinthe C., Bonneville S., and Van Cappellen P. (2005) Reactive iron(III) in sediments: Chemical versus microbial extractions. *Geochim. Cosmochim. Acta*, submitted.
- Hyacinthe C. and Van Cappellen P. (2004) An authigenic iron phosphate phase in estuarine sediments: composition, formation and chemical reactivity. *Mar. Chem.* **91**, 227-251.
- Jansen E., Kyek A., Schafer W., and Schwertmann U. (2002) The structure of six-line ferrihydrite. *Appl. Phys. A* **74** [suppl.], S1004-S1006.
- Jones J. G., Gardener S., and Simon B. M. (1983) Bacterial reduction of ferric iron in a stratified eutrophic lake. *J. Gen. Microbiol.* **129**, 131-139.
- Jones J. G., Gardener S., and Simon B. M. (1984) Reduction of ferric iron by heterotrophic bacteria in lake sediments. *J. Gen. Microbiol.* **130**, 45-51.
- Kadko D., Cochran J. K., and Lyle M. (1987) The effect of bioturbation and adsorption gradients on solid and dissolved radium profiles in sediments from the eastern equatorial Pacific. *Geochim. Cosmochim. Acta* **51**, 1613-1623.
- Kappler A., Benz M., Schink B., and Brune A. (2004) Electron shuttling via humic acids in microbial iron(III) reduction in a freshwater sediment. *FEMS Microbiol. Ecol.* **47**, 85-92.
- Kelly C. A. (1982) The potential importance of bacterial processes in regulating rate of lake acidification. *Limnol. Oceanogr.* **27**, 868-882.
- Kennedy C. B., Scott S. D., and Ferris F. G. (2004) Hydrothermal phase stabilization of 2-line ferrihydrite by bacteria. *Chem. Geol.* **212**, 269-277.
- Konhauser K. O. (1998) Diversity of bacterial iron reduction. *Elsevier Science Reviews* **43**, 91-121.
- Koretsky C. M., Moore C. M., Lowe K. L., Meile C., DiChristina T. J., and Van Cappellen P. (2003) Seasonal oscillation of microbial iron and sulfate reduction in saltmarsh sediments (Sapelo Island, GA, USA). *Biogeochemistry* **64**, 179-203.
- Lecuyer C. and Ricard Y. (1999) Long-term fluxes and budget of ferric iron: implication for the redox states of the Earth mantle and atmosphere. *Earth Planet. Sci. Lett.* **165**, 197-211.
- Lilienfein J., Qualls R. G., Uselman S. M., and Bridgman S. D. (2003) Soil formation and organic matter accretion in a young andesitic chronosequence at Mt. Shasta, California. *Geoderma* **116**, 249-264.
- Lindgren T., Wang H., Beermann N., Vayssieres L., Hagfeldt A., and Lindquist S.-E. (2002) Aqueous photoelectrochemistry of hematite nanorod array. *Solar Energy Materials and Solar Cells* **71**, 231-243.
- Lonergan D. J., Jenter H. L., Coates J. D., Phillips E. J. P., Schmidt T. M., and Lovley D. R. (1996) Phylogenetic analysis of dissimilatory Fe(III)-reducing bacteria. *J. Bacteriol.* **178**, 2402-2408.
- Lovley D. R. (1987) Organic matter mineralization with the reduction of ferric iron: a review. *Geomicrobiol. J.* **5**, 375-99.
- Lovley D. R. (1990) Magnetite formation during microbial dissimilatory iron reduction. In *Iron biominerals* (ed. R. B. Frankel and R. P. Blakemore). Plenum Publishing Corp.
- Lovley D. R. (1991) Dissimilatory iron(III) and manganese(IV) reduction. *Microbiol. Rev.* **55**, 259-287.
- Lovley D. R. (1993) Dissimilatory metal reduction. *Annu. Rev. Microbiol.* **47**, 263-290.
- Lovley D. R. (1995) Bioremediation of organic and metal contaminants with dissimilatory metal reduction. *J. Ind. Microbiol.* **14**, 85-93.
- Lovley D. R. (1997a) Microbial Fe(III) reduction in subsurface environments. *FEMS Microbiol. Rev.* **20**, 305-313.
- Lovley D. R. (1997b) Potential for anaerobic bioremediation of BTEX in petroleum-contaminated aquifers. *J. Ind. Microbiol. Biotechnol.* **18**, 75-81.
- Lovley D. R., Baedeker M. J., Lonergan D. J., Cozzarelli I. M., Phillips E. J. P., and Siegel D. I. (1989) Oxidation of aromatic contaminants coupled to microbial iron reduction. *Nature* **339**, 297-300.
- Lovley D. R. and Chapelle F. H. (1995) Deep subsurface microbial process. *Rev. Geophysic.* **33**, 365-381.
- Lovley D. R., Chapelle F. H., and Phillips E. J. P. (1990) Iron(III)-reducing bacteria in deeply buried sediments of the Atlantic Coastal Plain. *Geology* **18**, 954-957.
- Lovley D. R. and Goodwin S. (1988) Hydrogen concentrations as an indicator of the predominant terminal electron-accepting reactions in aquatic sediments. *Geochim. Cosmochim. Acta* **52**, 2993-3003.
- Lovley D. R. and Lloyd J. R. (2000) Microbes with a mettle for bioremediation. *Nat. Biotechnol.* **18**, 600-601.
- Lovley D. R. and Lonergan D. J. (1990) Anaerobic oxidation of toluene, phenol, and p-cresol by the dissimilatory iron-reducing organism, GS-15. *Appl. Environ. Microbiol.* **56**, 1858-1864.
- Lovley D. R. and Phillips E. J. P. (1986a) Availability of trivalent iron for microbial reduction in bottom sediments of the freshwater tidal Potomac River. *Appl. Environ. Microbiol.* **52**, 751-757.
- Lovley D. R. and Phillips E. J. P. (1986b) Organic matter mineralization with reduction of ferric iron in anaerobic

- sediments. *Appl. Environ. Microbiol.* **51**, 683-689.
- Lovley D. R. and Phillips E. J. P. (1988a) Manganese inhibition of microbial iron reduction in anaerobic sediments. *Geomicrobiol. J.* **6**, 145-155.
- Lovley D. R. and Phillips E. J. P. (1988b) Novel mode of microbial energy metabolism: organic carbon oxidation coupled to dissimilatory reduction of iron or manganese. *Appl. Environ. Microbiol.* **54**, 1472-1480.
- Lovley D. R., Phillips E. J. P., Gorby Y. A., and Landa E. R. (1991a) Microbial reduction of uranium. *Nature (London)* **350**, 413-416.
- Lovley D. R., Phillips E. J. P., and Lonergan D. J. (1991b) Enzymic versus nonenzymic mechanisms for iron(III) reduction in aquatic sediments. *Environ. Sci. Technol.* **25**, 1062-1067.
- Lovley D. R., Stolz J. F., Nord G. L., Jr., and Phillips E. J. P. (1987) Anaerobic production of magnetite by a dissimilatory iron-reducing microorganism. *Nature (London)* **330**, 252-254.
- Lowe K. L., Dichristina T. J., Roychoudhury A. N., and Van Cappellen P. (2000) Microbiological and geochemical characterization of microbial Fe(III) reduction in salt marsh sediments. *Geomicrobiol. J.* **17**, 163-178.
- Lower S. K., Hochella M. F., Jr., and Beveridge T. J. (2001) Bacterial recognition of mineral surfaces: nanoscale interactions between *Shewanella* and α -FeOOH. *Science (Washington, DC, U. S.)* **292**, 1360-1363.
- Luoma S. N. and Davis J. A. (1983) Requirements for modeling trace metal partitioning in oxidized estuarine sediments. *Mar. Chem.* **12**, 159-181.
- Mark Jensen M., Thamdrup B., Rysgaard S., Holmer M., and Fossing H. (2003) Rates and regulation of microbial iron reduction in sediments of the Baltic-North Sea transition. *Biogeochemistry* **65**, 295-317.
- McBride M. B., Goodman B. A., Russell J. D., Fraser A. R., Farmer V. C., and Dickson D. P. E. (1983) Characterization of iron in alkaline EDTA and ammonium hydroxide extracts of podzols. *J. Soil Sci.* **34**, 825-840.
- Means J. L., Crerar D. A., Borcsik M. P., and Duguid J. O. (1978) Radionuclide adsorption by manganese oxides and implications for radioactive waste disposal. *Nature* **274**, 44-47.
- Mesnager V., Bonneville S., Laignel B., Lefebvre D., Dupont J.-P., and Mikes D. (2002) Filling of a wetland (Seine estuary, France): natural eutrophication or anthropogenic process? A sedimentological and geochemical study of wetland organic sediments. *Hydrobiologia* **475/476**, 423-435.
- Miura Y., Watanabe A., Murase J., and Kimura M. (1992) Methane production and its fate in paddy fields. II. Oxidation of methane and its coupled ferric oxide reduction in subsoil. *Soil Sci. Plant Nutr.* **38**, 673-679.
- Mortimer C. H. (1941) The exchange of dissolved substances between mud and water in lakes. *J. Ecol.* **29**, 280-329.
- Munch J. C. and Ottow J. C. G. (1980) Preferential reduction of amorphous to crystalline iron oxides by bacterial activity. *Soil Sci.* **129**, 15-21.
- Munch J. C. and Ottow J. C. G. (1983) Reductive transformation mechanism of ferric oxides in hydromorphic soils. *Environ. Biogeochem. Ecol. Bull.* **35**, 383-394.
- Munch J. C. O., J. C. G. (1983) Effect of cell contact and iron(III) oxide form on bacterial iron reduction. *Zeitschrift fuer Pflanzenernaehrung und Bodenkunde* **145**, 66-77.
- Murray J. W. (1979) Iron oxides. In *Marine minerals* (ed. R. G. Burns), pp. 47-98. Mineralogical Society of America.
- Myers C. R. and Myers J. M. (1997a) Cloning and sequence of *cymA*, a gene encoding a tetraheme cytochrome c required for reduction of iron(III), fumarate, and nitrate by *Shewanella putrefaciens* MR-1. *J. Bacteriol.* **179**, 1143-1152.
- Myers C. R. and Myers J. M. (1997b) Outer membrane cytochromes of *Shewanella putrefaciens* MR-1: spectral analysis, and purification of the 83-kDa c-type cytochrome. *Biochim. Biophys. Acta* **1326**, 307-318.
- Myers C. R. and Myers J. M. (2003) Cell surface exposure of the outer membrane cytochromes of *Shewanella oneidensis* MR-1. *Letters in Applied Microbiology* **37**, 254-258.
- Myers C. R. and Myers J. M. (2004) The outer membrane cytochromes of *Shewanella oneidensis* MR-1 are lipoproteins. *Letters in Applied Microbiology* **39**, 466-470.
- Myers J. M. and Myers C. R. (2000) Role of the tetraheme cytochrome *CymA* in anaerobic electron transport in cells of *Shewanella putrefaciens* MR-1 with normal levels of menaquinone. *J. Bacteriol.* **182**, 67-75.
- Nevin K. P. and Lovley D. R. (2002) Mechanisms for Fe(III) oxide reduction in sedimentary environments. *Geomicrobiol. J.* **19**, 141-159.
- Obuekwe C. O., Westlake D. W. S., and Cook F. D. (1981) Effect of nitrate on reduction of ferric iron by a bacterium isolated from crude oil. *Can. J. Microbiol.* **27**, 692-697.
- Obuekwe C. O., Westlake D. W. S., and Plambeck J. A. (1987) Bacterial corrosion of mild steel under the condition of simultaneous formation of ferrous and sulfide ions. *Appl. Microbiol. Biotechnol.* **26**, 294-298.
- Ottow J. C. G. (1968) Evaluation of iron-reducing bacteria in soil and the physiological mechanism of iron reduction in *Aerobacter aerogenes*. *Z. Allg. Mikrobiol.* **8**, 441-443.

- Payne T. E., Davis J. A., and Waite T. D. (1994) Uranium retention by weathered schists - the role of iron minerals. *Radiochim. Acta* **66**, 297-303.
- Pedersen H. D., Postma D., Jakobsen R., and Larsen O. (2005) Fast transformation of iron oxyhydroxides by the catalytic action of aqueous Fe(II). *Geochim. Cosmochim. Acta* **69**, 3967-3977.
- Perret D., Gaillard J.-F., Dominik J., and Atteia O. (2000) The Diversity of Natural Hydrous Iron Oxides. *Environ. Sci. Technol.* **34**, 3540-3546.
- Perry E. C. (1973) Geology and stable isotope geochemistry of the Biwabik Iron Formation, northern Minnesota. *Econ. Geol.* **68**, 1110-1125.
- Pokrovsky O. S. and Schott J. (2002) Iron colloids/organic matter associated transport of major and trace elements in small boreal rivers and their estuaries (NW Russia). *Chem. Geol.* **190**, 141-179.
- Ponnamperuma F. N. (1972) Chemistry of submerged soils. *Adv. Agron.* **24**, 29-96.
- Poulton S. W. (2003) Sulfide oxidation and iron dissolution kinetics during the reaction of dissolved sulfide with ferrihydrite. *Chem. Geol.* **202**, 79-94.
- Poulton S. W., Krom M. D., and Raiswell R. (2004) A revised scheme for the reactivity of iron (oxyhydr)oxide minerals towards dissolved sulfide. *Geochim. Cosmochim. Acta* **78**, 3703-3715.
- Qi Y., Roh Y., Carroll S. L., Blair B., Zhou J., Zhang C. L., and Fields M. W. (2004) Alkaline anaerobic respiration: Isolation and characterization of a novel alkaliphilic and metal-reducing bacterium. *Appl. Environ. Microbiol.* **70**, 5595-5602.
- Reeburgh W. S. (1983) Rates of biogeochemical processes in anoxic sediments. *Ann. Rev. Earth Planet. Sci.* **11**, 269-298.
- Reguera G., McCarthy K. D., Mehta T., Nicoll J. S., T. T. M., and Lovley D. R. (2005) Extracellular electron transfer via microbial nanowires. *Nature* **435**, 1098-1101.
- Roden E. E. and Edmonds J. W. (1997) Phosphate mobilization in iron-rich anaerobic sediments. Microbial Fe(III) oxide reduction versus iron-sulfide formation. *Arch. Hydrobiol.* **139**, 347-378.
- Roden E. E. and Scheibe T. D. (2005) Conceptual and numerical model of uranium(VI) reductive immobilization in fractured subsurface sediments. *Chemosphere* **59**, 617-628.
- Roden E. E. and Urrutia M. M. (2002) Influence of biogenic Fe(II) on bacterial crystalline Fe(III) oxide reduction. *Geomicrobiology Journal* **19**, 209-251.
- Roden E. E. and Zachara J. M. (1996) Microbial reduction of crystalline iron(III) oxides: Influence of oxide surface area and potential for cell growth. *Environ. Sci. Technol.* **30**, 1618-28.
- Roemheld V. (1991) The role of phytosiderophores in acquisition of iron and other micronutrients in graminaceous species: an ecological approach. *Plant Soil* **130**, 127-134.
- Röling W. F. M., van Breukelen B. M., Braster M., Bin L., and van Verseveld H. W. (2001) Relationships between Microbial Community Structure and Hydrochemistry in a Landfill Leachate-Polluted Aquifer. *Appl. Environ. Microbiol.* **67**, 4619-4629.
- Rooney-Varga J. N., Anderson R. T., Fraga J. L., Ringelberg D., and Lovley D. R. (1999) Microbial communities associated with anaerobic benzene degradation in a petroleum-contaminated aquifer. *Appl. Environ. Microbiol.* **65**, 3056-3063.
- Rosso K. M., Zachara J. M., Fredrickson J. K., Gorby Y. A., and Smith S. C. (2003) Nonlocal bacterial electron transfer to hematite surfaces. *Geochim. Cosmochim. Acta* **67**, 1081-1087.
- Runov E. V. (1926) Die Reduktion der Eisenoxyde auf microbiologischem Wege. *Vestn. Bakter-Agronomich. Stantsii* **24**, 75-82.
- Schaefer T., Artinger R., Dardenne, Bauer A., Schuessler W., and Kim J. I. (2003) Colloid-Borne Americium Migration in Gorleben Groundwater: Significance of Iron Secondary Phase Transformation. *Environ. Sci. Technol.* **37**, 1528-1534.
- Schwertmann U. and Fitzpatrick R. W. (1977) Occurrence of lepidocrocite and its association with goethite in Natal soils. *Soil Sci. Soc. Am. J.* **41**, 1013-1018.
- Schwertmann U., Friedl J., and Stanjek H. (1999) From Fe(III) ions to ferrihydrite and then to hematite. *J. Colloid Interface Sci.* **209**, 215-233.
- Sparks N. H. C., Mann S., Bazylinski D. A., Lovley D. R., Jannasch H. W., and Frankel R. B. (1990) Structure and morphology of magnetite anaerobically-produced by a marine magnetotactic bacterium and a dissimilatory iron-reducing bacterium. *Earth Planet. Sci. Lett.* **98**, 14-22.
- Stauffer R. E. and Armstrong D. E. (1986) Cycling of iron, manganese, silica, phosphorus, calcium and potassium in two stratified basins of Shagawa Lake, Minnesota. *Geochim. Cosmochim. Acta* **50**, 215-229.
- Straub K. L., Benz M., and Schink B. (2001) Iron metabolism in anoxic environments at near neutral pH. *FEMS Microbiol. Ecol.* **34**, 181-186.
- Straub K. L., Schoenhuber W., Buchholz-Cleven B., and Schink B. (2004) Diversity of Ferrous Iron-Oxidizing, Nitrate-Reducing Bacteria and their Involvement in Oxygen-Independent Iron Cycling. *Geomicrobiol. J.*

21, 371-378.

- Stumm W., Furrer G., Wieland E., and Zinder B. (1985) The effect of complex-forming ligands on the dissolution of oxide and aluminosilicate. In *The chemistry of weathering* (ed. J. I. Drever), pp. 55-74. Reidel, D.
- Stumm W. and Sulzberger B. (1992) The cycling of iron in natural environments: considerations based on the laboratory studies of heterogeneous redox processes. *Geochim. Cosmochim. Acta* **56**, 3233-3257.
- Swarzenski P. W., McKee B. A., Skei J. M., and Todd J. F. (1999) Uranium biogeochemistry across the redox transition zone of a permanently stratified fjord: Framvaren, Norway. *Mar. Chem.* **67**, 181-198.
- Taillefert M. and Gaillard J.-F. (2002) Reactive transport modeling of trace elements in the water column of a stratified lake: Iron cycling and metal scavenging. *J. Hydrol.* **256**, 16-34.
- Tardy Y. and Nahon D. (1985) Geochemistry of laterites, stability of Al-goethite, Al-hematite, and Fe³⁺-kaolinite in bauxites and ferricretes: an approach to the mechanism of concretion formation. *Am. J. Sci.* **285**, 865-903.
- Todd J. F., Elsinger R. J., and Moore W. S. (1988) The distributions of uranium, radium and thorium isotopes in two anoxic fjords: Framvaren Fjord (Norway) and Saanich Inlet (British Columbia). *Mar. Chem.* **23**, 393-415.
- Torrent J. and Cabedo A. (1986) Sources of iron oxides in reddish brown soil profiles from calcarenites in southern Spain. *Geoderma* **37**, 57-66.
- Trefry J. H. and Presley B. J. (1982) Manganese fluxes from Mississippi Delta sediments. *Geochim. Cosmochim. Acta* **46**, 1715-1726.
- Van Breemen N. (1988) Effects of seasonal redox processes involving iron on the chemistry of periodically submerged soils. In *Iron in soils and clay minerals* (ed. J. W. Stucki, B. A. Goodman, and U. Schwertmann). D. Reidel Publishing Co.
- van der Marel H. W. (1951) Gamma ferric oxide in sediments. *J. Sed. Petrol.* **21**, 12-21.
- van der Zee C., Roberts D. R., Rancourt D. G., and Slomp C. P. (2003) Nanogoethite is the dominant reactive oxyhydroxide phase in lake and marine sediments. *Geology* **31**, 993-996.
- Verdouw H. and Dekkers E. M. J. (1980) Iron and manganese in Lake Vechten (the Netherlands); dynamics and role in the cycle of reducing power. *Archiv. Hydrobiol.* **89**, 509-522.
- Vuorinen A., Carlson L., and Tuovinen O. H. (1986) Ground water biogeochemistry of iron and manganese in relation to well water quality. In *International Symposium on Biofouled Aquifers: Prevention and Restoration* (ed. D. R. Cullimore). American Water Resources Association.
- Walker J. C. G. (1984) Suboxic diagenesis in banded iron formations. *Nature* **309**, 340-342.
- Walker J. C. G. (1987) Was the Archaean biosphere upside down? *Nature* **329**, 710-712.
- Watteau F. and Berthelin J. (1990) Iron solubilization by mycorrhizal fungi producing siderophores. *Symbiosis* **9**, 59-67.
- Xiong J., Fischer W. M., Inoue K., Nakahara M., and Bauer C. E. (2000) Molecular Evidence for the Early Evolution of Photosynthesis. *Science* **289**, 1724-1730.
- Zehnder A. (1988) Geochemistry and biogeochemistry of anaerobic habitats. In *Biology of anaerobic microorganisms* (ed. A. Zehnder), pp. 1-38. John Wiley & Sons.

Chapter II

Microbial reduction of iron(III) oxyhydroxides: effects of mineral solubility and availability

Steeve Bonneville, Philippe Van Cappellen and Thilo Behrends

Published in the Special issue “Metal ions and bacteria interactions” of *Chemical Geology*
(2004) **212**, 255-268

Abstract

The rate of Fe(III) reductive dissolution by ascorbate has been shown by Larsen and Postma (2001) to decrease in the order ferrihydrite > lepidocrocite > goethite > hematite. The abiotic rate of reductive dissolution thus correlates with the solubility of the iron oxyhydroxides. We investigated whether this also holds for the microbial reduction kinetics of Fe(III) iron oxyhydroxides. The solubilities of nanoparticulate hematite, lepidocrocite, ferrihydrite and amorphous Fe(III) oxyhydroxide were obtained from pe-pH titrations of oxyhydroxide/Fe²⁺(aq) suspensions, in pH range 4 to 7. The solubility of low surface area (LSA) hematite was estimated from redox potential measurements at pH 2. The same solid phases and soluble Fe(III)-citrate were then reduced by the iron reducing bacterium *Shewanella putrefaciens* using lactate as the electron donor. In all cases, the microbial Fe(III) reduction rates exhibited saturation behavior with respect to the initial Fe(III) concentration. The maximum specific rate of reduction (v_{\max} , in $\mu\text{mol cell}^{-1} \text{h}^{-1}$) correlated positively with the solubility of the Fe(III) oxyhydroxides, with the highest values of v_{\max} for ferrihydrite and amorphous Fe(III) oxide, the lowest for LSA hematite. Hence, the solubility appears to be a rate-controlling parameter in both the abiotic and enzymatic reduction of Fe(III) oxyhydroxides.

Keywords: Microbial iron reduction, Michaelis-Menten kinetics, Fe(III) oxyhydroxide solubility.

2.1 Introduction

Iron oxyhydroxides are ubiquitous reactive constituents of soils, sediments and aquifers. They exhibit large surface areas, which bind trace metals, nutrients and organic molecules. Under suboxic conditions, Fe(III) solids are reductively dissolved via a number of alternative abiotic and microbial pathways (Lovley, 1987; Roden and Wetzel, 2002; Van Cappellen and Wang, 1996). In particular, they serve as terminal electron acceptors for the oxidation of organic matter by iron reducing bacteria. In addition to being an important oxidation pathway of organic matter degradation and generating soluble ferrous iron, microbial iron reduction can have a major impact on the persistence and mobility of metals, phosphate, radionuclides and organic contaminants (Anderson and Lovley, 1999; Roden and Edmonds, 1997). The metabolic activity of iron reducing bacteria may further enhance the natural or engineered bioremediation of contaminated sites (Lovley, 1995; McCormick et al., 2002).

The rate and extent of microbial reduction of Fe(III) oxyhydroxides are influenced by a variety of factors, including the microbial community structure and biomass, the type and abundance of Fe(III) oxyhydroxides, and the sorption affinity between the oxide phases and bacteria (Caccavo et al., 1992). In addition, the Fe(III) reduction rate may be inhibited by adsorption, on the Fe(III) solid (Roden et al., 2000) or cell surface (Urrutia et al., 1998), of Fe²⁺ formed as by-product of microbial Fe(III) reduction. While many of the rate-determining factors have been identified, in most cases mathematical relationships expressing their effects on the kinetics of microbial Fe(III) reduction are lacking.

Rates of microbial processes typically exhibit saturation behavior with respect to external substrates. That is, with increasing concentration of a given substrate, the rate levels off at a maximum value. The so-called Michaelis-Menten (or Monod) rate expression forms the basis for representing microbial reaction pathways in biogeochemical reactive transports models (McNab and Narasimhan, 1994; Van Cappellen et al., 1993). Whether the Michaelis-Menten expression describes the dependence of dissimilatory Fe(III) reduction kinetics on the availability of Fe(III) oxyhydroxides has not been experimentally demonstrated, however.

The kinetics of abiotic reductive dissolution of Fe(III) iron oxyhydroxides by organic reductants have been extensively studied (Kuma et al., 1993; Larsen and Postma, 2001; Postma, 1993). In particular, Larsen and Postma (2001) have shown that the Fe(III) reduction rate by ascorbate, normalized to the mineral surface area, decreases in the order ferrihydrite 2-lines > ferrihydrite 6-lines > lepidocrocite > goethite > hematite. The observed reaction rate order sequence

is suggestive of a linear free energy relationship between the solubility of an iron oxyhydroxide and its rate of reductive dissolution by ascorbate.

In this paper, we investigate the dependence of the rate of dissimilatory Fe(III) reduction on the concentration of various Fe(III) oxyhydroxides, as well as on the bacterial density. The goal is to determine if the reduction rate follows the Michaelis-Menten expression with respect to the Fe(III) substrate concentration. The results obtained with the solid Fe(III) phases are compared to the microbial reduction kinetics of dissolved Fe(III)-citrate. We further investigate the relationship between the microbial reduction kinetics and the solubility of the Fe(III) oxyhydroxides. The microbial Fe(III) reduction experiments are performed using the facultative anaerobic Gram-negative bacterium *Shewanella putrefaciens* as model iron reducing bacterium, and lactate as electron donor.

2.2 Materials and methods

2.2.1 Fe(III) oxyhydroxides

Hematite nanoparticles were prepared by adding 100 mL of a 0.1 M $\text{Fe}(\text{NO}_3)_3$ solution to 1 L of boiled and vigorously stirred water, and allowing the suspension to cool down at room temperature, according to the method described by Schwertmann and Cornell (1991). Nanoparticles of 6-lines ferrihydrite were synthesized by dissolving 20 g of $\text{Fe}(\text{NO}_3)_3$ in 2 L of demineralized water at 75°C under rapid stirring (Schwertmann and Cornell, 1991). The solution was maintained at 75°C for 10 min and then rapidly cooled by plunging it into ice water. In order to remove the NO_3^- ions, the hematite and ferrihydrite nanosuspensions were dialyzed with demineralized water adjusted to pH 4 (Liger et al., 1999). Lepidocrocite (Bayferrox 943) and low surface area (LSA) hematite (Bayferrox 105M) were purchased from Scholz. Amorphous Fe(III) oxide was synthesized by neutralizing a 0.4 M solution of $\text{FeCl}_3 \cdot 6\text{H}_2\text{O}$ with 1 M NaOH, and subsequently dialyzing it to remove Na^+ and Cl^- ions. The specific surface areas of the solids are given in Table 2.1. Fe(III)-citrate (purum) was purchased from Fluka; a 0.5 M solution was prepared and autoclaved before being diluted in the experimental medium.

2.2.2 Bacteria

Cultures of *Shewanella putrefaciens* 200R were provided by T. DiChristina of Georgia Institute of Technology (DiChristina and DeLong, 1994; DiChristina et al., 2002). Cells were kept aerobically on Luria Bertani medium (LB) plates (Tryptone water 15 g L⁻¹, agar 15 g L⁻¹, NaCl 5 g L⁻¹, yeast 5 g L⁻¹) and routinely cultured in liquid LB medium on a rotary shaker (150 rpm) at room temperature.

Table 2.1 Solubilities determined in pe* -pH titrations.

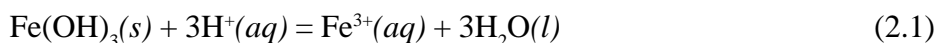
Iron oxyhydroxide	log *K _{so}	std. dev.	Slope	Reported log *K _{so}	Surf. Area (m ² g ⁻¹)
LSA Hematite	-0.82 to -0.02	-	-	-1.88 ^{a)} to 1.69 ^{b)}	12
Lepidocrocite	0.46	0.10	-2.65	-0.48 ^{c)} to 2.72 ^{d)}	83
Nano hematite	0.52	0.15	-2.85	-	125
6-lines ferrihydrite	1.62	0.27	-2.75	-	205 ^{g)}
Amorph. Fe(III) oxyhydroxide	1.90	0.13	-2.71	2.5 ^{e)} to 4.3 ^{f)}	600 ^{h)}

For LSA hematite log *K_{so} is derived from pe measurements at pH 2, assuming a range of *n* from 2.65 to 3. ^{a)} Baes and Mesmer (1976); ^{b)} Tardy and Nahon (1985); ^{c)} Vlek et al. (1974); ^{d)} Van Schuilenborgh (1973); ^{e)} Langmuir and Whittemore (1971); ^{f)} Byrne and Kester (1976); ^{g)} Larsen and Postma (2001); ^{h)} Roden and Zachara (1996).

The cultured cells were washed three times with the experimental medium solution to remove the growth medium, and then concentrated by centrifugation just before inoculation. The bacteria cultures were harvested during the late exponential/early stationary growth phase, and cell densities were estimated from optical density measurements at 660 nm wavelength. The relationship between the optical density and cell density was calibrated by direct cell counts using epifluorescence microscopy (Hobbie et al., 1977).

2.2.3 Solubility determinations

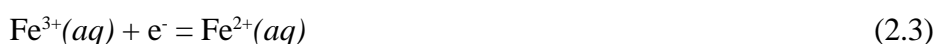
The solubility of a Fe(III) oxyhydroxide can, in theory, be obtained by measuring the pe of an oxyhydroxide suspension. Taking, for example, pure Fe(III) oxyhydroxide,



the solubility product can be expressed as,

$$*K_{so} = a_{\text{Fe}^{3+}} \cdot a_{\text{H}^+}^{-3} \quad (2.2)$$

Combining Equation (2.2) with the equilibrium constant, $K_{\text{red}} (= 10^{13.05}$ at 25°C), for the reduction half-reaction



yields

$$\text{pe}^* = \log(*K_{so} K_{\text{red}}) - 3\text{pH} \quad (2.4)$$

where

$$pe^* = pe + \log a_{Fe^{2+}} \quad (2.5)$$

Thus, at equilibrium, the simultaneous determination of pe , pH and the activity of dissolved Fe^{2+} allows one to derive the value of the solubility product, $*K_{so}$. In addition, Equation (2.4) predicts that pe^* values plotted versus pH should define a straight line with a slope of -3 . The -3 slope, however, assumes idealized, end-member compositions for the $Fe(III)$ oxyhydroxides considered in this study. In practice, deviations from the theoretical -3 value occur because of non-stoichiometric compositions (see section 2.3.1).

Duplicate titrations of suspensions of nanohematite, 6-lines ferrihydrite, amorphous $Fe(III)$ and lepidocrocite were performed from pH 4 to pH 7 in an anaerobic glove box at $25^\circ C$. The suspensions were prepared by adding 2 mM of $Fe(III)$ to 250 mL of a 0.01 M $NaCl$ and 0.01 M lactate solution. The solid concentration was kept relatively low to prevent extensive Fe^{2+} adsorption. Using reported surface site densities (see, for example, Liger et al., 1999), the concentration of adsorption sites on the oxyhydroxide particles in the suspensions were estimated to be below $2 \times 10^{-4} \text{ mol L}^{-1}$. The oxyhydroxide suspensions were purged overnight with argon gas and the initial pH was adjusted to 3.5–4 with HCl . $Fe(II)Cl_2$ was then added to a final Fe^{2+} concentration of 500 μM . The oxyhydroxide/ Fe^{2+} suspension was titrated by additions of 0.01 M $NaOH$, using a Metrohm automatic titrator equipped with a Ross glass electrode. A combined platinum electrode (Orion) monitored the redox potential in the suspension during the titration.

After each pH adjustment, the suspension was left to equilibrate for three–four hours until a stable redox potential reading was reached. Two aliquots of the suspension were then collected in order to determine the concentrations of dissolved and total Fe^{2+} . One aliquot was filtered through a 0.22 μm poresize filter and dissolved Fe^{2+} was measured using the ferrozine method (Viollier et al., 2000). Total Fe^{2+} concentration was determined on the other aliquot using the same analytical method, but after extracting the sample for 1 h with 0.5 M HCl . Activity coefficients of aqueous Fe^{2+} were calculated with the extended Debye-Hückel equation (Stumm and Morgan, 1995).

Preliminary redox potential measurements on LSA hematite suspensions showed very slow equilibration at $pH > 4$, probably due to the large particle size and, therefore, reduced contact area between oxyhydroxide and the Pt electrode, plus the rather low solubility of LSA hematite at $pH > 4$. Under highly acidic conditions, however, stable and reproducible redox measurements were obtained. Therefore, triplicate suspensions of LSA hematite were equilibrated at pH 2 for 4 days, prior to adding 500 μM Fe^{2+} as $Fe(II)Cl_2$. Redox potentials were monitored for several hours to insure stable readings.

2.2.4 Microbial Fe(III) reduction kinetics

Batch reduction experiments with *Shewanella putrefaciens* were conducted in 100 mL glass bottles, under strict anaerobic conditions. Three different concentrations of bacteria were exposed to a wide concentration range of Fe(III) substrate, either under the form of particulate Fe(III) oxyhydroxide or soluble Fe(III)-citrate. The composition of the experimental medium was: 10 mM lactate, 10 mM Hepes buffer, 28 mM NH₄Cl and 1mM CaCl₂·2H₂O. Neither phosphate, vitamins, nor trace elements were added.

The pH of the experimental media containing variable concentrations of a given Fe(III) substrate was adjusted to 7. The solutions were then degassed for 2 h, prior to being inoculated with bacteria from the same growth culture. The bottles were kept on a shaking table at room temperature (22-23°C) and aliquots were collected regularly to monitor the build-up of total Fe²⁺ during 24 h following the addition of the bacteria to the media. Controls without bacteria showed no production of Fe²⁺. Total Fe²⁺ concentrations were measured as described in section 2.3.

2.3 Results

2.3.1 Fe(III) oxyhydroxide solubilities

Duplicate titrations for each oxyhydroxide, except LSA hematite, yielded 7 to 11 individual (pe*, pH) points (Figure 2.1), which were fitted by linear least square regression. The slopes of the pe* versus pH trends were close, but not equal, to the theoretical value of -3 (Equation 2.4); the values varied from -2.65 for lepidocrocite to -2.85 for nanohematite. Comparison of dissolved and total Fe²⁺ concentrations indicated that up to 25% of the Fe²⁺ was adsorbed by the mineral surfaces, with the highest adsorption observed for nanohematite and lepidocrocite at pH 7.

In order to account for the non-stoichiometric slopes of the pe* versus pH relationships, the approach proposed by Fox (1988) was adopted (see section 2.4.1), and the solubility products of the solids were expressed as

$$^*K_{so} = a_{Fe^{3+}} \cdot a_{H^+}^{-n} \quad (2.6)$$

where $-n$ is the observed slope of the linear relationship between pe* and pH (Figure 2.1). For each measured (pe*, pH) point, a value of the solubility product was calculated using Equation (2.4), but substituting the observed slope $-n$ for the theoretical value -3 . Experimentally-derived average solubility products and their standard deviations, as well as the values of $-n$ are given in Table 2.1.

Equilibrium redox measurements for LSA hematite were performed at only one pH value. Hence, no information on the pe^*/pH relationship was obtained for this mineral phase. The range of the solubility product listed in Table 2.1 was calculated from the experimental data with an assumed interval of n from 2.65 to 3.

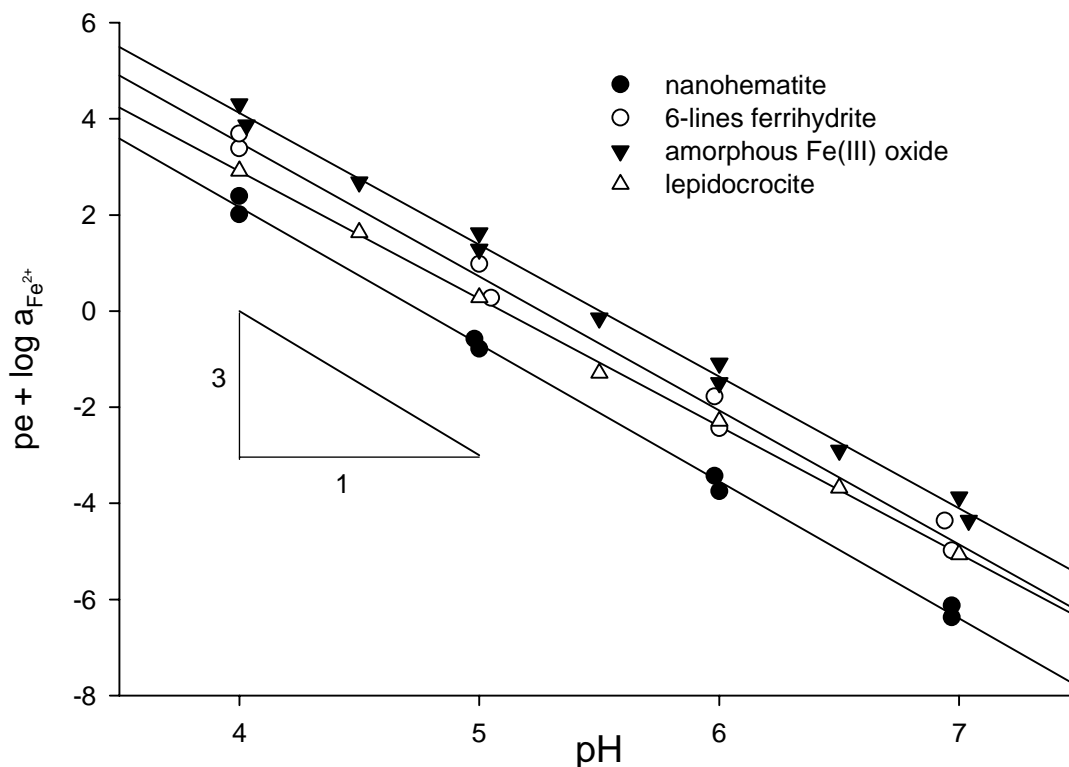


Figure 2.1 pe^* -pH titrations of nanohematite, 6-lines ferrihydrite, amorphous Fe(III) oxide and lepidocrocite. Solid lines are linear fits to the data for each of the Fe(III) oxyhydroxides.

2.3.2 Microbial Fe(III) reduction kinetics

For each Fe(III) substrate, incubations were performed at eight different substrate concentrations and three different cell densities. Under all conditions tested, the total Fe^{2+} concentration increased quasi-linearly over the 24 h of incubation (Figure 2.2). Reduction rates were calculated by linear least square regression of the total Fe^{2+} concentration versus time over the duration of the experiments.

The rates of Fe^{2+} production exhibited saturation behavior with increasing substrate concentration (Figure 2.3). For each cell density, the rate was fitted to the Michaelis-Menten rate expression:

$$R = v_{\max} \cdot B \cdot \frac{[Fe(III)]}{K_m + [Fe(III)]} \quad (2.7)$$

where v_{\max} is the maximum specific Fe(III) reduction rate per cell, B is the cell density, K_m is the affinity constant for the substrate, and $[\text{Fe(III)}]$ is the initial substrate concentration per unit volume of the suspension. In Equation (2.7), the rate R expresses the mass of Fe(III) reduced per unit volume of the suspension per unit time. Best-fit values of v_{\max} and K_m derived from the experimental data are given in Table 2.2.

Iron reduction rates normalized to cell density are plotted in Figure 2.3 for the six Fe(III) substrates. The solid lines correspond to the best fit of the Michaelis-Menten expression to the entire set of 24 experiments per Fe(III) substrate. The results summarized in Figure 2.3 and Table 2.2 show no systematic dependence of the maximum specific rate v_{\max} on the cell density. Values of v_{\max} ranged from 0.2×10^{-11} to $399 \times 10^{-11} \mu\text{mol h}^{-1} \text{cell}^{-1}$, with the lowest rates for LSA hematite and the highest for Fe(III)-citrate.

The affinity constants K_m , expressed in units of mass of Fe(III) per unit volume suspension, ranged from 0.6 to 4.9 mM for the various oxyhydroxides and Fe(III)-citrate, with the exception of lepidocrocite, which exhibited much higher K_m values (from 14.5 to 27.9 mM). As shown in Figure 2.5, the K_m values for the solid phase Fe(III) substrates systematically increased with cell density, with the possible exception of amorphous Fe(III) oxyhydroxide.

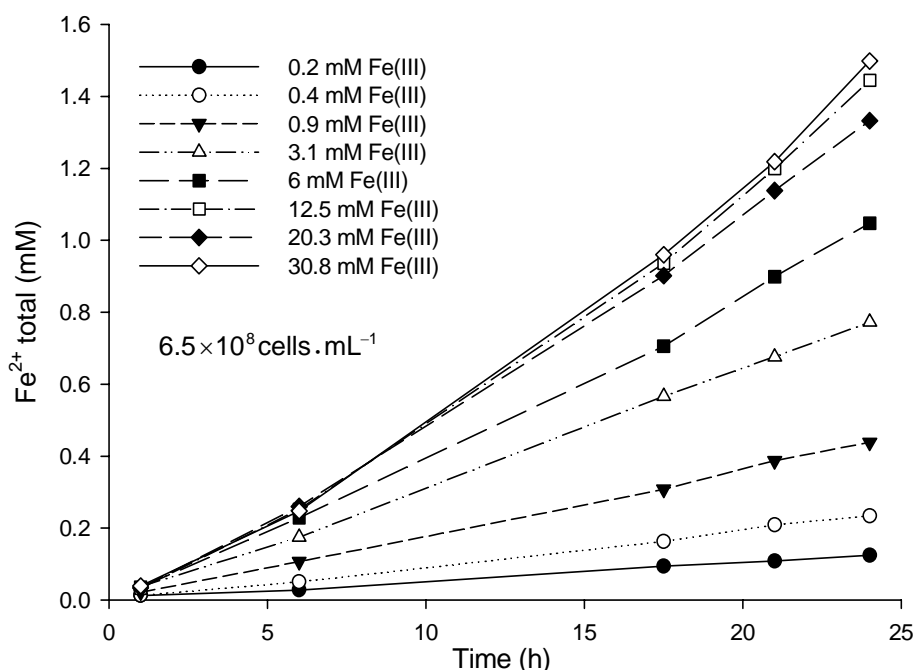


Figure 2.2 Example of the kinetic data obtained for 6-lines ferrihydrite reduction by *S. putrefaciens* 200R.

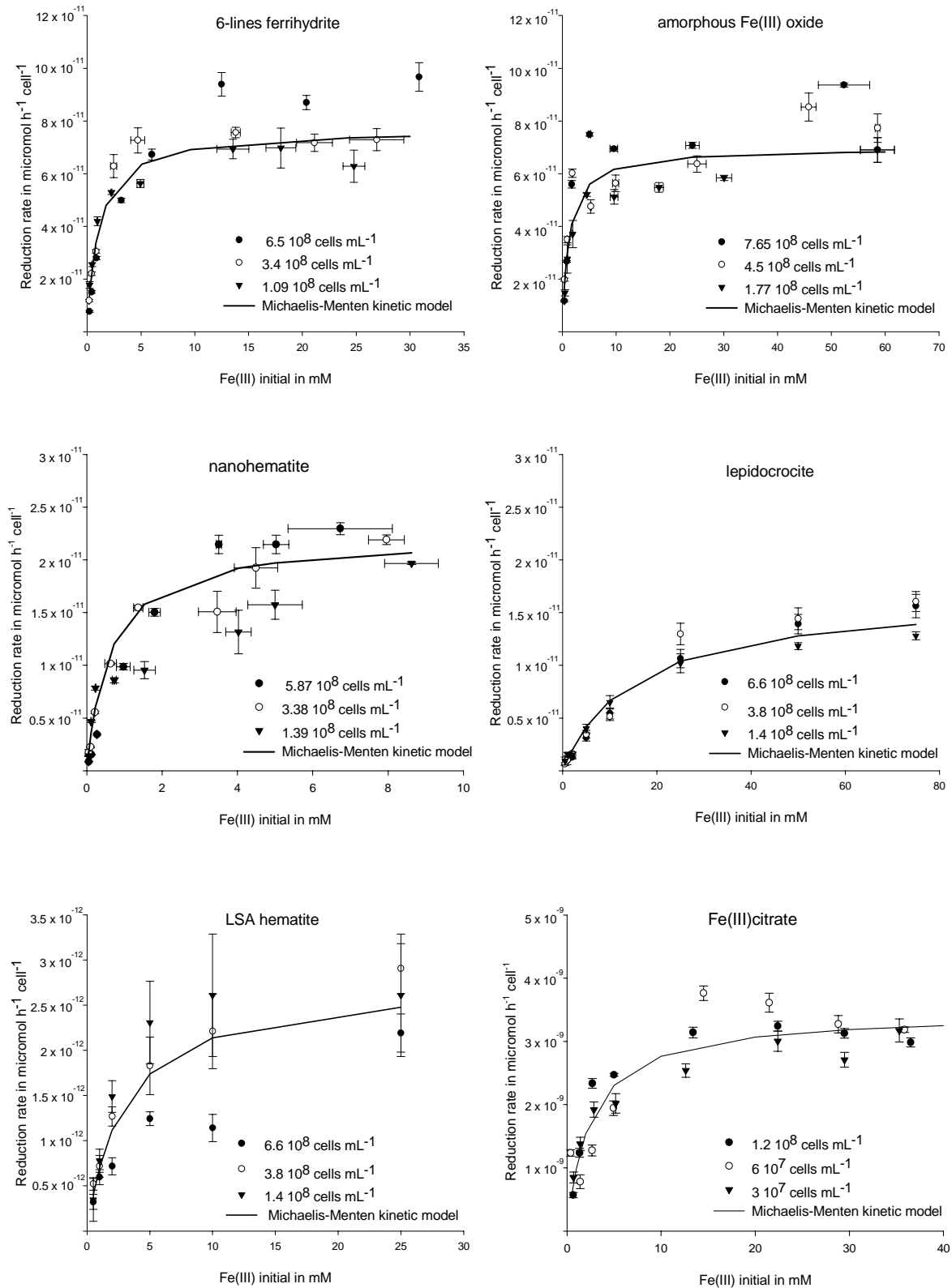


Figure 2.3 Rates of Fe(III) reduction by *S. putrefaciens* as a function of the initial concentration of Fe(III) substrate. Errors bars for the rates indicate the standard deviation of the slope of the linear least squares regression of the total Fe²⁺ concentration build-up over 24 hours (Figure 2.2).

2.4 Discussion

2.4.1 Fe(III) oxyhydroxide solubilities

Solubility products of Fe(III) oxyhydroxides reported in the literature often vary over several orders of magnitude (Table 2.1). Differences in solubility of a given Fe(III) oxyhydroxide may arise from variations in specific surface area, crystallinity and impurity content. They may also reflect difficulties associated with the experimental determination of Fe(III) oxyhydroxide solubilities. Because one of the objectives of this study is to determine the relationship between microbial Fe(III) reduction rates and Fe(III) oxyhydroxide solubility, it is essential to constrain the solubilities of the mineral phases actually used in the reduction experiments.

The solubility product of a Fe(III) oxyhydroxide can be determined by precipitating Fe³⁺ from a supersaturated solution upon addition of base, while simultaneously measuring the pH and aqueous Fe³⁺ concentration. The practicality of this approach is limited by the long equilibration times, from 10 days for ferrihydrite to several years for goethite (Feitknecht and Schindler, 1963; Schindler, 1963), as well as the low solubility of aqueous Fe³⁺ in all but highly acidic solutions.

Alternatively, one can measure the redox potential of a suspension of a Fe(III) oxyhydroxide to which soluble Fe²⁺ has been added (Equation 2.4). One advantage of this method is that it involves the determination of the concentration of aqueous Fe²⁺, rather than Fe³⁺, which makes it applicable over a wider range of pH (Figure 2.1). The method, however, assumes it is possible to determine equilibrium redox potentials. Coating of the electrode surface (Whitfield, 1974), mixed potentials (Power and Ritchie, 1983), lack of internal redox equilibrium (Jackson and Patterson, 1982) or slow kinetics of electrode exchange currents (Stumm and Morgan, 1995) may all interfere with redox potential measurement.

Stumm and Morgan (1995) conclude that few environmentally relevant redox couples produce Nernstian electrode responses. A notable exception, however, is the Fe(III)/Fe(II) couple. In homogeneous solution, equilibrium pe values can be measured under strictly anaerobic conditions, for Fe(III) and Fe(II) activities in excess of 10⁻⁶ (Grenthe et al., 1992). In heterogeneous systems, it has been demonstrated that equilibrium pe values can be obtained with colloidal Fe(III) oxyhydroxide suspensions in the presence of Fe²⁺ concentrations ≥10⁻⁵ M, even at neutral pH (Macalady et al., 1990). Doyle (1968) concludes that “the platinum electrode mediates the exchange of electrons with insoluble ferric oxide itself, either in colloidal suspension or coating the surface”.

Table 2.2 Michaelis-Menten kinetic parameters for iron(III) reduction by *S. putrefaciens*.

Iron oxyhydroxide		K_m (mM)		v_{max} (10^{-11} $\mu\text{mol h}^{-1}$ cell $^{-1}$)		v_{max}^\dagger (10^{-11} $\mu\text{mol h}^{-1}$ cell $^{-1}$)	
			std dev		std dev		std dev
lepidocrocite	H	27.9	2.1	2.1	0.07	2.0	0.1
	M	23.4	5.7	2.1	0.2		
	L	14.5	1.3	1.6	0.05		
LSA Hematite	H	4.9	2.6	0.23	0.04	0.27	0.03
	M	3.3	0.5	0.31	0.01		
	L	2.3	0.5	0.3	0.02		
nanohematite	H	1.8	0.2	3.0	0.15	2.4	0.15
	M	0.7	0.2	2.2	0.15		
	L	0.6	0.3	1.7	0.2		
6-lines ferrihydrite	H	3.0	0.5	10	0.5	8.1	0.3
	M	1.0	0.2	7.9	0.3		
	L	0.7	0.1	6.9	0.2		
amorph. Fe(III) oxyhydroxide	H	1	0.4	8.9	0.6	6.5	0.3
	M	1.4	0.3	7.8	0.3		
	L	0.6	0.1	6.7	0.2		
Fe(III)-citrate	H	1.9	0.4	346	16	345	16
	M	4.1	1.9	399	49		
	L	2.0	0.3	309	12		

Values of K_m and v_{max} are given for the three bacterial concentrations: $6\text{-}7 \times 10^8$ (H), 3×10^8 (M) and 10^8 (L) cells mL $^{-1}$. The v_{max}^\dagger values are derived from the global fit to the set of 24 experiments for each Fe(III) substrate.

Our results agree with the findings of Doyle (1968) and Macalady et al. (1990). In pH range 4-7, the platinum electrode yields stable and reproducible redox potentials for suspensions of fine-grained Fe(III) oxyhydroxides spiked with aqueous Fe $^{2+}$ (Figure 2.1). The response of the redox potentials to pH closely follows the theoretical relationship of Equation (2.4). Furthermore, the values of $*K_{so}$ derived from the pe*-pH titrations are consistent with values found in the literature (Table 2.1). Thus, it appears that the platinum electrode records redox equilibrium between colloidal Fe(III) oxyhydroxides and aqueous Fe $^{2+}$.

While close to the theoretical value, the slopes of the experimental pe*-pH relations systematically yield $n < 3$. Deviations from end-member compositions are typical of synthetic and natural Fe(III) oxyhydroxides. Due to the incorporation in the mineral structure of counter ions, such as NO $_3^-$, Cl $^-$ and SO $_4^{2-}$, or water molecules, freshly precipitated Fe(III) oxyhydroxides exhibit stoichiometric ratios, n , that fall mostly in the range 2 to 2.7 (Biedermann and Chow, 1966; Dousma and De Bruyn, 1978; Fox, 1988; Murphy et al., 1976; Spiro et al., 1966). To compare solubilities of Fe(III) oxyhydroxides, Fox (1988) therefore proposes to use the effective solubility product $*K_{so} = a_{Fe^{3+}} \cdot a_{H^+}^{-n}$, which account for non-stoichiometry of the solid phases.

The variable nature of n is a source of uncertainty in thermodynamic calculations involving Fe(III) oxyhydroxides. Most discussions of the thermodynamics of microbial iron reduction assume ideal mineral formulas (Liu et al., 2001; Roden, 2003). As free energy yields ($-\Delta G$) are often invoked to explain the occurrence of particular microbial reaction pathways in environmental settings (McNab and Narasimhan, 1994), a correct representation of the reaction quotients is paramount. For colloidal suspensions, the pe^*/pH titrations presented in this paper provide a means to directly obtain values of the effective solubility product and stoichiometric ratio, n , of a particular oxyhydroxide.

For coarse-grained oxyhydroxides, the $pe^* - pH$ method does not work because the low contact surface area hinders electron transfer between the platinum electrode and the Fe(III) solid (Doyle, 1968). This limitation can be overcome by performing potential measurements under highly acidic conditions. Equilibrium speciation calculations for the LSA hematite suspensions indicate that, at pH 2, Fe^{3+} becomes a quantitatively important species, with equilibrium concentrations around 3 μM . At low pH, proton-promoted dissolution accelerates the establishment of solubility equilibrium between the oxyhydroxide and aqueous Fe^{3+} . Under these conditions, the platinum electrode records the equilibrium potential between $Fe^{3+}(aq)$ produced by dissolution of the solid phase and $Fe^{2+}(aq)$ added to the suspension (Grenthe et al., 1992).

2.4.2 Microbial iron reduction kinetics

The Michaelis-Menten rate expression successfully reproduces the dependence of Fe(III) dissimilatory reduction rates on the initial concentrations of the various Fe(III) substrates used in this study (Figure 2.3). Liu and Zachara (2001) and Liu et al. (2002), previously used the Michaelis-Menten expression to describe the microbial reduction of aqueous Fe(III)-citrate by *S. putrefaciens* and *S. alga*, while Arnold et al. (1986) suggested that the microbial reduction of hematite may exhibit saturation behavior. Our study, however, is the first to systematically show saturation kinetics for a range of Fe(III) oxyhydroxides, and to present a complete set of kinetic parameters, v_{max} and K_m .

The Michaelis-Menten rate expression was originally derived for enzyme-catalyzed reactions in which one reactant species, the substrate, is transformed into a product via an enzyme-substrate complex. It relates the initial rate of the reaction to the total concentration of the enzyme, which is assumed to remain constant over time, and the initial concentration of substrate

(Segel, 1975). The rate of transformation of the substrate reaches a maximum value when all enzyme molecules are complexed with the substrate. When more than one substrate is limiting, more complete rate expressions for multi-substrate enzymatic reactions can be derived (Henderson, 1992; Laidler, 1987).

The formalism of the Michaelis-Menten expression has been shown to apply to complex microbially-mediated reaction pathways (Abdelmagid and Tabatabai, 1987; Kaksonen et al., 2003; Martin-Nieto et al., 1992; Ulrich et al., 2003). In case of one limiting substrate, the expression is usually recast as Equation (2.7), whereby the cell density replaces the total enzyme concentration. This assumes that, on average, each cell has the same enzymatic capability.

The dissimilatory reduction of Fe(III) oxyhydroxides by *S. putrefaciens* has been shown to require direct contact between microorganism and solid, indicating that the electron transfer to Fe(III) likely occurs at membrane-bound sites (Arnold et al., 1988; Beliaev and Saffarini, 1998; Caccavo, 1999; Caccavo et al., 1992). The identical functional dependence on the Fe(III) concentration of the reduction rate of Fe(III)-citrate and the various Fe(III) oxyhydroxides suggests that, with increasing substrate concentration, the active sites at the outer membrane of the bacteria become saturated, whether Fe(III) is dissolved or solid-bound. For any given Fe(III) substrate, the maximum Fe(III) reduction rate per cell (v_{\max}) should then be independent of the cell density. The results in Table 2.2 and Figure 2.3 show this to be the case for all the Fe(III) substrates.

While the systematic saturation behavior observed in Figure 2.3 is ascribed to saturation of electron transfer sites at the outer membrane of *S. putrefaciens* cells, there is a major difference between aqueous and solid Fe(III) substrates. For dissolved Fe(III) species, every Fe(III) center is potentially available for binding to active sites on the cell. For particulate species, however, only those Fe(III) centers within the contact region between bacterium and mineral act as direct substrates. Yet, saturation of the active sites is still likely, because membrane-bound Fe(III) reductase systems are large macromolecular structures (Beliaev and Saffarini, 1998; Beliaev et al., 2001). At the interface between a cell and a mineral surface, the number of electron transfer sites, per unit surface area, must therefore be much smaller than the surface density of Fe(III) centers of oxyhydroxides, which is on the order of two Fe(III) per nm² (Liger et al., 1999). Thus, as more and more of the cell wall contacts mineral surface, the higher abundance of interfacial Fe(III) centers should ultimately cause saturation of the active membrane sites.

2.4.3 Maximum specific reduction rate, v_{max}

The values of the maximum Fe(III) reduction rate per cell, v_{max} , obtained here are comparable to the maximum rates reported by Roden (2003) for Fe(III) oxyhydroxide reduction by *Shewanella alga*. His maximum rates, normalized to cell density, are 13.5×10^{-11} , 4.5×10^{-11} and 1×10^{-11} $\mu\text{mol h}^{-1}$ cell^{-1} for amorphous Fe(III) oxide, lepidocrocite and hematite, respectively. The hematite used by Roden has a specific surface area of $10 \text{ m}^2 \text{ g}^{-1}$ and is, thus, more akin to the LSA hematite than the nanohematite in our experiments (Table 2.1). Hence, in both studies, the maximum Fe(III) reducing activity of the cells shows a similar dependence on the solubility of the Fe(III) solids.

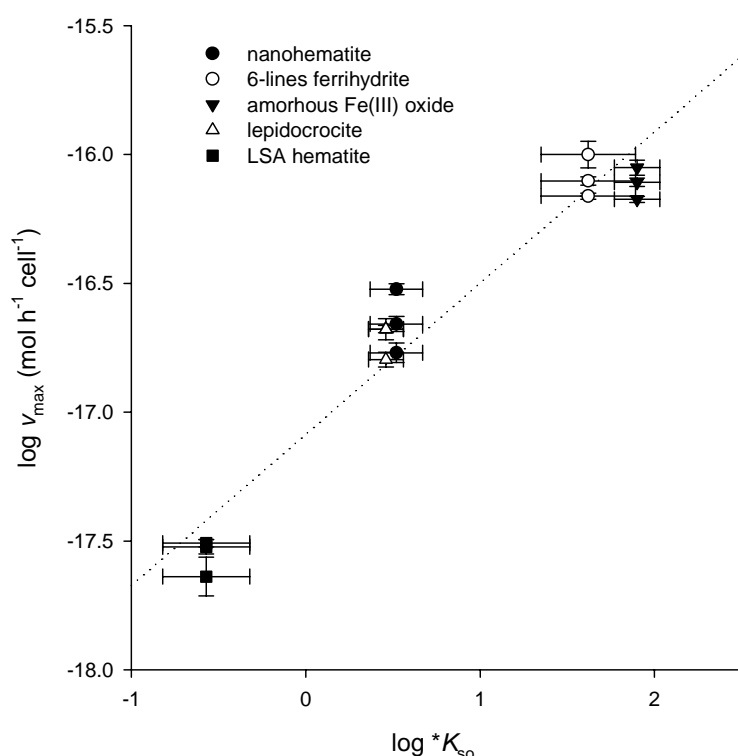


Figure 2.4 Positive relationship between maximum reduction rate per cell (v_{max}) and solubility of the Fe(III) oxyhydroxides studied.

The correlation between v_{max} and the solubility of the oxyhydroxide phases (Figure 2.4) is reminiscent of linear free energy relationships reported for abiotic mineral dissolution rates. Wollast (1974), for example, showed that the dissolution rate constant of silica polymorphs in aqueous solution correlates to their solubility. More directly relevant are the rates of reductive dissolution of Fe(III) oxyhydroxides by ascorbate of Postma (1993) and Larsen and Postma (2001), which show a similar dependence on solubility as observed here. It should be noted, however, that a direct comparison between the ascorbate dissolution rates and our v_{max} values is complicated by major differences in experimental design. The reported abiotic rates were obtained under acidic conditions (pH 3), where proton-promoted dissolution strongly influences the reaction kinetics (Suter et al., 1991).

Furthermore, the rates were measured in the presence of a large excess of ascorbate, relative to the Fe(III) concentration, while our maximum reduction rates correspond to excess Fe(III) oxyhydroxide, relative to the available active sites on the bacteria.

The trend in Figure 2.4 implies that the thermochemical properties of Fe(III) oxyhydroxides play a role in dissimilatory Fe(III) reduction by *S. putrefaciens*. This is consistent with a reaction pathway where Fe(III) centers at the mineral surface directly bind to active membrane sites of the cell prior to reduction. Because oxidation or reduction rates of metals depend on their coordination environment (Wehrli et al., 1989), the mineral lattice in which the surface Fe(III) centers are imbedded is expected to affect the reaction kinetics.

The relation between v_{\max} and oxyhydroxide solubility forms an important constraint for any mechanistic model proposed to describe microbial Fe(III) reduction kinetics and may, ultimately, help predict Fe(III) reduction rates in environmental settings. Equally important, our results illustrate the need for accurate estimates of the solubility of Fe(III) phases when relating microbial reduction rates to thermodynamic driving forces.

2.4.4 Affinity constant, K_m

For an enzymatic reaction in homogeneous solution, the meaning of K_m is straightforward. The affinity constant corresponds to the substrate concentration at which the rate reaches half the maximum rate. Because all substrate molecules can potentially bind to the enzyme, the value of K_m can directly be equated to a concentration of substrate, expressed per unit volume solution. The value of K_m is specific for the enzyme-substrate complex and is generally viewed as a measure of the affinity of the enzyme for the substrate: the smaller K_m , the stronger the affinity.

The situation is different when considering the reduction by *S. putrefaciens* of an Fe(III) oxyhydroxide, because only those Fe(III) centers in direct contact with the cells' outer membranes can potentially bind to active sites (sections 2.4.2 and 2.4.3). Therefore, K_m values expressed in terms of total Fe(III) concentrations are apparent affinity constants, whose values reflect the extent to which Fe(III) particles and cells are associated with one another. While K_m still depends on the intrinsic affinity of the bacteria for a given mineral phase, its value may also be influenced by the solid to cell ratio in the experimental system.

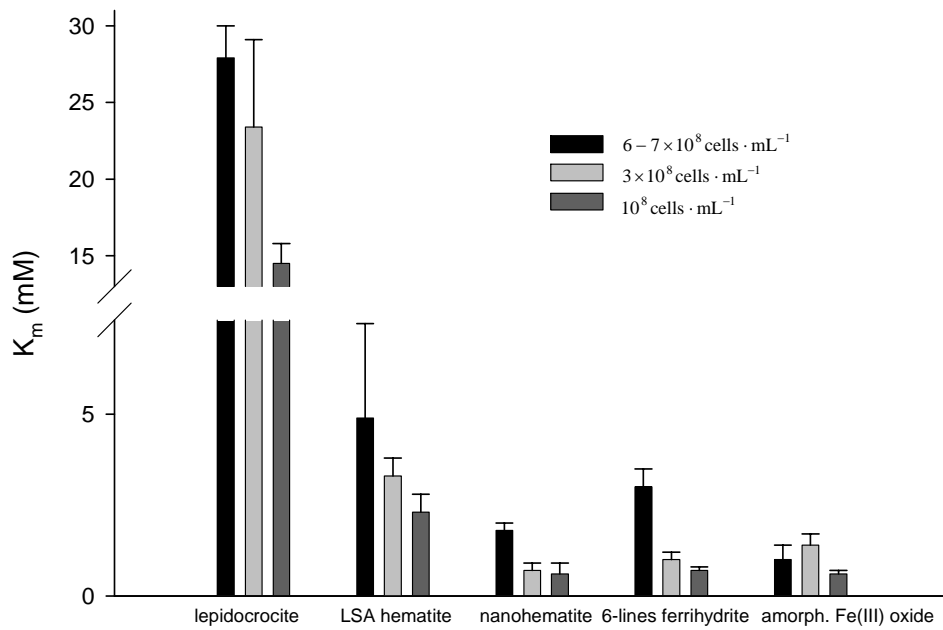


Figure 2.5 Fitted K_m values as a function of cell density for the microbial reduction of the Fe(III) oxyhydroxides. The K_m values increase systematically with increasing cell density.

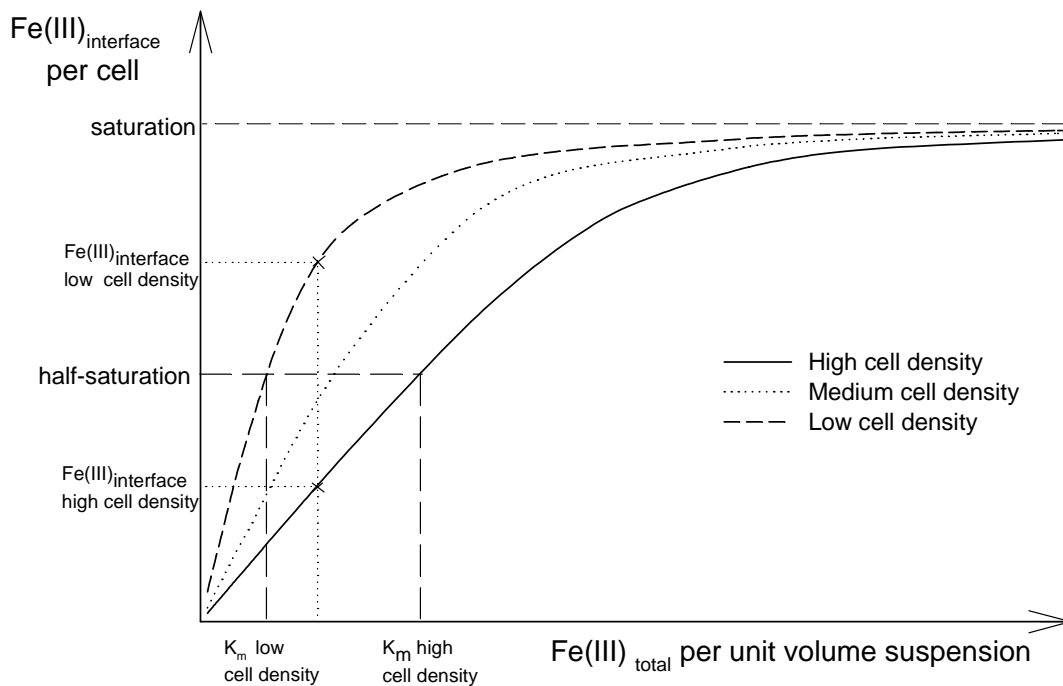


Figure 2.6 Schematic representation of the concentration of Fe(III) centers in direct contact with the cell's outer membranes, as a function of the total concentration of an oxyhydroxide and the cell density. The effect of the cell density on the apparent K_m values assume that the rate of Fe(III) reduction per cell is directly related to the abundance of Fe(III) centers at the mineral-bacterium contact. See text for complete discussion.

Figure 2.6 illustrates qualitatively how K_m may vary with the solid to cell ratio: the average concentrations of interfacial Fe(III) centers per cell are plotted as a function of the total Fe(III) concentration and the cell density. Interfacial Fe(III) centers are those mineral surface Fe(III) centers that are in direct contact with the bacterial cells. The curves assume that with increasing Fe(III) concentration, the cell surfaces are ultimately saturated with Fe(III) centers. When saturation is reached, the rate of Fe(III) reduction per cell is equal to the maximum value, v_{\max} . However high the Fe(III) becomes, the concentration of interfacial Fe(III) is limited by the finite amount of cell surface area. When the total Fe(III) concentration decreases, the average interfacial Fe(III) concentration will, at some point, become sensitive to the cell density. If a large number of cells are present relative to the Fe(III) particle density, then a large fraction of the total cell surface will not be in contact with mineral. That is, the interfacial Fe(III) concentration, normalized to cell density, will be fairly small. In contrast, if only a few cells are present, there is excess mineral surface and the average interfacial Fe(III) concentration per cell will be high. This is schematically represented on Figure 2.6 by the three curves corresponding to high, medium and low cell density.

Assuming that the Fe(III) reduction rate is directly related to the abundance of Fe(III) centers at the interface between bacterium and mineral, the theoretical curves on Figure 2.6 imply that differences in cell density should lead to differences in apparent K_m values. Actual values of K_m , and their sensitivity to cell density, are expected to be influenced by any property of the solid phase that affects the extent of mineral-bacteria association, including the specific surface area and shape of the mineral particles. It is important to note that the above discussion focuses on the effect of cell density on the Fe(III) reduction rate per cell. The total rate of Fe(III) reduction in a cell-mineral suspension, R in Equation (2.7), is the product of the reduction rate per cell, times the cell density. Thus, increasing the cell density, at a given total concentration of Fe(III) oxyhydroxide, has two opposing effects on the reduction rate R : an enhancing effect via the explicit linear dependence of R on the cell density, B , in Equation (2.7), and a negative one via the positive correlation between K_m and B (Figure 2.5).

2.5 Conclusions

The Michaelis-Menten expression for enzyme-catalyzed reactions describes the dependence of the rates of dissimilatory reduction by *S. putrefaciens* of five Fe(III) oxyhydroxides and soluble Fe(III)-citrate on the Fe(III) substrate concentration. For the mineral phases, the maximum reduction rate per cell, v_{\max} , is positively correlated with the effective solubility product of the oxyhydroxide, $*K_{so} = a_{Fe^{3+}} \cdot a_{H^+}^{-n}$, which accounts for deviations from the end-member mineral compositions via the stoichiometric ratio, n .

The systematic saturation behavior observed for the various Fe(III) oxyhydroxides is consistent with direct binding of the Fe(III) centers from the mineral surface to electron transfer sites on the cells of *S. putrefaciens*. With increasing concentration of the Fe(III) substrate, more and more of the cell membrane is in contact with mineral surface and, ultimately, the limited number of active sites on the cells becomes saturated. The observed relationship between v_{\max} and $*K_{so}$ indicates that the reduction activity of the cells is a function of the mineral lattice in which the Fe(III) surface centers are imbedded.

For practical reasons, the affinity constants, K_m , in Table 2.2 are expressed in units of total Fe(III) concentration per unit volume suspension. In principle, however, K_m is a measure of the affinity of the direct substrate for the active binding site. In case of Fe(III) oxyhydroxides, the direct substrate are Fe(III) centers located within the interfacial region between mineral and bacterium. The reported K_m values are therefore apparent coefficients that depend on the cell density. A major challenge ahead will be to relate total Fe(III) concentrations to concentrations of Fe(III) centers in direct contact with cells, in order to derive true affinity constants for the dissimilatory reduction of Fe(III) solids.

Acknowledgements

This study is part of TRIAS project 835.80.004, co-funded by the Centre for Soil Quality Management and Knowledge Transfer (SKB), Delft Cluster (DC) and the Council for the Earth and Life Sciences (ALW) of the Netherlands Organisation for Scientific Research (NWO). The authors thank Dr. D. Perret and Dr. J. Haas for their constructive reviews.

References

- Abdelmagid, H.M. and Tabatabai, M.A., 1987. Nitrate reductase activity of soils. *Soil Biol. Biochem.*, **19**: 421-427.
- Anderson, R.T. and Lovley, D.R., 1999. Naphthalene and benzene degradation under Fe(III)-reducing conditions in petroleum-contaminated aquifers. *Biorem. J.*, **3**: 121-135.
- Arnold, R.G., DiChristina, T.J. and Hoffmann, M.R., 1988. Reductive dissolution of iron(III) oxides by *Pseudomonas* sp. 200. *Biotechnol. Bioeng.*, **32**: 1081-96.
- Arnold, R.G., Olson, T.M. and Hoffmann, M.R., 1986. *Biotechnol. Bioeng.*, **28**: 1657-1671.
- Baes, C.F. and Mesmer, R.E., 1976. *The Hydrolysis of Cations*. Wiley, New York, 496 pp.
- Beliaev, A.S. and Saffarini, D.A., 1998. *Shewanella putrefaciens* mtrB encodes an outer membrane protein required for Fe(III) and Mn(IV) reduction. *J. Bacteriol.*, **180**: 6292-6297.
- Beliaev, A.S., Saffarini, D.A., McLaughlin, J.L. and Hunnicutt, D., 2001. MtrC, an outer membrane decahaem c cytochrome required for metal reduction in *Shewanella putrefaciens* MR-1. *Mol. Microbiol.*, **39**: 722-730.
- Biedermann, G. and Chow, J.T., 1966. Hydrolysis of metal ions. LVII. Hydrolysis of the Fe(III) ion and the solubility product of the $\text{Fe}(\text{OH})_{2.70}\text{Cl}_{0.30}$ in 0.5M $\text{Na}^+ \text{Cl}^-$ medium. *Acta Chem. Scand.*, **20**: 1376-1388.
- Byrne, R.H. and Kester, D.R., 1976. Solubility of hydrous ferric oxide and iron speciation in seawater. *Mar. Chem.*, **4**: 255-274.
- Caccavo, F., Jr., 1999. Protein-mediated adhesion of the dissimilatory Fe(III)-reducing bacterium *Shewanella alga* BrY to hydrous ferric oxide. *Appl. Environ. Microbiol.*, **65**: 5017-5022.
- Caccavo, F., Jr., Blakemore, R.P. and Lovley, D.R., 1992. A hydrogen-oxidizing, iron(III)-reducing microorganism from the Great Bay estuary, New Hampshire. *Appl. Environ. Microbiol.*, **58**: 3211-3216.
- DiChristina, T.J. and DeLong, E.F., 1994. Isolation of anaerobic respiratory mutants of *Shewanella putrefaciens* and genetic analysis of mutants deficient in anaerobic growth on Fe^{3+} . *J. Bacteriol.*, **176**: 1468-1474.
- DiChristina, T.J., Moore, C.M. and Haller, C.A., 2002. Dissimilatory Fe(III) and Mn(IV) reduction by *Shewanella putrefaciens* requires ferE, a homolog of the pulE (gspE) type II protein secretion gene. *J. Bacteriol.*, **184**: 142-151.
- Dousma, J. and De Bruyn, P.L., 1978. Hydrolysis-precipitation studies of iron solutions. II. Aging studies and the model for precipitation from iron(III) nitrate solutions. *J. Colloid Interface Sci.*, **64**: 154-170.
- Doyle, R.C., 1968. The origin of the ferrous ion-ferric oxide Nernst potential in environments containing dissolved ferrous iron. *Am. J. Sci.*, **266**: 840-859.
- Feitknecht, W. and Schindler, P.W., 1963. Löslichkeitskonstanten von Metalloxiden, -hydroxiden und hydroxidsalzen in wässrigen Lösungen. *Pure Appl. Chem.*, **6**: 125-199.
- Fox, L.E., 1988. The solubility of colloidal ferric hydroxide and its relevance to iron concentrations in river water. *Geochim. Cosmochim. Acta*, **52**: 771-777.
- Grenthe, I., Stumm, W., Laaksuharju, M., Nilsson, A.C. and Wikberg, P., 1992. Redox potentials and redox reactions in deep groundwater systems. *Chem. Geol.*, **98**: 131-50.
- Henderson, P.J.F., 1992. Statistical analysis of enzyme kinetic data. In: R. Eisenthal and M.J. Danson (Editors), *Enzyme Assays*. IRL, Oxford, UK, pp. 277-316.
- Hobbie, J.E., Daley, R.J. and Jasper, S., 1977. Use of nuclepore filters for counting bacteria by fluorescence microscopy. *Appl. Environ. Microbiol.*, **33**: 1225-8.
- Jackson, R.E. and Patterson, R.J., 1982. Interpretation of pH and Eh trends in a fluvial-sand aquifer system. *Water Resour. Res.*, **18**: 1255-68.
- Kaksonen, A.H., Franzmann, P.D. and Puhakka, J.A., 2003. Performance and ethanol oxidation kinetics of a sulfate-reducing fluidized-bed reactor treating acidic metal-containing wastewater. *Biodegradation*, **14**: 207-217.
- Kuma, K., Suzuki, Y. and Matsunaga, K., 1993. Solubility and dissolution rate of colloidal g-iron oxyhydroxide in seawater. *Wat. Res.*, **27**: 651-657.
- Laidler, K.J., 1987. *Chemical Kinetics*. Harper and Rows Publishers, New-York, 490 pp.
- Langmuir, D. and Whittemore, D.O., 1971. Variations in the stability of precipitated ferric oxyhydroxides. *Advan. Chem. Ser.*, **106**: 209-234.
- Larsen, O. and Postma, D., 2001. Kinetics of reductive bulk dissolution of lepidocrocite, ferrihydrite and goethite. *Geochim. Cosmochim. Acta*, **65**: 1367-1379.
- Liger, E., Charlet, L. and Van Cappellen, P., 1999. Surface catalysis of uranium (VI) reduction by iron(II). *Geochim. Cosmochim. Acta*, **63**: 2939-2955.
- Liu, C., Gorby, Y.A., Zachara, J.M., Fredrickson, J.K. and Brown, C.F., 2002. Reduction kinetics of Fe(III), Co(III), U(VI), Cr(VI), and Tc(VII) in cultures of dissimilatory metal-reducing bacteria. *Biotechnol. Bioengin.*, **80**: 637-649.

- Liu, C., Kota, S., Zachara, J.M., Fredrickson, J.K. and Brinkman, C.K., 2001. Kinetic analysis of the bacterial reduction of goethite. *Environ. Sci. Technol.*, **35**: 2482-2490.
- Liu, C. and Zachara, J.M., 2001. Uncertainties of Monod Kinetic Parameters Nonlinearly Estimated from Batch Experiments. *Environ. Sci. Technol.*, **35**: 133-141.
- Lovley, D.R., 1987. Organic matter mineralization with the reduction of ferric iron: a review. *Geomicrobiol. J.*, **5**: 375-399.
- Lovley, D.R., 1995. Bioremediation of organic and metal contaminants with dissimilatory metal reduction. *J. Ind. Microbiol.*, **14**: 85-93.
- Macalady, D.L., Langmuir, D., Grundl, T. and Elzerman, A., 1990. Use of model-generated Fe³⁺ ion activities to compute Eh and ferric oxyhydroxide solubilities in anaerobic systems. *ACS Symposium Series*, **416**: 350-367.
- Martin-Nieto, J., Flores, E. and Herrero, A., 1992. Biphasic kinetic behavior of nitrate reductase from heterocystous, nitrogen-fixing cyanobacteria. *Plant Physiol.*, **100**: 157-163.
- McCormick, M.L., Bouwer, E.J. and Adriaens, P., 2002. Carbon tetrachloride transformation in a model iron-reducing culture: relative kinetics of biotic and abiotic reactions. *Environ. Sci. Technol.*, **36**: 403-410.
- McNab, W.W. and Narasimhan, T.N., 1994. Modeling reactive transport of organic compounds in groundwater using a partial redox disequilibrium approach. *Water Resources Res.*, **30**: 2619-2635.
- Murphy, P.J., Posner, A.M. and Quirk, J.P., 1976. Characterization of hydrolyzed ferric ion solutions. A comparison of the effects of various anions on the solutions. *J. Colloid Interface Sci.*, **56**: 312-319.
- Postma, D., 1993. The reactivity of iron oxides in sediments: a kinetic approach. *Geochim. Cosmochim. Acta*, **57**: 5027-5034.
- Power, G.P. and Ritchie, I.M., 1983. Mixed potentials: experimental illustrations of an important concept in practical electrochemistry. *J. Chem. Ed.*, **60**: 1022-1026.
- Roden, E.E., 2003. Fe(III) Oxide reactivity toward biological versus chemical reduction. *Environ. Sci. Technol.*, **37**: 1319-1324.
- Roden, E.E. and Edmonds, J.W., 1997. Phosphate mobilization in iron-rich anaerobic sediments. Microbial Fe(III) oxide reduction versus iron-sulfide formation. *Arch. Hydrobiol.*, **139**: 347-378.
- Roden, E.E., Urrutia, M.M. and Mann, C.J., 2000. Bacterial reductive dissolution of crystalline Fe(III) oxide in continuous-flow column reactors. *Appl. Environ. Microbiol.*, **66**: 1062-1065.
- Roden, E.E. and Wetzel, R.G., 2002. Kinetics of microbial Fe(III) oxide reduction in freshwater wetland sediments. *Limnol. Oceanogr.*, **47**: 198-211.
- Roden, E.E. and Zachara, J.M., 1996. Microbial reduction of crystalline iron(III) oxides: Influence of oxide surface area and potential for cell growth. *Environ. Sci. Technol.*, **30**: 1618-1628.
- Schindler, P.W., 1963. Die Bestimmung der Löslichkeitkonstanten von Metalloxiden und -hydroxiden. *Chimia*, **17**: 313-330.
- Schwertmann, U. and Cornell, R.M., 1991. *Iron Oxides in the Laboratory: Preparation and Characterization*. VCH, Weinheim, 137 pp.
- Segel, I.H., 1975. *Enzyme Kinetics: Behavior and Analysis of Rapid Equilibrium and Steady-State Enzyme Systems*. John Wiley, New-York, 957 pp.
- Spiro, T.G. et al., 1966. The hydrolytic polymerization of iron(III). *J. Amer. Chem. Soc.*, **88**: 2721-2726.
- Stumm, W. and Morgan, J.J., 1995. *Aquatic Chemistry: Chemical Equilibria and Rates in Natural Waters*; Third Edition. Wiley, New York, 1022 pp.
- Suter, D., Banwart, S. and Stumm, W., 1991. Dissolution of hydrous iron(III) oxides by reductive mechanisms. *Langmuir*, **7**: 809-813.
- Tardy, Y. and Nahon, D., 1985. Geochemistry of laterites, stability of Al-goethite, Al-hematite, and Fe³⁺-kaolinite in bauxites and ferricretes: an approach to the mechanism of concretion formation. *Am. J. Sci.*, **285**: 865-903.
- Ulrich, G.A., Breit, G.N., Cozzarelli, I.M. and Suflita, J.M., 2003. Sources of sulfate supporting anaerobic metabolism in a contaminated aquifer. *Environ. Sci. Technol.*, **37**: 1093-1099.
- Urrutia, M.M., Roden, E.E., Fredrickson, J.K. and Zachara, J.M., 1998. Microbial and surface chemistry controls on reduction of synthetic Fe(III) oxide minerals by the dissimilatory iron-reducing bacterium *Shewanella alga*. *Geomicrobiol. J.*, **15**: 269-291.
- Van Cappellen, P., Gaillard, J.-F. and Rabouille, C., 1993. Biogeochemical transformations in sediments: kinetic models of early diagenesis. In: R. Wollast, F.T. Mackenzie and L. Chou (Editors), *Interactions of C, N, P and S Biogeochemical Cycles and Global Change*. Springer, Berlin, pp. 401-455.
- Van Cappellen, P. and Wang, Y., 1996. Cycling of iron and manganese in surface sediments: a general theory for the coupled transport and reaction of carbon, oxygen, nitrogen, sulfur, iron, and manganese. *Am. J. Sci.*, **296**: 197-243.

- Van Schuilenborgh, J., 1973. Sesquioxide formation and transformation. In: E. Schlichting, U. Schwertmann (Editors), Pseudogleys and Gley. VCH, Weinheim, pp. 91-102.
- Viollier, E., Inglett, P.W., Hunter, K., Roychoudhury, A.N. and Van Cappellen, P., 2000. The ferrozine method revisited: Fe(II)/Fe(III) determination in natural waters. *Appl. Geochem.*, 15: 785-790.
- Vlek, P.L.G., Blom, T.J.M., Beek, J. and Lindsay, W.L., 1974. Determination of the solubility product of various iron hydroxides and jarosite by the chelation method. *Soil Sci. Soc. Am. Proc.*, 38: 429-432.
- Wehrli, B., Sulzberger, B. and Stumm, W., 1989. Redox processes catalyzed by hydrous oxide surfaces. *Chem. Geol.*, 78: 167-179.
- Whitfield, M., 1974. Thermodynamic limitations on the use of the platinum electrode in Eh measurements. *Limnol. Oceanogr.*, 19: 857-865.
- Wollast, R., 1974. Silica problem. In: M.N. Hill, A.E. Maxwell and E.D. Goldberg (Editors), *The Sea*. Wiley, New-York, pp. 5359-5392

Chapter III

Microbial reduction of Fe(III) oxyhydroxide colloids: a kinetic model

Steeve Bonneville, Thilo Behrends, Hyacinthe Christelle, Wilfred Röling and Philippe Van Cappellen

Submitted to *Geochimica Cosmochimica Acta*

Abstract

A kinetic model for the microbial reduction of Fe(III) oxyhydroxide colloids in the presence of excess electron donor is presented. The model assumes a two-step mechanism: (1) attachment of Fe(III) colloids to the cell surface, and (2) reduction of Fe(III) centers at the surface of attached colloids. The validity of the model is tested using *Shewanella putrefaciens* and nanohematite as model dissimilatory iron reducing bacteria and Fe(III) colloidal particles, respectively. Iron reduction rates are shown to correlate linearly with the relative coverage of the cell surface by nanohematite particles, hence supporting a direct electron transfer from membrane bound reductases to mineral particles attached to the cells. Using internally consistent parameter values for the maximum attachment capacity of Fe(III) colloids to the cells, M_{max} , the attachment constant, K_p , and the first-order Fe(III) reduction rate constant, k , the model reproduces the reduction rates of a variety of fine-grained Fe(III) oxyhydroxides by *S. putrefaciens*. The model explains the observed dependency of the Fe(III) half saturation constant, K_m^* , on the solid to cell ratio, and it predicts that iron reduction rates exhibit saturation with respect to both the cell density and the abundance of the Fe(III) oxyhydroxide substrate.

3.1 Introduction

The dissimilatory reduction of ferric iron is an important geomicrobial process in soils, sediments, aquifers and stratified water bodies, where it relies primarily on Fe(III) oxyhydroxide minerals as terminal electron acceptors (Albrechtsen and Christensen, 1994; Canfield, 1988; Taillefert et al., 2000). In addition to being an important oxidation pathway of organic matter under suboxic conditions and generating soluble ferrous iron, microbial iron reduction can have a major impact on the persistence and mobility of metals, radionuclides, and organic contaminants (Anderson and Lovley, 1999; Cummings et al., 1999; Lovley and Coates, 1997; Lovley et al., 1993; McCormick et al., 2002; Zachara et al., 2001). A particular challenge facing iron reducing microorganisms is the very low solubility of Fe(III) oxyhydroxides under near-neutral pH conditions. The simplest strategy to overcome this limitation is for the microorganisms to associate directly with the mineral surfaces (Arnold et al., 1988; Caccavo, 1999; Caccavo and Das, 2002). In the absence of direct cell-mineral contact, soluble electron shuttles or chelating agents are needed to transfer electrons from membrane-bound electron transport proteins to Fe(III) (Kappler et al., 2004).

In a recent study, we showed that the initial reduction kinetics of a variety of Fe(III) oxyhydroxides by the iron reducing bacterium *Shewanella putrefaciens* systematically exhibit saturation with respect to the Fe(III) substrate availability (Bonneville et al., 2004). The observed parabolic dependence of the Fe(III) reduction rate on the mineral concentration could be fitted with the Michaelis-Menten rate equation, yielding a maximum reduction rate per cell, v_{\max} , and an apparent half-saturation constant, K_m^* . The value of v_{\max} was found to be characteristic of the oxyhydroxide mineral undergoing reduction, generally increasing with increasing mineral solubility (Bonneville et al., 2004).

Our previous experimental results, and evidence from other studies (Caccavo and Das, 2002; Das and Caccavo, 2000), indicate that the reduction kinetics of iron oxyhydroxides by *S. putrefaciens* occurs predominantly via the transfer of electrons to Fe(III) centers at the cell-mineral interface. When the cell surface is saturated by the solid-state Fe(III) substrate, the iron reducing activity of *S. putrefaciens* reaches its maximum value, v_{\max} . Further increasing the concentration of the Fe(III) substrate then no longer has an effect on the rate of iron reduction. This saturation behavior is captured by the Michaelis-Menten rate equation.

The usual form of the Michaelis-Menten rate equation for enzymatic reactions assumes that the enzyme concentration is small. The amount of substrate associated with the enzyme can then be neglected, and the bulk and “free” concentrations of the substrate are identical. For a dissolved substrate, this simplification is usually adequate, and the half-saturation constant is uniquely defined when expressed in

terms of bulk substrate concentration units. Its value provides a direct measure of the affinity of the enzyme to combine chemically with the substrate.

The reduction of Fe(III) oxyhydroxide minerals by *S. putrefaciens* presents a more complex situation, however. The Fe(III) centers that can undergo reduction are located in the contact region between cell and mineral. The direct Fe(III) substrate therefore only represents a fraction of the bulk Fe(III) in the system. Furthermore, under typical experimental conditions, the approximation that the amount of Fe(III) associated with cells is negligible, compared to the total amount of Fe(III), may not be valid. As a result, K_m^* values expressed in units of bulk concentration of the Fe(III) substrate (e.g., in moles of Fe(III) per unit volume suspension) are conditional, rather than intrinsic, kinetic parameters. For instance, in our earlier study, K_m^* values were shown to depend on the solid-to-cell ratio of the experimental suspensions (Bonneville et al., 2004).

The present study explicitly links the association of mineral particles and iron reducing microorganisms to the rate of dissimilatory iron reduction, using suspensions of *Shewanella putrefaciens* and nanoparticulate hematite as model experimental system. Iron reduction rates measured in the presence of excess electron donor are related to the relative coverage of the cells by the iron colloids. Based on the results, a kinetic model for the microbial reduction of nanohematite is developed, which takes into account the abundance and size of the mineral particles. The predictive capability of the model is tested by extending it to a number of other colloidal Fe(III) oxyhydroxides.

3.2 Materials and Experimental Methods

3.2.1 Fe(III) oxyhydroxides

Hematite nanoparticles were prepared by adding 100 mL of a 0.1 M $\text{Fe}(\text{NO}_3)_3$ solution at a flow rate of 3 mL min^{-1} to 1 L of boiling and vigorously stirred demineralized water (Liger, 1996). After allowing the hematite suspension to cool down to room temperature, it was dialyzed in demineralized water adjusted to pH 4 with 0.5 M HCl, in order to remove the nitrate counter ions. Thereafter, the mineral suspension was filtered successively through $0.45 \mu\text{m}$ and $0.2 \mu\text{m}$ poresize filters (Millipore). The average grain size of the hematite nanoparticles, measured using electron transmission microscopy (TEM), was $8 \text{ nm} (\pm 2 \text{ nm})$. X-ray diffraction and ^{57}Fe Mossbauer spectroscopy analyses revealed highly crystalline hematite, with trace amounts of ferrihydrite (Dr. D. Rancourt, University of Ottawa, personal communication). A surface site density of 2.07 sites per nm^2 and a pH of zero net proton charge of 8.15 were derived from acid-base titrations (Liger et al., 1999).

Amorphous ferric oxide (HFO) and ferrihydrite 6 lines were prepared following the procedures described in (Bonneville et al., 2004). Lepidocrocite (Bayferrox 943) and low surface area (LSA) hematite (Bayferrox 105M) were purchased from Harold Scholz & Co., GmbH, and used as received. The grain size and shape (obtained using TEM), and the specific surface area (measured by N₂BET) of the different Fe(III) oxyhydroxides are listed in Table 3.1.

Table 3.1. Properties of the Fe(III) oxyhydroxides considered in this study.

Iron oxyhydroxide	Dimensions (nm)	Shape	Surface area (m ² g ⁻¹)	v_{\max}^1 (10 ⁻¹¹ μmol h ⁻¹ cell ⁻¹)
Nanohematite	8	sphere	125	2.4
6-line ferrihydrite	8	sphere	175	8.1
LSA ² hematite	90	sphere	12	0.27
Lepidocrocite	50×300	needle	83	2.0
HFO ³	1.3	sphere	600	6.5

¹Maximum cell-normalized iron reduction rate by *S. putrefaciens* in the presence of excess lactate (from Bonneville et al., 2004); ²LSA = Low Surface Area; ³HFO = Hydrous Ferric Oxide.

3.2.2 Bacteria

Cultures of *Shewanella putrefaciens* 200 R were provided by Dr. T. DiChristina, Georgia Institute of Technology (DiChristina and DeLong, 1994; DiChristina et al., 2002). Cells were kept aerobically on Luria Bertani (LB) medium plates (Tryptone water 15 g L⁻¹, agar 15 g L⁻¹, NaCl 5 g L⁻¹, yeast 5 g L⁻¹) and routinely cultured in liquid LB medium on a rotary shaker (150 rpm) at room temperature. The bacteria were harvested in the late exponential-early stationary growth phase. The cells were washed with 10 mM NaCl solution, followed by centrifugation (6800 g) and resuspension. The washing procedure was repeated three times. After the last centrifugation step, cells were concentrated in 50 mL of 10 mM NaCl solution. The bacteria were harvested and washed just before being used in the experiments.

Cell numbers were determined by epifluorescence microscopy after acridine orange staining (Hobbie et al., 1977): 100 μL of bacterial suspension were mixed with 4.4 mL of phosphate buffer solution (8 g L⁻¹ NaCl, 2 g L⁻¹ KCl, 1.44 g L⁻¹ Na₂HPO₄, 0.24 g L⁻¹ KH₂PO₄), 200 μL of a 0.25 g L⁻¹ acridine orange solution and 0.5 mL of a 30% formaldehyde solution. After 10 min, 100-200 μL of the suspension was transferred to a 17 mm diameter filter tower to which 5 mL phosphate buffer solution and 200 μL of acridine orange solution were added in advance. The content of the tower

was mixed by swirling and then filtrated through a black 0.2 μm polycarbonate filter (Millipore). An epifluorescence microscope equipped with a camera was used to take five pictures of each filter. The counting of the cells was performed automatically using imaging software.

3.2.3 Microbial attachment and reduction of nanohematite

Attachment of nanohematite particles to *S. putrefaciens* cells was measured under aerobic conditions and in the absence of electron donor. The experiments were performed in 5 mM NaCl solutions, whose pH was adjusted to 5 using HCl. Preliminary tests showed that under these conditions the nanohematite particles formed a stable colloidal suspension. The absence of aggregation was a prerequisite for separating nanohematite particles attached to bacteria from those remaining as free colloids.

Concentrated cell suspensions of *S. putrefaciens* were added to nanohematite suspensions giving a final volume of 50 mL. The experiments were performed at three cell densities (3.0×10^8 , 1.0×10^9 and 1.25×10^9 cells mL^{-1}), while the nanohematite concentration was varied from 25 to 2820 $\mu\text{mol Fe(III) L}^{-1}$. After 4 hours of continuous agitation on a horizontal shaker, aliquots of the suspensions were centrifuged at 900 g for 40 minutes. In preliminary experiments, this centrifugation procedure was shown to quantitatively pelletize the bacterial cells (>97% recovery), while avoiding sedimentation of free nanohematite particles (<9% loss). In a limited number of cases, aliquots of cell-mineral suspensions were periodically sampled over the duration of an experiment, in order to follow the time-dependent attachment of nanohematite colloids to the cells.

Total Fe(III) concentrations were determined on the aliquots, before and after centrifugation: 750 μL of suspension was mixed with 250 μL of 2 M HCl and kept at 60°C overnight in order to completely dissolve the nanohematite. Hydroxylamine hydrochloride solution (1.4 M in 2 M HCl) was then added to reduce Fe(III) to Fe(II), followed by the determination of total iron concentration by ferrozine essay (Viollier et al., 2000). The amount of hematite attached to the bacteria was calculated from the difference between the iron concentrations measured before and after centrifugation.

The attachment experiments were directly followed by microbial Fe(III) reduction experiments. After centrifugation, the suspension of free nanohematite colloids overlying the pellet was decanted. The pellet, containing the bacterial cells with attached nanohematite, was resuspended in a medium of 10 mM lactate, 5.6 mM KCl, 14 mM Na_2SO_4 , 20 mM NH_4Cl , 1.2 mM $\text{CaCl}_2 \cdot 6\text{H}_2\text{O}$, 1 mM MgSO_4 and 10 mM Hepes buffer. The medium pH was adjusted to 7. The incubation experiments were performed in 100 mL septum bottles, under anaerobic conditions at room temperature (22 °C). The bottles

were kept on a rotary shaker and sampled regularly during 250 hours. Concentrated HCl was added to the samples, to a final concentration of 0.5 M HCl. After 1 hour, the total Fe(II) concentration was measured, following the method of (Viollier et al., 2000). The measured total Fe(II) concentration includes dissolved Fe(II) as well as Fe(II) sorbed to the nanohematite or the bacterial cell walls.

3.2.4 Detachment experiments

The reversibility of nanohematite attachment to cells of *S. putrefaciens* was tested in three sets of seven experiments. Each experimental set was carried out with a different concentration of nanohematite particles, 2044, 1089 and 102 μM Fe(III) nanohematite, exposed to a bacterial density of 2.8×10^8 cells mL^{-1} . Attachment of nanohematite to the bacteria followed the procedure described in section 2.3. After centrifugation, pellets containing bacteria and attached nanohematite were resuspended under aerobic conditions in 5 mM NaCl solution, at seven different pH values: 5, 5.5, 6, 6.5, 7, 8, 9. No electron donor was added to the experimental media. The bottles were kept on a shaking table under aerobic conditions; samples were collected 10 minutes and 24 hours after resuspending the bacteria. The samples were filtered through 0.2 mm pore size filters to retain bacterial cells and attached nanohematite particles. Total Fe(III) concentrations in the filtrate solution were measured as described in section 2.3. The amount of nanohematite detached from the cells was calculated as the difference between the initial amounts of hematite attached at pH 5 and that remaining after 24 hours of resuspension in 5 mM NaCl solution at variable pH.

3.3 Experimental Results

3.3.1 Nanohematite attachment to *S. putrefaciens*

The results of the 25 individual attachment experiments are summarized in Figure 3.1. At low mineral to cell ratios ($< 5 \times 10^{-10}$ $\mu\text{mol Fe(III) cell}^{-1}$), on the order of 90% of the added nanohematite was associated with the bacteria. With increasing mineral loading, the cell-normalized amount of attached nanohematite ultimately reached a maximum value. The observed saturation of the cells with nanohematite could be fitted to a Langmuir isotherm (Figure 3.1), with an attachment constant, K_p , of 2.0×10^{-2} L μmol^{-1} Fe(III) and a maximum attachment capacity on the cells, M_{max} , of 1.1×10^{-9} $\mu\text{mol Fe(III) cell}^{-1}$.

The attachment kinetics were fast, with little change in cell-bound nanohematite concentration beyond the first 10 minutes after adding cells to the colloidal suspensions (results not shown). Furthermore, in all of the 21 detachment experiments, less than 10% of cell-bound nanohematite was released in the course of 24 hours, irrespective of the medium pH (pH range 5-9, results not shown). Henceforth, it

was assumed that nanohematite colloids attached to the cells at pH 5 remained cell-bound during the subsequent reduction experiments at pH 7.

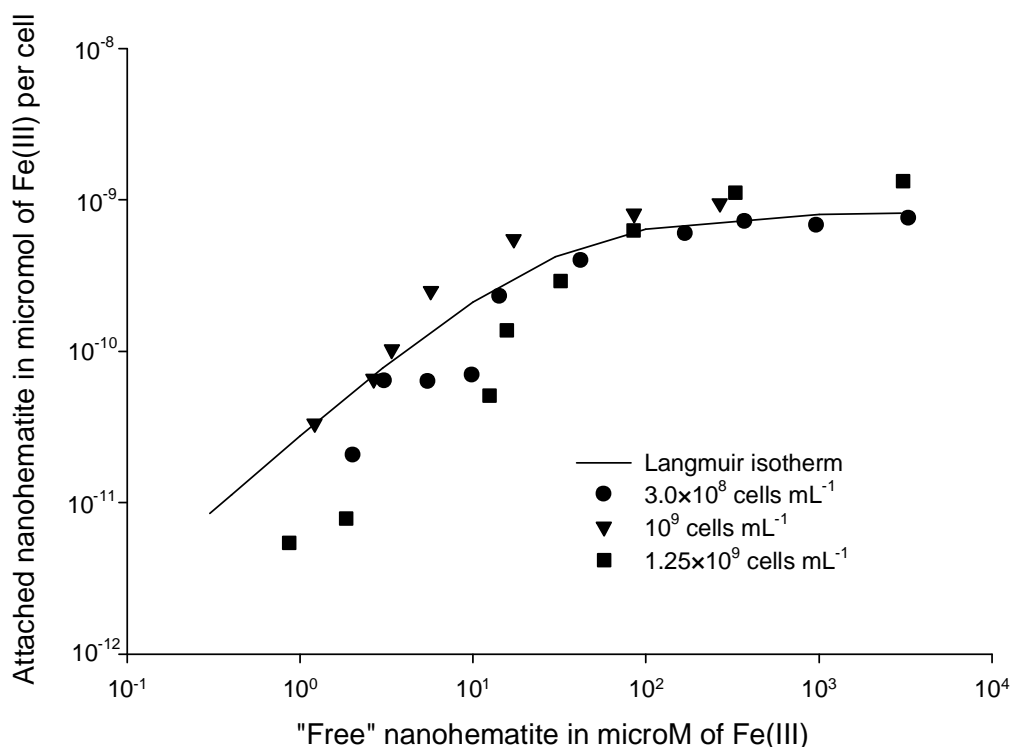


Figure 3.1: Attachment of nanohematite to *S. putrefaciens* 200R, upon exposure of three bacterial densities (3.0×10^8 , 1.0×10^9 , 1.25×10^9 cells mL^{-1}) to a range of total nanohematite concentrations (from 25 to 2820 $\mu\text{mol Fe(III) L}^{-1}$) in 5 mM NaCl, at pH 5. The horizontal axis corresponds to the concentration of nanohematite particles that do not attach to the cells. The solid line is the best-fit Langmuir isotherm to the entire data set.

3.3.2 Nanohematite reduction by *S. putrefaciens*

Upon resuspension of cells with attached nanohematite in lactate containing pH 7 medium, Fe(II) started building up after a lag time on the order of 24 hours. The Fe(II) concentration first increased near-linearly for about 100 hours followed by a progressive slowing down of the rate of Fe(II) build-up (not shown). Microbial Fe(III) reduction exhibited a first-order dependence on the amount of cell-bound nanohematite, as shown by the log-linear plot in Figure 3.2a. In this plot, time zero corresponds to the beginning of the observed build-up of Fe(II), that is, ignoring the initial lag time. Linear regression of the data points on the log-linear plot yielded a first-order rate constant of $3.9 \times 10^{-3} \text{ h}^{-1}$ for the reduction of nanohematite by *S. putrefaciens*. Figure 3.2b further illustrates the linear dependence of the initial, cell normalized Fe(III) reduction rate on the initial amount of attached nanohematite. The initial rates were calculated from the build-up of Fe(II) during the first 100 hours following the lag time.

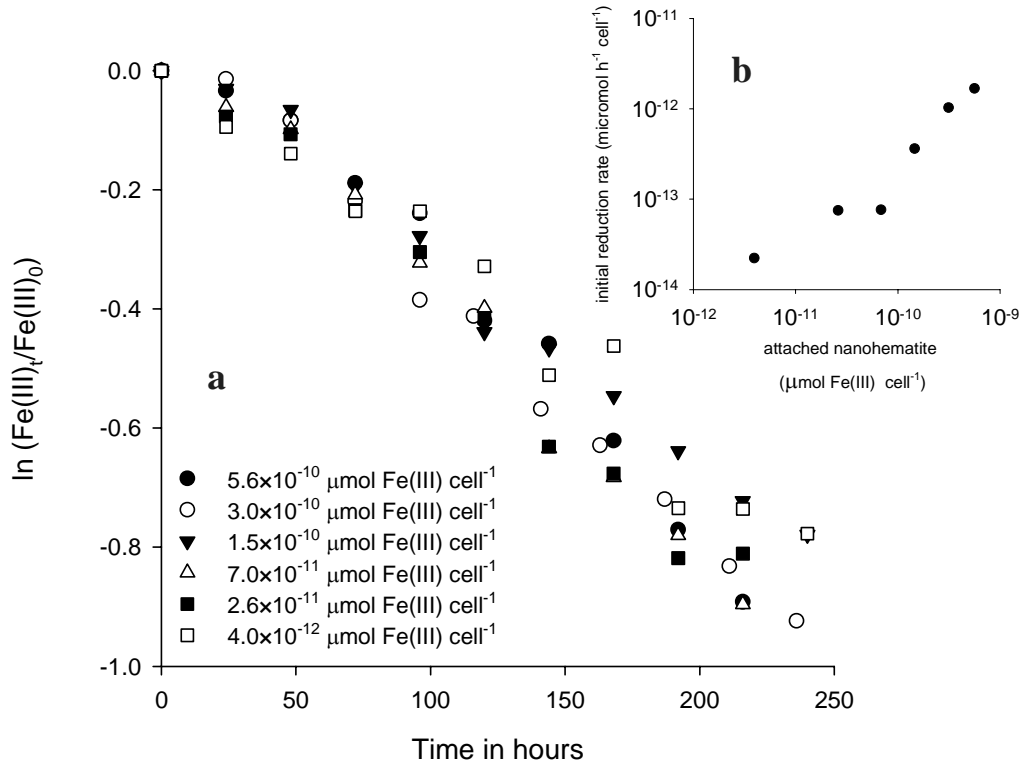


Figure 3.2: Iron reduction kinetics by *S. putrefaciens* as a function of the attached nano hematite concentration. (a) Log-linear plot showing first order rate dependency on the concentration of cell-bound nano hematite, $\text{Fe(III)}_t/\text{Fe(III)}_0$ is the fraction of attached nano hematite remaining at time t . (b) Linear dependency of the initial iron reduction rate on the initial mass of cell-bound nano hematite. See text for complete description and discussion of the experiments.

3.4 Kinetic Model of Microbial Reduction of Fe(III) Colloids

The conceptual model for the reduction of Fe(III) colloids by *S. putrefaciens* is illustrated in Figure 3.3. Reduction is assumed to occur via transfer of electrons from membrane-bound reductases to nearby Fe(III) centers at the surface of attached Fe(III) colloids. Far-field Fe(III) reduction, involving soluble electron shuttles, is not considered in the model. Therefore, the total reduction rate should reflect the abundance of Fe(III) colloids directly bound to the bacterial cells.

Based on the results presented in Figure 3.1 for nano hematite, the model assumes that the partitioning of Fe(III) colloids to initially mineral-free cells of *S. putrefaciens* can formally be represented by a Langmuir isotherm:

$$\theta_B = \frac{[\text{Fe}_{\text{cell}}^{\text{III}}]}{BM_{\text{max}}} = \frac{K_P[\text{Fe}_{\text{free}}^{\text{III}}]}{1 + K_P[\text{Fe}_{\text{free}}^{\text{III}}]} \quad (3.1)$$

where θ_B represents the relative coverage of the cells by the colloids, $[\text{Fe}_{\text{free}}^{\text{III}}]$ is the concentration of “free” colloidal particles, that is, particles not attached to cells, $[\text{Fe}_{\text{cell}}^{\text{III}}]$ is the concentration of

colloids attached directly to the cells, M_{max} is the maximum attachment capacity per cell, B is the bacterial density per unit volume suspension, and K_p is the attachment constant.

Assuming a homogenous distribution of reductase sites at the cell surface, plus a uniform size of the iron colloids, the number of reaction centers for electron transfer should be proportional to the relative coverage of the cells, θ_B . The initial Fe(III) reduction rate is then given by:

$$R = -\frac{d[\text{Fe}_{\text{tot}}^{\text{III}}]}{dt} = k B M_{\text{max}} \theta_B = \frac{k B M_{\text{max}} [\text{Fe}_{\text{free}}^{\text{III}}]}{\frac{1}{K_p} + [\text{Fe}_{\text{free}}^{\text{III}}]} \quad (3.2)$$

where k is a first-order reduction rate constant, and $[\text{Fe}_{\text{tot}}^{\text{III}}]$ is the total (initial) concentration of Fe(III) colloids in units of mass Fe(III) per unit volume total suspension. According to equation (3.2), the maximum cell-normalized iron reduction rate, v_{max} , is:

$$v_{\text{max}} = k M_{\text{max}} \quad (3.3)$$

Combining equations (3.2) and (3.3), and defining the reciprocal value of K_p as K_m , results in:

$$R = \frac{B v_{\text{max}} [\text{Fe}_{\text{free}}^{\text{III}}]}{K_m + [\text{Fe}_{\text{free}}^{\text{III}}]} \quad (3.4)$$

Equation (3.4) is formally identical to the Michaelis-Menten rate equation, with $[\text{Fe}_{\text{free}}^{\text{III}}]$ as the substrate concentration. Direct application of equation (3.4) to data sets on microbial Fe(III) reduction, however, is hindered by the fact that usually the total, rather than the “free”, concentration of the Fe(III) substrate is known (for examples, see, Roden and Zachara, 1996; Bonneville et al., 2004). Furthermore, it may not be appropriate to approximate the concentration of free Fe(III) colloids by the total Fe(III) concentration. For instance, in the case of nanohematite, at low mineral-to-cell ratios, the majority of particles are attached to the cells (Figure 3.1). Under these circumstances, $[\text{Fe}_{\text{free}}^{\text{III}}]$ represents only a small fraction of $[\text{Fe}_{\text{tot}}^{\text{III}}]$.

In systems where the partitioning of Fe(III) colloids can be described by equation (3.1), incorporation of the mass balance for ferric iron ($[\text{Fe}_{\text{tot}}^{\text{III}}] = [\text{Fe}_{\text{free}}^{\text{III}}] + [\text{Fe}_{\text{cell}}^{\text{III}}]$) into equation (3.1) yields a quadratic equation in $[\text{Fe}_{\text{free}}^{\text{III}}]$. Combining the solution to the quadratic equation with equation (3.4), we then obtain:

$$R = k \frac{1 + A + C - \sqrt{1 + A(2 + A - 2C) + 2C(1 + C)}}{2K_p} \quad (3.5)$$

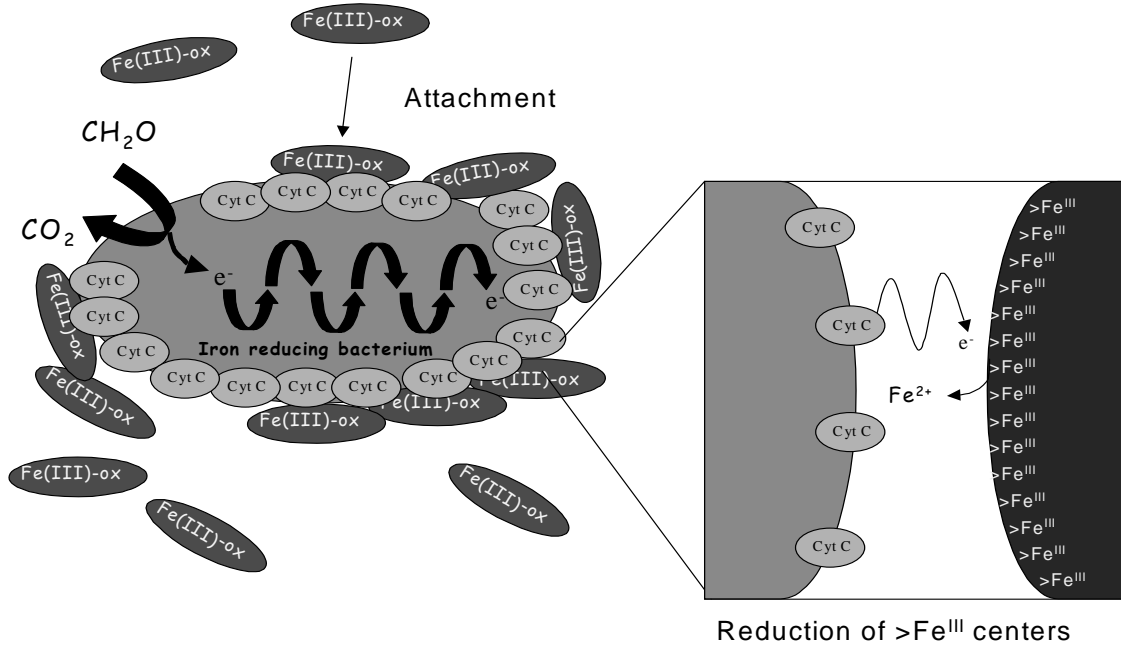


Figure 3.3 Conceptual model of the microbial reduction of Fe(III) colloids. The reduction process consists of two consecutive steps: (1) attachment of the Fe(III) colloids to the iron reducing microorganism, and (2) reduction of Fe(III) centers at the surface of attached colloids by electron transfer from membrane-bound Fe(III) reductases.

where $A = K_p [\text{Fe}_{\text{tot}}^{\text{III}}]$ and $C = M_{\text{max}} B K_p$. In rate equation (3.5), the initial reduction rate is expressed as a function of the total initial concentration of Fe(III) colloids, $[\text{Fe}_{\text{tot}}^{\text{III}}]$, and the cell density, B . The equation contains three adjustable parameters, k , K_p and M_{max} , which are specific for the Fe(III) colloid-microbe system under consideration.

Assuming that only the Fe(III) centers in direct contact with the cell membrane are susceptible of being reduced, the maximum capacity, M_{max} , in rate equation (3.5) should reflect the size of the Fe(III) colloids, relative to that of the cells (Figure 3.4). For colloids that are much smaller than the cells (as in the case of nanohematite), a simple geometrical estimate of M_{max} can be calculated as:

$$M_{\text{max}} = \frac{n_{\text{Fe}} V_p \rho}{M_p} \times \frac{A_B}{A_p} \quad (3.6)$$

where A_B is the surface area of the cell, while A_p is the projected surface area of a mineral particle onto the cell (Figure 3.4a); V_p , ρ , M_p , are the volume, density and molar mass of the Fe(III) colloids, and n_{Fe} is the number of iron atoms in the stoichiometric formula of the Fe(III) oxyhydroxide mineral. Figure 3.4a illustrates how an order-of-magnitude estimate of M_{max} can be derived for spherical colloids, assuming a simple, two-dimensional cubic surface packing of the colloids.

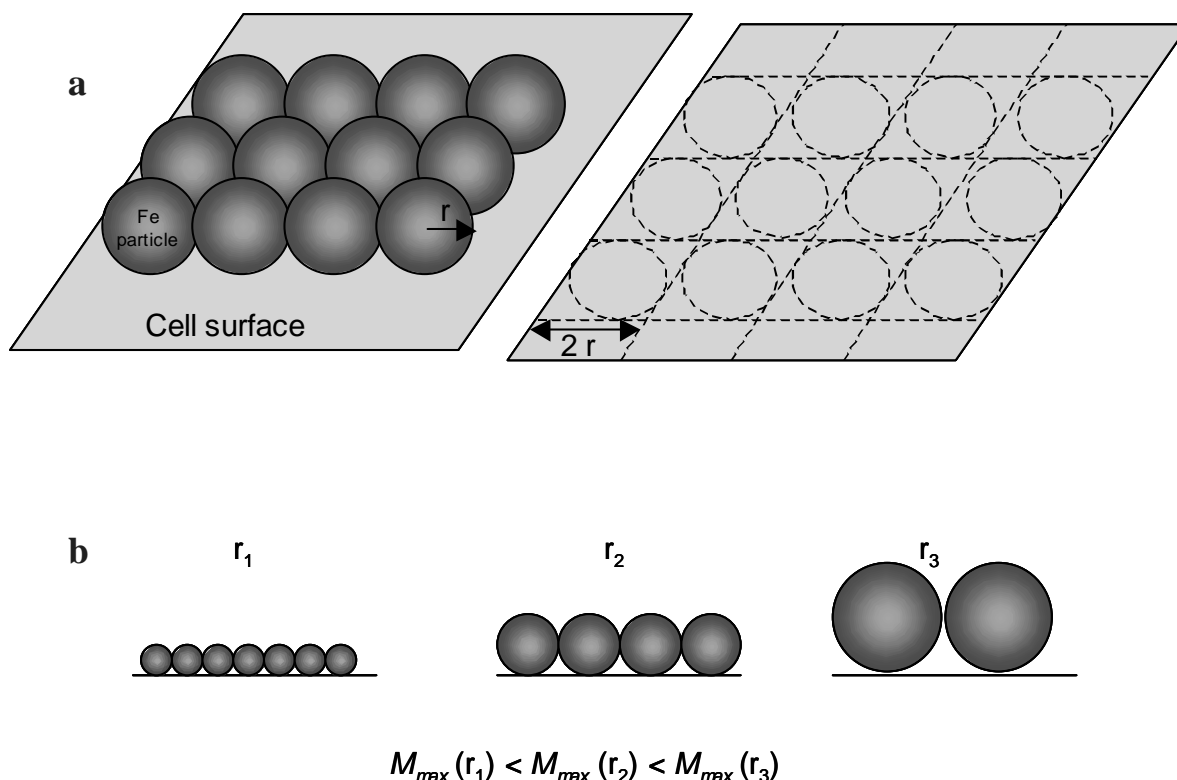


Figure 3.4 (a) Geometric estimation of the maximum mass of Fe(III) colloids, M_{max} , that can bind directly to the cell surface, assuming a cubic packing of the colloids. (b) Particle size dependency of M_{max} .

It is important to note that the above rate model applies to the initial stage of reduction, when the amount of Fe(III) reduced is negligible compared to the total amount of Fe(III) initially present. Upon desorption of a reduced Fe(II) ion from the surface of a cell-bound Fe(III) colloid, an underlying Fe(III) center is exposed, which, in turn, becomes available for reduction. This recycling mechanism ensures that the concentration of Fe(III) centers at the bacterium-mineral interface remains initially constant, justifying the steady-state assumption for $[\text{Fe}_{\text{free}}^{\text{III}}]$ implied in the derivation of the rate law.

3.5 Discussion

3.5.1 Nanohematite attachment to *S. putrefaciens*

The kinetic model presented in section 3.4, couples the iron reduction rate to the relative coverage of the iron reducing bacteria by Fe(III) colloids. In particular, the assumption that attachment of the colloids to the cells follows a Langmuir isotherm (equation 3.1) implies that the half-saturation constant, K_m , appearing in rate equation (3.4) equals the reciprocal of the attachment constant, K_p , of the isotherm. Furthermore, the iron reduction rate approaches its maximum value when the cells approach monolayer coverage by Fe(III) colloids.

The Langmuir isotherm provides an adequate macroscopic description of the attachment of nano hematite to *S. putrefaciens* at pH 5 (Figure 3.1). A progressive increase in cell coverage by nano hematite with increasing mineral loading is also apparent in electron micrographs of cells exposed to variable nano hematite concentrations (Figure 3.5). As can be seen, for very high nano hematite to cell ratios, the cells become surrounded by a near-continuous layer of attached Fe(III) colloids (Figure 3.5a).

Furthermore, the maximum attachment capacity, M_{max} , measured in the attachment experiments at pH 5 (Figure 3.1; $M_{max} = 1.1 \times 10^{-9} \mu\text{mol Fe(III) cell}^{-1}$) is in good agreement with the value inferred from the relative sizes of the cells and Fe(III) colloids. A geometric surface area for *S. putrefaciens* of $8.3 \pm 2.1 \mu\text{m}^2$ is derived from the average intact bacteria cells ($n = 63$) diameter ($0.7 \pm 0.1 \mu\text{m}$) and length ($3.1 \pm 0.7 \mu\text{m}$) of intact bacterial cells observed with transmission electron microscopy. With this surface area, and assuming an average diameter of 8 nm for the nano hematite particles (section 3.2.1), a density of hematite of 5.26 g cm^{-3} , and a cubic packing of the Fe(III) colloids on the cell wall (Figure 3.4a), equation (3.6) yields $M_{max} = 2.3 \times 10^{-9} \mu\text{mol Fe(III) cell}^{-1}$. This value falls within a factor of two of that obtained independently from the attachment experiments, that is, well within the uncertainties of both estimations of M_{max} .

Strictly speaking, the Langmuir isotherm applies to reversible adsorption reactions of molecular species to two-dimensional surfaces, that is, processes that differ fundamentally from the adhesion of mineral particles to bacterial cell walls. Thus, the Langmuir isotherm is used here as an empirical equation that accounts for the observed saturation behavior of the concentration of cell-bound nano hematite (see Appendix for further justification). Similarly, Das and Caccavo (2001) found that the attachment of bacterial cells to large iron oxide particles could be described by a Langmuir isotherm.

Electrophoretic mobility measurements and acid-base titrations show that *S. putrefaciens* cells carry a net negative charge at $\text{pH} > 4$ (Claessens et al., 2004). In contrast, nano hematite is positively charged between pH 4 and its zero point of charge of 8.15 (Liger et al., 1999). Consequently, under the conditions of the attachment experiments (pH 5 and low ionic strength), electrostatic repulsion among nano hematite particles and coulombic attraction between nano hematite particles and bacteria facilitates the attachment of the Fe(III) colloids to the cells. The available evidence, however, indicates that short-range, non-ionic interactions play a major role in binding the nano hematite particles to the cells.

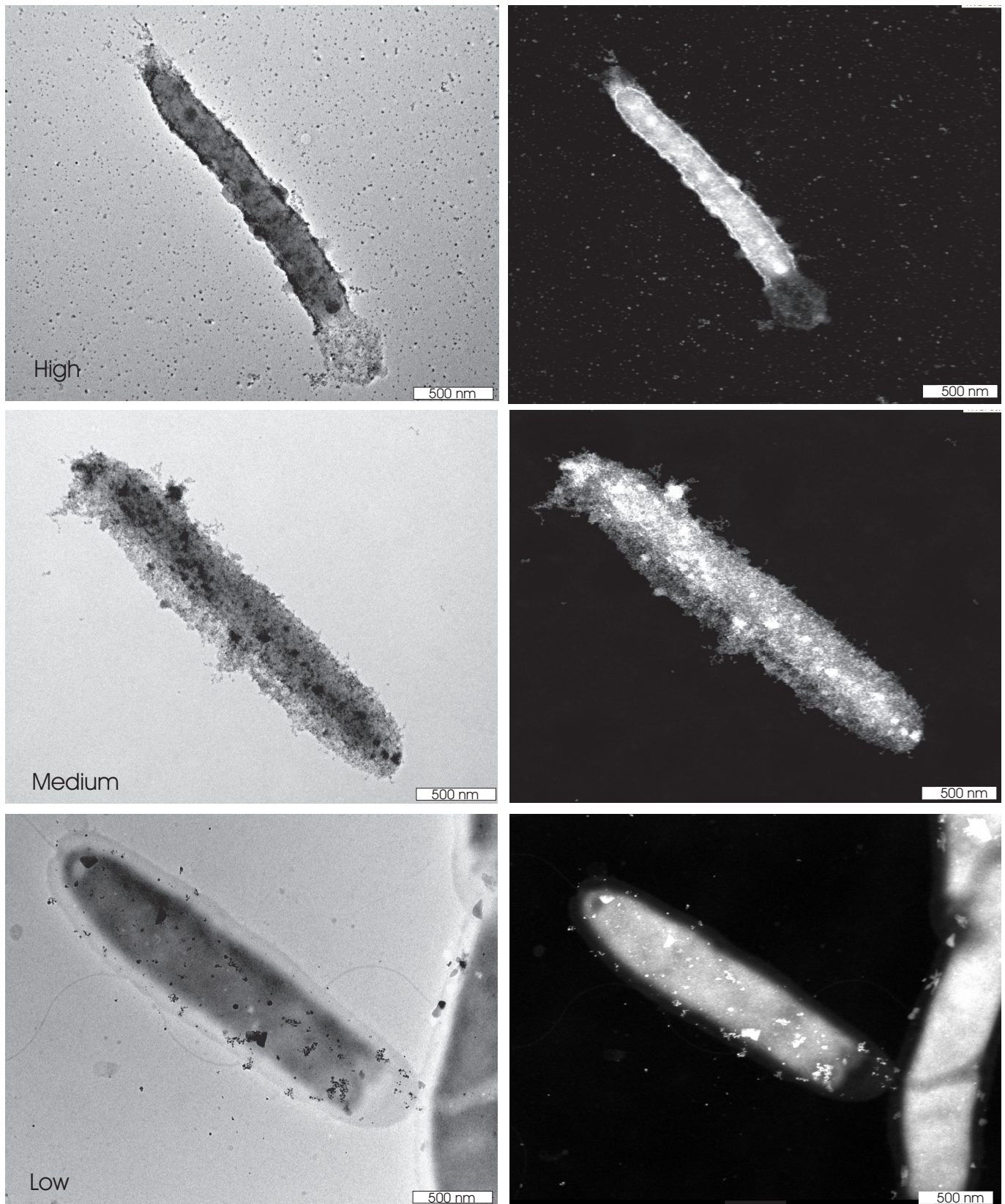


Figure 3.5: TEM (right) and STEM (left) micrographs of *S. putrefaciens* cells that have been exposed to 20 (Low), 100 (Medium) and 500 (High) $\mu\text{mol L}^{-1}$ of nanohematite (cell density = 2×10^8 cells mL^{-1} , pH 7).

Cells of *Shewanella* species can apparently synthesize specific proteins that enhance adhesion of Fe(III) oxyhydroxide particles (Caccavo, 1999; Lower et al., 2001; Lower et al., 2000). Even in the absence of specifically synthesized proteins, however, non-ionic interactions between structural components of the outer cell wall of Gram-negative bacteria and Fe(III) oxide minerals likely generate strong attractive forces at short distances. In particular, the flexible O side chain of lipopolysaccharides, a major constituent of the outer membrane of Gram-negative bacteria, may account for the “non-specific” attractive forces measured upon retraction of *S. oneidensis* from Fe(III) oxyhydroxide mineral surfaces (Lower et al., 2001). The absence of significant release of attached nanohematite in pH range 5-9 (section 3.3.1) further implies that strong, non-ionic forces maintain the colloidal particles attached to the cells.

In the following sections, kinetic data on iron reduction by *S. putrefaciens* obtained at circumneutral pH will be discussed. For the reduction experiments carried out in the present study, nanohematite attachment to the cells was carried out at pH 5, prior to initiating reduction at pH 7, in order to avoid coagulation of the nanohematite particles. In general, however, iron reduction experiments are started by directly introducing the cells in suspensions of Fe(III) oxyhydroxides at circumneutral pH. For colloidal Fe(III) phases, this may cause the mineral particles to aggregate.

Because in the conceptual model for iron reduction only Fe(III) centers located at the mineral-cell interface are potential electron acceptors (Figure 3.3), aggregation is assumed to have little effect on M_{max} . That is, for a given cell size, the maximum number of Fe(III) particles that can attach directly to the cells still depends principally on the shape and size of the individual mineral particles. In contrast, deviations in the attachment constant, K_p , may be expected as attachment of a Fe(III) colloid to the cell now competes with attachment to other Fe(III) colloids (Appendix).

3.5.2 Microbial reduction of nanohematite

Several outer-membrane c-type cytochromes capable of mediating electron transfer to Fe(III) and Mn(IV) oxides have been isolated from *Shewanella* cultures (Arnold et al., 1988; Beliaev and Saffarini, 1998; Blakeney et al., 2000; Caccavo, 1999; Myers and Myers, 1997). Their abundance depends on the growth conditions of the bacteria, with values of 0.45×10^{-2} and 1.96×10^{-2} μmol c-type cytochrome per mg of protein reported for cultures of *S. putrefaciens* 200 grown under aerobic and microaerobic conditions, respectively (Picardal et al., 1993). Based on the average protein content of *S. putrefaciens* 200 cells grown aerobically in LB medium (56% of the cell dry weight, Bin Lin, Free University of Amsterdam, personal communication), and their dry cell mass (3×10^{-13} g cell⁻¹), a *S.*

putrefaciens cell should contain on the order of 7×10^{-19} moles of c-type cytochromes. If these cytochromes can be assimilated to reduction sites for Fe(III) then, for an estimated cell surface area of $8.3 \mu\text{m}^2$ (section 3.5.1), we obtain a density of 0.054 sites per nm^2 , or an average of about 3 reductase sites per cell-bound nanohematite particle. The reductase abundance is thus sufficient to insure that every nanohematite particle becomes a potential electron acceptor upon attachment to the cell surface.

As the coverage of the outer membrane by nanohematite increases, so does the number of reaction centers for electron transfer from the cell to Fe(III) (Figure 3.3). Irrespective of the details of the reaction mechanism, the overall Fe(III) reduction rate should then also increase. This model prediction is verified by the observed proportionality between the initial Fe(III) reduction rate and the surface coverage of the cells by nanohematite (Figure 3.2b), as well as the continued first-order dependence of the reduction kinetics on the concentration of cell-bound Fe(III) over the entire duration of the reduction experiments (Figure 3.2a).

The first-order dissolution rate constant obtained in the reduction experiments presented here ($k = 3.9 \times 10^{-3} \text{ h}^{-1}$, Figure 3.2a), is smaller than that derived from the maximum nanohematite reduction rate by *S. putrefaciens* reported in our earlier study, $v_{\text{max}} = 2.4 \times 10^{-11} \mu\text{mol h}^{-1} \text{ cell}^{-1}$ (Bonneville et al., 2004). Combining the latter value of v_{max} with the estimated maximum attachment capacity of nanohematite to *S. putrefaciens* cells, $M_{\text{max}} = 2.3 \times 10^{-9} \mu\text{mol cell}^{-1}$, yields a rate constant of $k = 1.0 \times 10^2 \text{ h}^{-1}$ (equation 3.3). The lower iron reducing activity observed here is most likely due to the pH 5 conditions experienced by the cells prior to initiating reduction at pH 7. Claessens et al. (2004, 2005) provide clear evidence for a loss of cell viability when *S. putrefaciens* cells are exposed to acid conditions.

3.5.3 Half saturation constants

Bonneville et al. (2004) fitted initial reduction rates of a variety of fine grained Fe(III) oxyhydroxide minerals by *S. putrefaciens* to a rate expression of the form of equation (3.4), but using the total Fe(III) concentration, $[\text{Fe}_{\text{tot}}^{\text{III}}]$, as the substrate concentration. Given the high affinities of the Fe(III) oxides for the cells, $[\text{Fe}_{\text{tot}}^{\text{III}}]$ is expected to deviate significantly from the concentration of non-attached particles, $[\text{Fe}_{\text{free}}^{\text{III}}]$ especially at low mineral to cell ratios. The fitted saturation constants, K_m^* , should therefore be regarded as conditional parameters. Indeed, the optimized values of K_m^* reported by Bonneville et al. (2004) depend on the mineral to cell ratio. As shown below, such a dependence is predicted by the kinetic model presented in section 3.3.4.

Model-derived rates of iron reduction are plotted in Figure 3.6a as a function of the total Fe(III) concentration, for variable cell densities (10^6 up to $10^{10} \text{ cells mL}^{-1}$). The reduction rates are

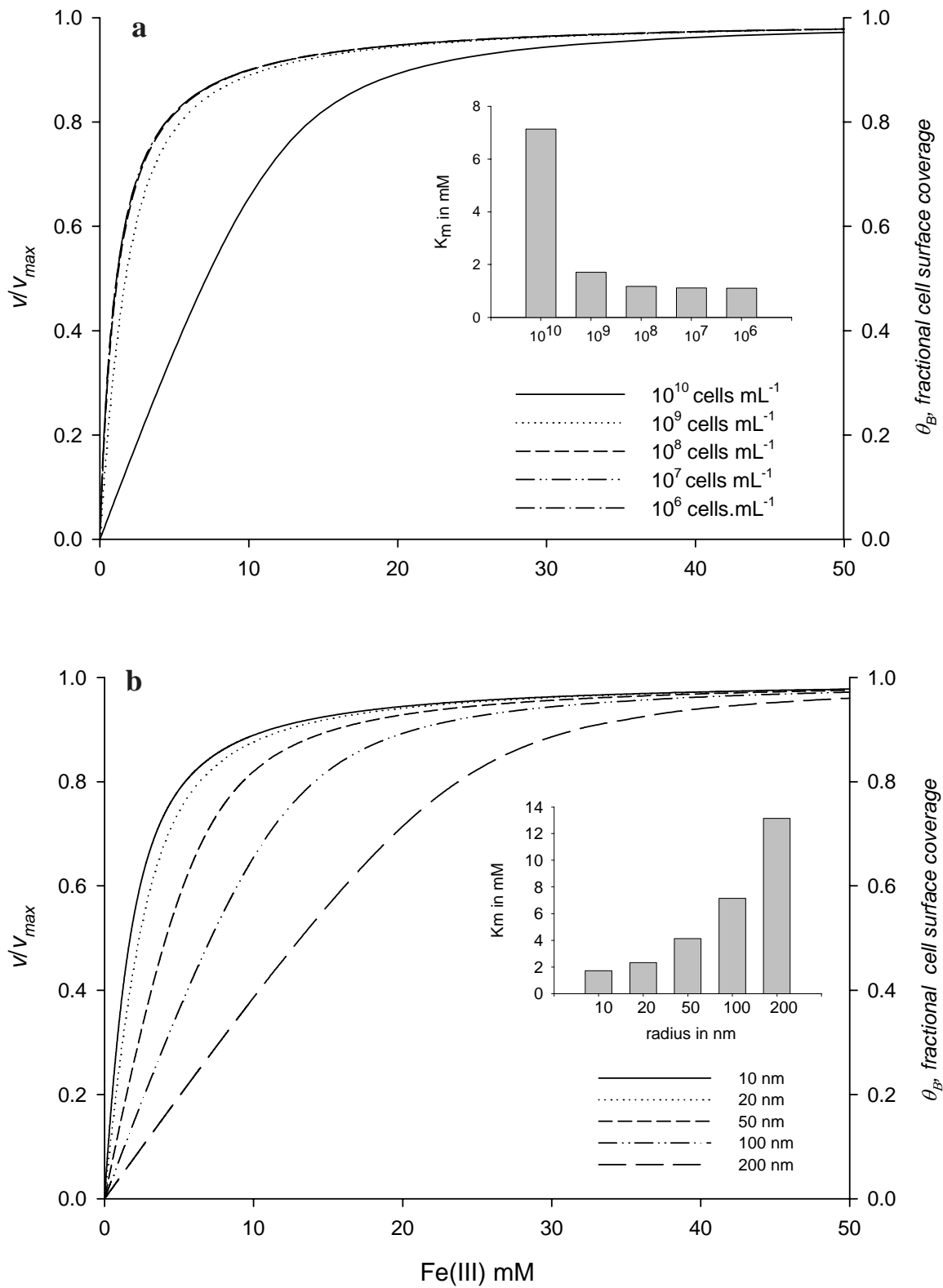


Figure 3.6: Model-predicted microbial iron reduction kinetics for spherical Fe(III) colloids, as a function of cell density (a) and particle diameter (b). See text for details.

calculated using equation (3.5), which relates v to $[\text{Fe}_{\text{tot}}^{\text{III}}]$. A constant value of K_p of $10^{-3} \text{ L } \mu\text{mol}^{-1}$ is imposed, and the Fe(III) particles are assumed to be spherical with a diameter of 10 nm. For all cell densities considered, the model-derived iron reduction rates exhibit a Michaelis-Menten-type dependence on the total Fe(III) concentration (Figure 3.6a).

At low to intermediate cell densities (10^6 - 10^8 cells mL^{-1}), the v versus $[\text{Fe}_{\text{tot}}^{\text{III}}]$ curves are nearly identical, and the apparent K_m^* values approach the intrinsic half saturation constant, $K_m = 1/K_p$. At the higher cell densities (10^9 and 10^{10} cells mL^{-1}), K_m^* values exceed K_m . This is because, at a given $[\text{Fe}_{\text{tot}}^{\text{III}}]$, the relative coverage of individual cells by Fe(III) colloids, θ_b , decreases with increasing cell density. It is important to stress that the higher K_m^* values at the higher cell to mineral ratios are not due to a decrease in the affinity of the Fe(III) particles for attachment to the cells, but to a change in the partitioning of $[\text{Fe}_{\text{tot}}^{\text{III}}]$ between cell-bound and free Fe(III) particles.

For practical reasons, the Fe(III) substrate availability is expressed in mass-based concentration units. However, the actual Fe(III) centers that undergo reduction are located at the surface of Fe(III) particles attached to the cells. Because particle mass and surface area are not linearly related, apparent half saturation constants should also depend on particle size. This is shown in Figure 3.6b, which shows iron reduction rates calculated at a fixed bacterial density (5×10^8 cells mL^{-1}) and a fixed value of K_p ($10^{-3} \text{ L } \mu\text{mol}^{-1}$). The spherical Fe(III) colloids are assigned diameters varying from 10 to 200 nm. With increasing particle size, the model predicts increasing K_m^* values, because of decreasing mineral-cell contact area. Again, the observed variability in K_m^* reflects apparent, rather than true, changes in the attachment affinity of the mineral particles for the cells.

Table 3.2. Kinetic model parameters.

Iron oxyhydroxide	M_{max} ($\mu\text{mol cell}^{-1}$)	K_p ($\text{L } \mu\text{mol}^{-1}$)	k (h^{-1})
Nanoematite	2.3×10^9	1.1×10^{-3}	1.0×10^{-2}
6-line ferrihydrite	8.6×10^{10}	8.0×10^{-4}	9.4×10^{-2}
LSA hematite	2.6×10^8	2.0×10^{-3}	1.0×10^{-4}
Lepidocrocite	1.5×10^8	5.0×10^{-5}	1.3×10^{-3}
HFO	4.3×10^{10}	1.0×10^{-3}	1.5×10^{-1}

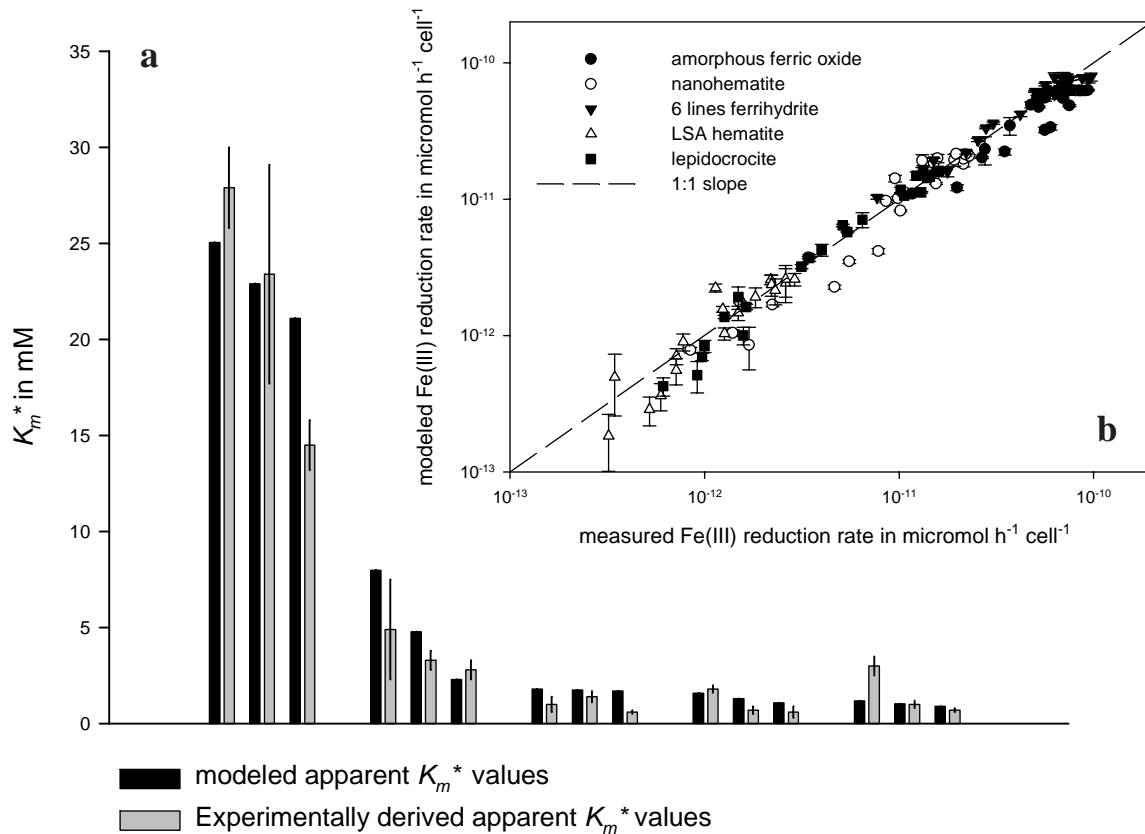


Figure 3.7: Application of the proposed kinetic model to the reduction of different fine-grained Fe(III) oxyhydroxides by *S. putrefaciens*. (a) Apparent half saturation constants, K_m^* , at three different bacterial densities, high (H), medium and low (L), ranging from 1.1 to 7.6×10^8 cells mL^{-1} . (b) Modeled versus measured microbial iron reduction rates for the different Fe(III) oxyhydroxides considered (see Table 3.1). All data are from Bonneville et al. (2004). See text for detailed discussion.

3.5.4 Application to other Fe(III) oxyhydroxides

The kinetic model successfully reproduces the observed saturation of the rate of nanohematite reduction by *S. putrefaciens* with increasing mineral loading. A similar behavior has been observed for the reductive dissolution of a number of other colloidal Fe(III) oxyhydroxides by *S. putrefaciens* (Bonneville et al., 2004). Thus it seems reasonable to hypothesize that rate equation (3.5) provides a general description of the dependence of the reduction rate of Fe(III) colloids on the Fe(III) substrate concentration, $[\text{Fe}_{\text{tot}}^{\text{III}}]$, and the cell density, B .

As for nanohematite, the maximum mass of iron particles that can directly attach to the cell surface, M_{max} , is calculated based on the size, shape and density of the Fe(III) oxyhydroxides (Table 3.1). The estimates of M_{max} vary by more than two orders of magnitude (Table 3.2). These variations primarily reflect the large differences in size, and hence specific surface area, of the different minerals

considered. By combining the estimates of M_{max} with the maximum cell-normalized reduction rates, v_{max} , reported by Bonneville et al. (2004), values for the first-order reduction rate constants, k , are obtained (Table 3.2). The rate constants range over four orders of magnitude, with the highest value for amorphous hydrous ferric oxide (HFO) and the lowest for low surface area (LSA) hematite. Using the predetermined values of M_{max} and k , the only remaining adjustable parameter in rate equation (3.5) is the attachment constant K_p . For each Fe(III) oxyhydroxide phase, an optimized value of K_p is obtained by fitting equation (3.5) to the rates measured by Bonneville et al. (2004). As summarized in Figure 3.7b, the kinetic model successfully reproduces the order-of-magnitude variations in iron reduction rates of the five oxyhydroxides, for variable Fe(III) substrate concentrations and bacterial cell densities.

The value of K_p derived for nanohematite from fitting equation (3.5) to Fe(III) reduction rate data ($1.1 \times 10^{-3} \text{ L } \mu\text{mol}^{-1}$, Table 3.2) deviates from that determined in the attachment experiments ($2.0 \times 10^{-2} \text{ L } \mu\text{mol}^{-1}$, section 3.3.1). This discrepancy is ascribed to differences in pH and ionic strength conditions. At the higher ionic strength (0.02 *versus* 0.005 M NaCl) and pH (7 *versus* 5) of the incubations of Bonneville et al. (2004), colloidal suspensions of nanoparticulate hematite are not stable and coagulation is observed. That is, attachment of mineral particles to one another competes with attachment to the cells, resulting in a lower value of K_p (Appendix).

Similar values of K_p are obtained for all the oxyhydroxides, with the exception of lepidocrocite (Table 3.2). The order-of-magnitude smaller K_p value for lepidocrocite suggests a lower tendency of this mineral to attach to the cells. Possibly, this is due to the elongated shape of the lepidocrocite (Table 3.1), which may interfere with a close packing of the particles at the bacterial surface. In contrast, all other Fe(III) colloids are spherical. Further studies are needed, however, to determine whether steric effects related to particle shape explain the deviating K_p value for lepidocrocite.

From the optimized K_p values, it is possible to derive apparent K_m^* values as a function of the cell density (section 3.5.3, Figure 3.6a). The model-derived K_m^* values can then be compared directly to the values obtained experimentally for different bacterial cell densities in the study of Bonneville et al. (2004). As shown in Figure 3.7a, the model correctly predicts the magnitudes of the K_m^* values, and reproduces the observed dependency of K_m^* on cell density.

3.5.5 Bioreduction kinetics and cell density

So far, emphasis has been on explaining the saturation of the rate of microbial iron reduction with respect to the concentration of the Fe(III) solid phase (e.g., Figure 3.6). As shown by Roden and Zachara (1996) and Roden (2003), iron reduction rates also asymptotically approach maximum values

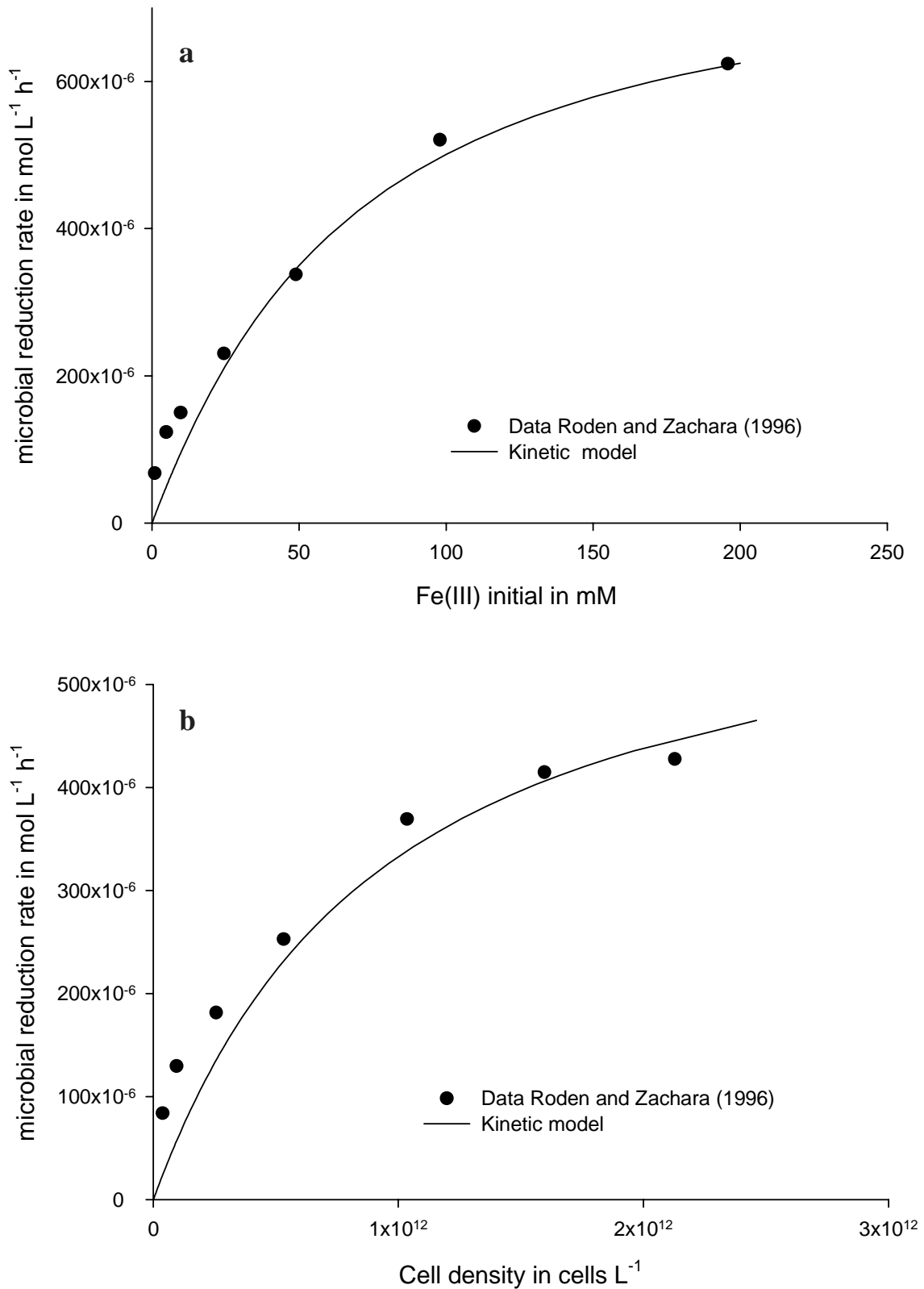


Figure 3.8: Rates of hydrous ferric oxide (HFO) reduction by *S. alga* strain BrY. (a) Fit of equation (3.5) to rates measured at variable HFO concentrations and a fixed cell density of 2×10^8 cells mL^{-1} . (b) Model predicted rates as a function of cell density, at a fixed HFO concentration of 20 mM Fe(III). All data are from Roden and Zachara (1996). See text for complete discussion.

when increasing the cell density in bacteria-mineral suspensions. This behavior is not directly apparent from equations (3.2) and (3.4), which may seem to imply a linear dependence of the reduction rate on the cell density, B . This linear dependence, however, is only apparent, because, at a given total concentration of the Fe(III) colloids, the relative coverage of the cells, θ_b , is itself dependent on B .

To demonstrate that the kinetic model presented here reproduces the saturation of microbial Fe(III) reduction kinetics with increasing cell density, equation (3.5) is applied to the data for hydrous ferric oxide (HFO) reduction by *S. alga* strain BrY reported in Roden and Zachara (1996). These authors measured initial iron reduction rates at constant bacterial density while varying the HFO concentration (Figure 1 in Roden and Zachara, 1996), but also at constant HFO concentration while varying the cell density (Figure 3 in Roden and Zachara, 1996). Equation (3.5) is therefore first fitted to the reduction rates measured for variable HFO concentrations, assuming a mineral particle size of 6 nm. From the fit, a value for K_p of $2 \times 10^{-5} \text{ L } \mu\text{mol}^{-1}$ is obtained. Next, rate equation (3.5) is used to forecast HFO reduction rates as a function of cell density, at a constant HFO concentration. The model-predicted rates are then compared to the measured rates. The results of the initial model fit and the subsequent model forecast are shown in Figure 3.8. The observed parabolic dependence of the Fe(III) reduction rate on the HFO concentration (Figure 3.8a) is similar to that found for the microbial reduction of HFO and other Fe(III) oxyhydroxides by Bonneville et al. (2004). Therefore, not surprisingly, the data in Figure 3.8a can be fitted by equation (3.5). However, with the same set of model parameters, equation (3.5) also correctly predicts the observed dependence of the HFO reduction rate on the density of iron reducing bacterial cells (Figure 3.8b).

3.6 Conclusions

The proposed kinetic model relates the reduction kinetics of fine-grained Fe(III) oxyhydroxides by iron reducing microorganisms to the relative coverage of the cells by the mineral particles. The experimental and modeling results highlight the central role of cell-mineral adhesion processes in the direct, enzymatic reduction of solid phase Fe(III). The model captures some of the essential features of microbial iron reduction observed in mixed suspensions of iron reducing bacteria and Fe(III) minerals. In particular, the model reproduces the saturation of the bioreduction rate with respect to the solid phase Fe(III) substrate concentration, as well as the cell density. The model further accounts for the particle size dependency of the first-order rate constant for microbial iron reduction, k , and the apparent half-saturation constant, K_m^* . Under otherwise identical conditions, the model predicts decreasing rates of microbial iron reduction with decreasing specific surface area of the Fe(III) mineral particles.

Appendix

A simple stochastic model is used to simulate colloid attachment to initially mineral-free cell surfaces that contain a limited number of attachment sites, n . It is assumed that every colloidal particle either attaches to a free cell wall site, or to another particle already associated with the bacteria. The first particle added to the system attaches to the cell wall. The probability that the next particle entering the system attaches to a free cell wall site is then $(n-1)/n$, and so on, until for the x -th particle the probability is $(n-k)/n$, where k is the number of occupied sites. The approach implies that the tendency of a particle to attach to a free cell wall site or to another particle is identical.

Results for $n = 50$ and 150 particles are shown in Figure 3.A1. The points on the plot represent the average numbers of occupied sites for 200 simulation runs. The broken line is the best-fit Langmuir isotherm when imposing a cell wall site density of 50. The resulting attachment constant is $K_p = 0.1$. Also shown is the best-fit Langmuir isotherm when both the site density and K_p are optimized. The fit yields a maximum attachment density of 55 and $K_p = 0.07$ (continuous line). Both fits illustrate that the irreversible binding of the colloids to the cell wall can be represented by a Langmuir isotherm.

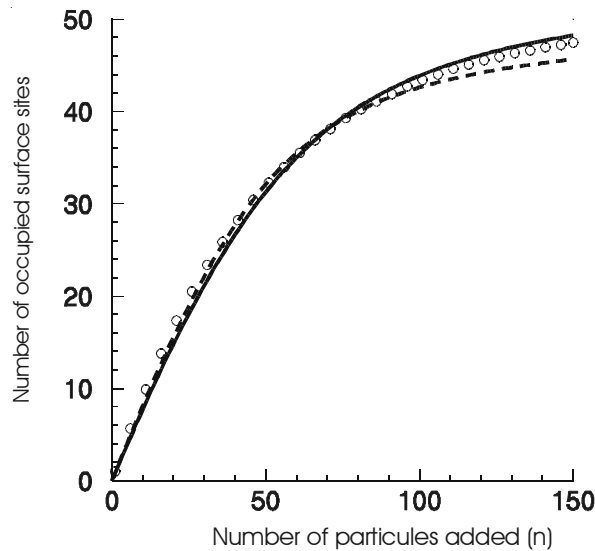


Figure 3.A1

The above scenario can easily be modified to account for preferential attachment of the mineral particles to the cell wall or to other particles. Introducing the adjustable weighing factors, a and b , the probability of attachment of the x -th particle to a free cell wall site is written as $p = a(n-k)/n$, while the probability of attachment to another particle is given by $q = b(k/n)$. Per definition, $p + q = 1$ and, consequently,

$$a \left(1 - \frac{k}{n} \right) + b \frac{k}{n} = 1 \quad (\text{equation 3.AP 1})$$

The attachment preference of the mineral particles is then reflected in the ratio $r = a/b$. Setting $r > 1$ implies a greater affinity of the particles for direct attachment to the cell wall than to other particles, and vice versa for $r < 1$. Substituting b by a/r in equation AP 1 then yields:

$$a = \frac{rn}{rn - rk + k} \quad (\text{equation 3.AP 2})$$

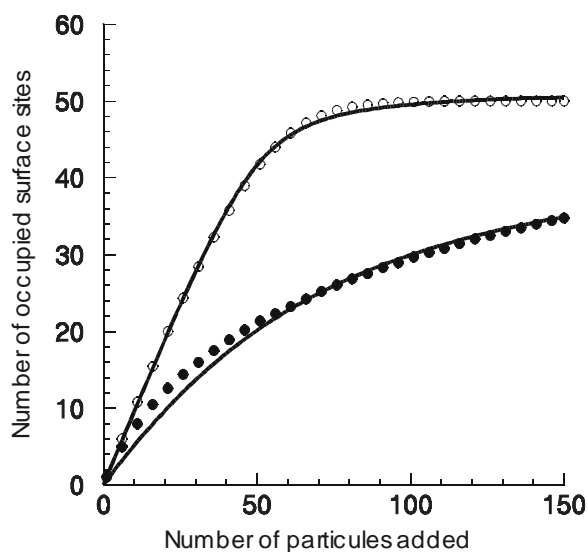


Figure 3.A2

The open circles on Figure 3.A2 correspond to the results of stochastic simulations similar to those in Figure 3.A1, except that $r = 5$. A best-fit Langmuir isotherm with $K_p = 0.5$ is obtained, when the maximum number of surface sites is fixed at 50. When the cell wall site density is treated as an adjustable parameter, the best-fit Langmuir isotherm yields nearly the same K_p value and a slightly higher maximum site density of 51.1 (continuous line). Thus, the preference for direct attachment of the mineral particles to the cells results in a K_p value that is five times higher than when the particles exhibit no attachment preference (i.e., $r = 1$, Figure 3.A1). Effectively, $r > 1$ also simulates scenarios where the mineral particles repulse one another.

In contrast, using a weighing factor $r = 0.2$ leads to decreased attachment densities of the particles to the cells (filled circles on Figure 3.A2). The attachment behavior, however, still follows a (pseudo-)Langmuir isotherm, albeit with a much lower K_p value of 0.025. The results of the stochastic experiments thus imply that particle-particle interactions among the Fe(III) colloids affect their attachment behavior to the cell wall. Because in the kinetic model presented in section 3.4 only those mineral colloids that are directly bound to the cells are susceptible of undergoing reduction, the particle-particle interactions also influence the enzymatic iron reduction kinetics.

References

- Albrechtsen H.-J. and Christensen T. H. (1994) Evidence for microbial iron reduction in a landfill leachate-polluted aquifer (Vejen, Denmark). *Appl. Environ. Microbiol.* **60**, 3920-3925.
- Anderson R. T. and Lovley D. R. (1999) Naphthalene and benzene degradation under Fe(III)-reducing conditions in petroleum-contaminated aquifers. *Biorem. J.* **3**, 121-135.
- Arnold R. G., DiChristina T. J., and Hoffmann M. R. (1988) Reductive dissolution of iron(III) oxides by *Pseudomonas* sp. 200. *Biotechnol. Bioeng.* **32**, 1081-1096.
- Beliaev A. S. and Saffarini D. A. (1998) *Shewanella putrefaciens* mtrB encodes an outer membrane protein required for Fe(III) and Mn(IV) reduction. *J. Bacteriol.* **180**, 6292-6297.
- Blakeney M. D., Moulaei T., and DiChristina T. J. (2000) Fe(III) reduction activity and cytochrome content of *Shewanella putrefaciens* grown on ten compounds as sole terminal electron acceptor. *Microbiol. Res.* **155**, 87-94.
- Bonneville S., Van Cappellen P., and Behrends T. (2004) Microbial reduction of iron(III) oxyhydroxides: effects of mineral solubility and availability. *Chem. Geol.* **212**, 255-268.
- Caccavo F., Jr. (1999) Protein-mediated adhesion of the dissimilatory Fe(III)-reducing bacterium *Shewanella* alga BrY to hydrous ferric oxide. *Appl. Environ. Microbiol.* **65**, 5017-5022.
- Caccavo F. J. and Das A. (2002) Adhesion of dissimilatory Fe(III)-reducing bacteria to Fe(III) minerals. *Geomicrobiol. J.* **19**, 161-177.
- Canfield D. E. (1988) Sulfate reduction and diagenesis of iron in anoxic marine sediments., Yale University, USA.
- Claessens J., Behrends T., and Van Cappellen P. (2004) What do acid-base titrations of live bacteria tell us? A preliminary assessment. *Aquat. Sci.* **66**, 19-26.
- Cummings D. E., Caccavo F., Jr., Fendorf S., and Rosenzweig R. F. (1999) Arsenic Mobilization by the Dissimilatory Fe(III)-Reducing Bacterium *Shewanella* alga BrY. *Environ. Sci. Technol.* **33**, 723-729.
- Das A. and Caccavo F., Jr. (2000) Dissimilatory Fe(III) oxide reduction by *Shewanella* alga BrY requires adhesion. *Curr. Microbiol.* **40**, 344-347.
- DiChristina T. J. and DeLong E. F. (1994) Isolation of anaerobic respiratory mutants of *Shewanella putrefaciens* and genetic analysis of mutants deficient in anaerobic growth on Fe³⁺. *J. Bacteriol.* **176**, 1468-1474.
- DiChristina T. J., Moore C. M., and Haller C. A. (2002) Dissimilatory Fe(III) and Mn(IV) reduction by *Shewanella putrefaciens* requires ferE, a homolog of the pulE (gspE) type II protein secretion gene. *J. Bacteriol.* **184**, 142-151.
- Hobbie J. E., Daley R. J., and Jasper S. (1977) Use of nucleopore filters for counting bacteria by fluorescence microscopy. *Appl. Environ. Microbiol.* **33**, 1225-1228.
- Kappler A., Benz M., Schink B., and Brune A. (2004) Electron shuttling via humic acids in microbial iron(III) reduction in a freshwater sediment. *FEMS Microbiol. Ecol.* **47**, 85-92.
- Liger E. (1996) Role catalytique des oxyhydroxides de Fe(III): Reduction de U(VI) par le Fe(II) adsorbé, Université Joseph Fourier, Grenoble, France. p 187.
- Liger E., Charlet L., and Van Cappellen P. (1999) Surface catalysis of uranium (VI) reduction by iron(II). *Geochim. Cosmochim. Acta* **63**, 2939-2955.
- Lovley D. R. and Coates J. D. (1997) Bioremediation of metal contamination. *Curr. Opin. Biotechnol.* **8**, 285-289.
- Lovley D. R., Giovannoni S. J., White D. C., Champine J. E., Phillips E. J. P., Gorby Y. A., and Goodwin S. (1993) *Geobacter metallireducens* gen. nov. sp. nov., a microorganism capable of coupling the complete oxidation of organic compounds to the reduction of iron and other metals. *Arch. Microbiol.* **159**, 336-344.
- Lower S. K., Hochella M. F., Jr., and Beveridge T. J. (2001) Bacterial recognition of mineral surfaces: nanoscale interactions between *Shewanella* and α -FeOOH. *Science (Washington, DC, U. S.)* **292**, 1360-1363.
- Lower S. K., Tadanier C. J., and Hochella M. F., Jr. (2000) Measuring interfacial and adhesion forces between bacteria and mineral surfaces with biological force microscopy. *Geochim. Cosmochim. Acta* **64**, 3133-3139.
- McCormick M. L., Bouwer E. J., and Adriaens P. (2002) Carbon Tetrachloride Transformation in a Model Iron-Reducing Culture: Relative Kinetics of Biotic and Abiotic Reactions. *Environ. Sci. Technol.* **36**, 403-410.
- Methe B. A., Nelson K. E., Eisen J. A., Paulsen I. T., Nelson W., Heidelberg J. F., Wu D., Wu M., Ward N., Beanan M. J., Dodson R. J., Madupu R., Brinkac L. M., Daugherty S. C., DeBoy R. T., Durkin A. S., Gwinn M., Kolonay J. F., Sullivan S. A., Haft D. H., Selengut J., Davidsen T. M., Zafar N., White O., Tran B., Romero C., Forberger H. A., Weidman J., Khouri H., Feldblyum T. V., Utterback T. R., Van Aken S. E., Lovley D. R., and M. F. C. (2003) Genome of *Geobacter sulfurreducens*: metal reduction in subsurface environments. *Science* **302**, 1967-1969.
- Myers C. R. and Myers J. M. (1997) Outer membrane cytochromes of *Shewanella putrefaciens* MR-1: spectral analysis, and purification of the 83-kDa c-type cytochrome. *Biochim. Biophys. Acta* **1326**, 307-318.

- Picardal F. W., Arnold R. G., Couch H., Little A. M., and Smith M. E. (1993) Involvement of cytochromes in the anaerobic biotransformation of tetrachloromethane by *Shewanella putrefaciens* 200. *Appl. Environ. Microbiol.* **59**, 3763-3770.
- Taillefert M., Bono A. B., and Luther G. W., III. (2000) Reactivity of Freshly Formed Fe(III) in Synthetic Solutions and (Pore)Waters: Voltammetric Evidence of an Aging Process. *Environ. Sci. Technol.* **34**, 2169-2177.
- Viollier E., Inglett P. W., Hunter K., Roychoudhury A. N., and Van Cappellen P. (2000) The ferrozine method revisited: Fe(II)/Fe(III) determination in natural waters. *Appl. Geochem.* **15**, 785-790.
- Zachara J. M., Fredrickson J. K., Smith S. C., and Gassman P. L. (2001) Solubilization of Fe(III) oxide-bound trace metals by a dissimilatory Fe(III) reducing bacterium. *Geochim. Cosmochim. Acta* **65**, 75-93.

Chapter IV

The role of solubility in microbial Fe(III) oxyhydroxide reduction kinetics

Steeve Bonneville, Thilo Behrends and Philippe Van Cappellen

Submitted to *Environmental Science & Technology*

Abstract

The solubilities of a variety of Fe(III) oxyhydroxides correlate positively with the maximum cell-normalized rates (v_{max}) of iron reduction by *Shewanella putrefaciens*, at near-neutral pH and in the presence of excess electron donor. This Free Energy Relationship (LFER) accounts for variations in v_{max} ranging over 1.5 orders of magnitude, and implies that the structure and energetics of the minerals play a determining role in microbial iron reduction kinetics. The observed positive correlation between v_{max} and the rate constant for detachment of Fe²⁺ from the mineral (k_{des}) further points to the release of reduced Fe²⁺ centers from the surface lattice as the key rate-controlling process.

4.1 Introduction

In many suboxic environments ferric iron is the most abundant potential electron acceptor for the anaerobic oxidation of organic compounds (Canfield et al., 1993; Jakobsen and Postma, 1999; Lyngkilde and Christensen, 1992; Van Breemen, 1988). Within the large group of Fe(III)-bearing minerals, Fe(III) oxyhydroxides are of particular environmental relevance because they often occur as fine grained particles and exhibit highly reactive surfaces (Fox and Doner, 2002; Kaplan et al., 1997; Luther et al., 1982; Scheidegger et al., 1993; Tipping et al., 1981). Due to their affinity for dissolved metal ions and oxyanions, Fe(III) oxyhydroxides play an important role in controlling the mobility and bioavailability of nutrients and contaminants (Anderson and Lovley, 1999; Fox and Doner, 2002; Roden and Edmonds, 1997). They are usually considered the main terminal electron acceptors for dissimilatory iron reduction (Lovley et al., 1991).

The rate and extent of microbially-mediated iron reduction is controlled by the bioavailability of suitable electron donors, primarily under the form of organic matter (Lovley and Phillips, 1989; Petruzzelli et al., 2005), but also that of the Fe(III) mineral substrates (van Breukelen et al., 2004). Among the various mineral properties that may affect the kinetics of dissimilatory iron reduction, the solubility is intuitively expected to be important, because it is a direct measurement of the stability of the iron(III) solid in aqueous solution. Furthermore, the rates of abiotic reductive dissolution of Fe(III) oxyhydroxides by ascorbate decrease in the order ferrihydrite > lepidocrocite > goethite > hematite, hence following their ranking order of solubility (Larsen and Postma, 2001).

Because for any given Fe(III) oxyhydroxide the reported range in solubility can be very large, it is important to determine the solubility and microbial reduction kinetics on the exact same solids. In a previous study, we determined the solubility products of four different colloidal Fe(III) oxyhydroxides by performing pe-pH titrations of suspensions of the minerals in the pH range 4-7 (Bonneville et al., 2004). As this approach only works for fine-grained minerals, we resorted to redox potential measurements at pH 2 to constrain the solubility of a low surface area (LSA) hematite. For the five Fe(III) oxyhydroxides studied, a positive correlation was found between the solubility product of the mineral and the maximum rate of Fe(III) reduction by the iron reducing bacterium *Shewanella putrefaciens*.

In order to validate the previously observed dependence of microbial iron reduction rates on mineral solubility, the solubilities of a number of additional Fe(III) oxyhydroxides were assessed using a dialysis bag dissolution method. With this method, which involves the direct measurement of the concentrations of ferric iron dissolving under acid conditions, it is possible to derive the solubility products

of coarser, more insoluble mineral phases. The reduction rates of the additional Fe(III) solids by *S. putrefaciens* were measured in exactly the same way as in our earlier study. Based on the expanded data set, the relationship between Fe(III) oxyhydroxide mineral solubility and microbial reduction kinetics is analyzed, and the possible underlying mechanism discussed.

4.2 Materials and Methods

4.2.1 Fe(III) oxyhydroxides

Nano hematite and 6-lines ferrihydrite were synthesized according to the methods described in (Bonneville et al., 2004). Amorphous ferric oxide (HFO) was synthesized by neutralizing a 0.4 M solution of $\text{FeCl}_3 \cdot 6\text{H}_2\text{O}$ with 1 M NaOH, followed by dialysis with demineralized water to remove Na^+ and Cl^- ions. Lepidocrocite 6.8 was prepared according to the method described in (1991): 11.93 grams of unoxidized crystals of $\text{FeCl}_2 \cdot 4\text{H}_2\text{O}$ were dissolved in 300 mL of demineralized water. After adjusting the pH to 6.8 with 1M NaOH, the solution was exposed to air at a flow rate of 100 mL min^{-1} . During oxidation, NaOH was added to neutralize proton production and maintain pH 6.8, until the color of the solution turned orange. Lepidocrocite (Bayferrox 943), low surface area (LSA) hematite (Bayferrox 105M) and goethite (Bayferrox 910) were purchased from Scholz & Co, whereas hematite Merck and lepidocrocite (Alfa) were purchased from Merck and Alfa Aesar, respectively.

4.2.2 Fe(III) oxyhydroxide dissolution experiments

Solubilities of Fe(III) oxyhydroxides were derived by measuring the activities of aqueous ferric iron, $\text{Fe}^{3+}(\text{aq})$, in equilibrium with the solids at variable pH and 25°C , using a method inspired from (Kuma et al., 1992). Dialysis membrane bags were filled with 20 mL of concentrated Fe(III) oxyhydroxide suspension, and then placed in 100 mL glass bottles. Iron concentrations of the Fe(III) oxyhydroxide suspension were around 100 mM. The glass bottles contained 10 mM NaNO_3 solutions whose pH was adjusted to 1, 1.5, 2 and 2.5 with 1M HNO_3 . The dialysis bags were completely immersed and kept in the dark under aerobic conditions in a thermostated water bath at 25°C .

Aliquots from the solution surrounding the dialysis membrane bags were collected regularly to monitor the build-up of total dissolved Fe and dissolved Fe^{2+} . Dissolved Fe^{2+} was measured directly after sampling by the ferrozine assay method (Viollier et al., 2000). Total dissolved Fe concentrations were determined by mixing 25 to 300 μL of sample with hydroxylamine hydrochloride solution (1.4 M in 2 M HCl). The hydroxylamine reduced Fe^{3+} to Fe^{2+} and, after 30 minutes, total dissolved Fe^{2+} was measured by ferrozine assay. In order to check for the presence of Fe(III) solids in the solution surrounding

the dialysis bags, 200 μL of sample was mixed with 100 μL of 2M HCl and placed in an oven overnight to dissolve any Fe(III) particles. The acidified solution was then mixed with hydroxylamine solution, and the Fe concentrations measured by ferrozine assay. The dissolution experiments were terminated when the total dissolved Fe concentration no longer increased. The final pH was then recorded using a Ross glass electrode calibrated by pH 1, 2 and 3 solutions freshly prepared by dilution of a 1 M HCl solution (Titrisol).

The concentration of total $\text{Fe}^{3+}(\text{aq})$ was obtained by subtracting the measured Fe^{2+} concentration from the measured total dissolved Fe concentration. The formation of Fe^{3+} solution complexes, predominantly $\text{Fe}(\text{OH})^{2+}$ in the pH range considered, and long-range electrostatic interactions were accounted for by equilibrium speciation calculations including the extended Debye-Hückel equation.

Table 4.1. Properties of Fe(III) oxyhydroxides used in this study.

Iron oxyhydroxide	v_{max} ($10^{-17} \text{ mol h}^{-1} \text{ cell}^{-1}$)	$\log *K_{so}$	Slope (-n)	Surface Area ($\text{m}^2 \text{ g}^{-1}$)	Reference v_{max} & $\log *K_{so}$
Nanohematite	2.40	0.52 (± 0.15)	2.85	125	(Bonneville et al., 2004)
LSA hematite	0.27	-1.22 (± 0.38)	2.60 (± 0.14)	12	this study
Hematite (Merck)	0.96	-1.05 (± 0.20)	2.66 (± 0.11)	3	this study
6 lines ferrihydrite	8.10	1.62 (± 0.27)	2.75	175	(Bonneville et al., 2004)
HFO (pe-pH)	6.50	1.90 (± 0.13)	2.71	600	(Bonneville et al., 2004)
HFO (Dialysis)		1.78 (± 0.04)	2.74 (± 0.04)		this study
Lepidocrocite (Bayferrox)	2.00	0.46 (± 0.10)	2.65	17	(Bonneville et al., 2004)
Lepidocrocite (Alfa)	3.30	0.68 (± 0.50)	2.61 (± 0.17)	83	this study
Lepidocrocite 6.8	5.40	1.11 (± 0.40)	2.83 (± 0.13)	70-80	this study
Goethite (Bayferrox)	1.15	-0.66 (± 0.17)	2.84 (± 0.1)	15	this study

4.2.3 Microbial reduction experiments

Cultures of *S. putrefaciens* 200R were provided by Dr. T. DiChristina of Georgia Institute of Technology (DiChristina et al., 1988; DiChristina et al., 2002). Cells were kept aerobically on Luria Bertani medium (LB) and routinely cultivated in liquid LB medium on a rotary shaker at room temperature. The bacteria were washed, concentrated in 50 mL of 0.1 M NaCl, and cell densities were estimated according to the method described in (Bonneville et al., 2004). For each Fe(III) oxyhydroxide, suspensions of *S. putrefaciens* were incubated at eight different Fe(III) concentrations and three different

cell densities. Batch incubation experiments were performed in 100 mL glass bottles, under anaerobic conditions. The composition of the medium was: 10 mM lactate, 10 mM Hepes buffer, 28 mM NH_4Cl and 1 mM $\text{CaCl}_2 \cdot 2\text{H}_2\text{O}$. The pH of the medium containing the Fe(III) oxyhydroxides was adjusted to 7 and degassed for 2 hours prior to being inoculated with bacteria. The bottles were kept on a rotary table at room temperature (22-23°C). Samples were collected periodically to monitor the production of Fe^{2+} during the 24 hours following inoculation (Bonneville et al., 2004).

4.3 Results

4.3.1 Fe(III) oxyhydroxide solubilities

The Fe concentrations measured on acid-digested samples from the solutions surrounding the dialysis bags were indistinguishable from the dissolved Fe concentrations, implying the effective retention of the Fe(III) oxyhydroxide particles by the dialysis membrane. For all Fe(III) oxyhydroxides, except HFO, the measured total dissolved Fe concentrations reached a plateau at the pH values tested, as shown for one of the lepidocrocites in Figure 4.1a. The noticeable exception was HFO, for which total dissolved Fe concentrations reached a maximum after about 400 hours, and then decreased with time (Figures 4.1a and 4.1b). The drop in dissolved Fe concentration, and the concomitant drop of the computed concentration of dissolved Fe^{3+} , most likely reflect a decrease in solubility due to aging processes (e.g., Ostwald ripening or recrystallisation). The maximum dissolved Fe^{3+} concentrations were used to compute the solubility product of HFO (see below). The time required to achieve dissolution equilibrium varied between around 500 hours for HFO and 4000 hours for LSA hematite. The amounts of added Fe(III) oxyhydroxide dissolved ranged from 0.01 % (LSA hematite, pH 2.5) to about 50 % (HFO, pH 1).

In all dissolution experiments, Fe^{2+} was detected in the surrounding solution. The highest concentration was observed for HFO at pH 1 ($82 \mu\text{M Fe}^{2+}$). In general, dissolved ferrous iron represented only a small fraction (< 10%) of total dissolved Fe in experiments at pH 1, 1.5 and 2. Most Fe^{2+} was released at the beginning of the experiments, with the dissolved Fe^{2+} concentration remaining fairly constant afterwards, while the total Fe concentration continued to increase. In contrast, at pH 2.5, higher contributions of Fe^{2+} were observed, in particular for dissolution experiments with Merck hematite, LSA hematite and goethite, where up to 50-70 % of the total dissolved Fe occurred in the reduced state. These very high Fe^{2+} concentrations imply Fe^{3+} reduction, possibly by reduced organic compounds released by the dialysis membrane. As shown in Fukushima et al. (1999), small amounts of dissolved organic matter can reduce aqueous Fe^{3+} in the dark, especially at low pH.

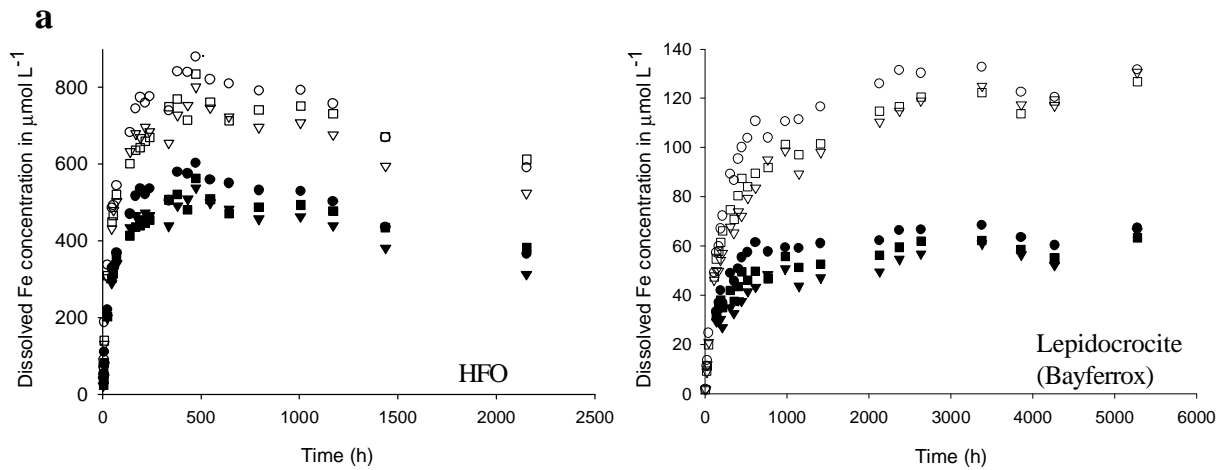


Figure 4.1. a. Build-up of total dissolved Fe (open symbols) and dissolved $\text{Fe}^{3+}_{(\text{aq})}$ (closed symbols) in triplicate dialysis bag dissolution experiments with HFO and lepidocrocite (Bayferrox) at pH 2. The concentrations plotted correspond to the hexaquo ion concentrations ($[\text{Fe}^{3+}_{(\text{aq})}] = [\text{Fe}^{\text{tot}}_{(\text{aq})}] - [\text{Fe}^{2+}_{(\text{aq})}] - [\text{Fe}(\text{OH})^{2+}_{(\text{aq})}]$).

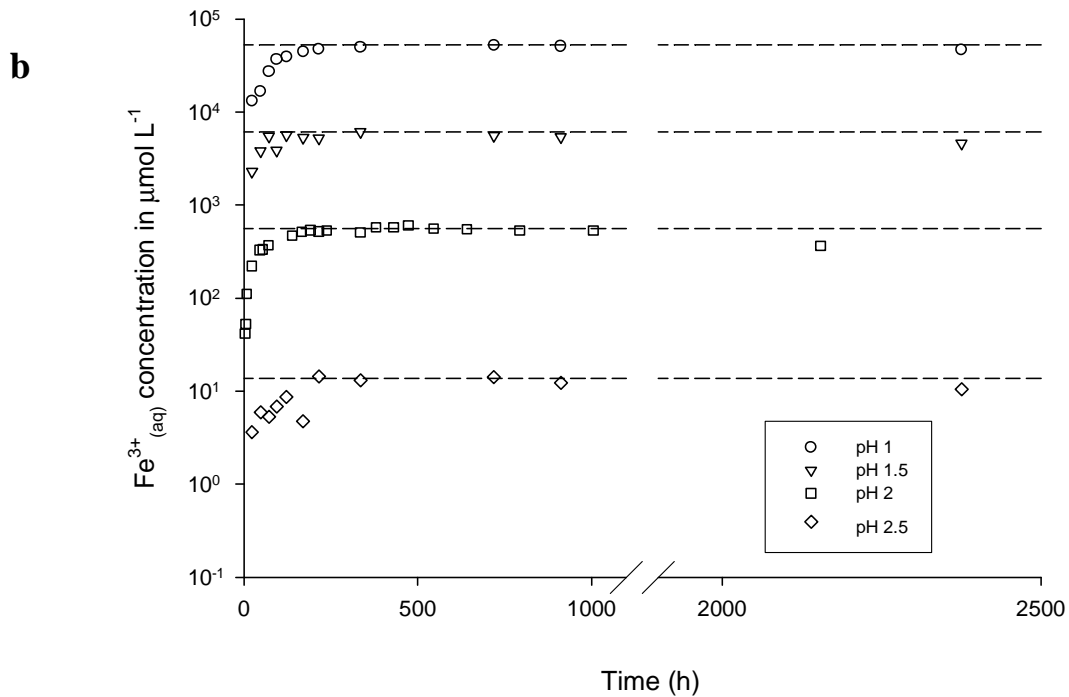


Figure 4.1.b. Build-up of during HFO dissolution at pH 1, 1.5, 2 and 2.5. The dotted lines represent the maximum concentrations used to calculate the solubility product of HFO.

When plotted on a logarithmic scale against pH, the computed Fe^{3+} activities, $a_{\text{Fe}^{3+}}$, exhibited slopes that were close, but not equal, to the theoretical stoichiometric value of -3 expected for pure Fe(III) oxyhydroxides (Figure 4.2). The slopes varied from -2.60 (LSA hematite) to -2.84 (goethite). Deviation from ideal stoichiometry has been systematically observed in studies on Fe(III) oxyhydroxide solubility (Biedermann and Chow, 1966; Byrne and Luo, 2000; Byrne et al., 2000; Dousma and De Bruyn, 1978; Fox, 1988; Murphy et al., 1976; Spiro et al., 1966). Following (Fox, 1988), solubility products, $^*K_{so}$, were therefore expressed as:

$$^*K_{so} = a_{\text{Fe}^{3+}} \times a_{\text{H}^+}^{-n} \quad (4.1)$$

where $-n$ is the slope between $\log a_{\text{Fe}^{3+}}$ and pH. The average solubility products and stoichiometric ratios $-n$ for the investigated Fe(III) phases are listed in Table 4.1.

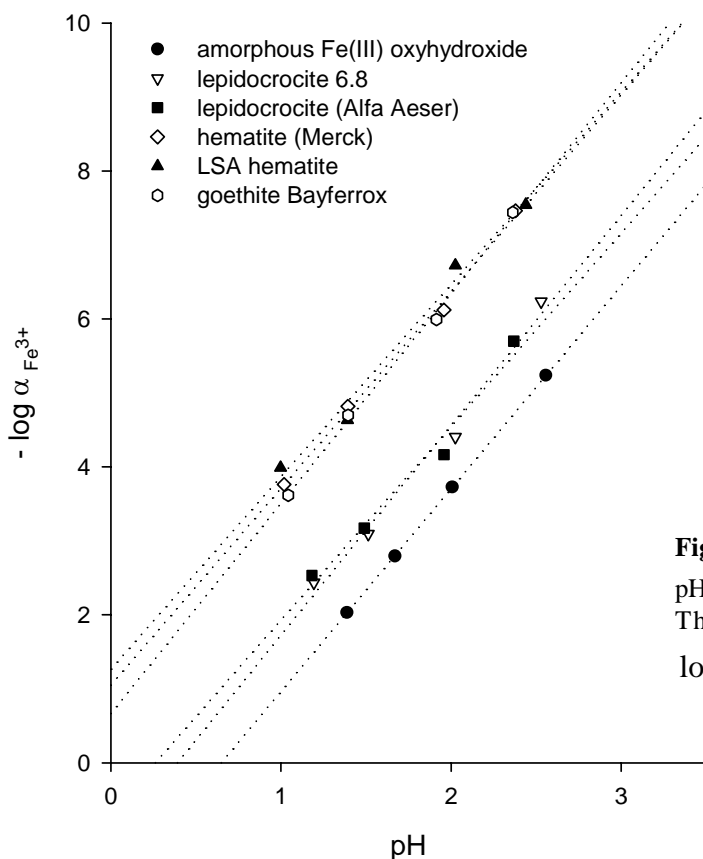


Figure 4.2. Activities of $\text{Fe}_{(\text{aq})}^{3+}$ as a function of pH for the various Fe(III) oxyhydroxides at 25°C. The dotted lines are linear fits of $\log a_{\text{Fe}^{3+}}$ versus pH, for the individual minerals.

4.3.2 Dialysis bag method versus pe-pH titrations

The solubility of the same HFO as used here was previously determined by measuring the redox potential of Fe^{2+} -amended mineral suspensions over pH range 4-7 (Bonneville et al., 2004). The values of $\log ^*K_{so}$ (1.90 ± 0.13) and n (-2.71) obtained from these pe-pH titrations are in excellent agreement with those derived from the dialysis bag dissolution experiments ($\log ^*K_{so} = 1.78 \pm 0.04$; $n =$

-2.74). Thus, for HFO, the two methods yielded internally consistent solubilities, despite the very different experimental approaches and pH conditions. The ranges of stoichiometric ratios n were also similar for both methods (Table 4.1), and comparable to n values reported in the literature for a variety of Fe(III) oxyhydroxides (Biedermann and Chow, 1966; Byrne and Luo, 2000; Byrne et al., 2000; Dousma and De Bruyn, 1978; Fox, 1988; Murphy et al., 1976; Spiro et al., 1966).

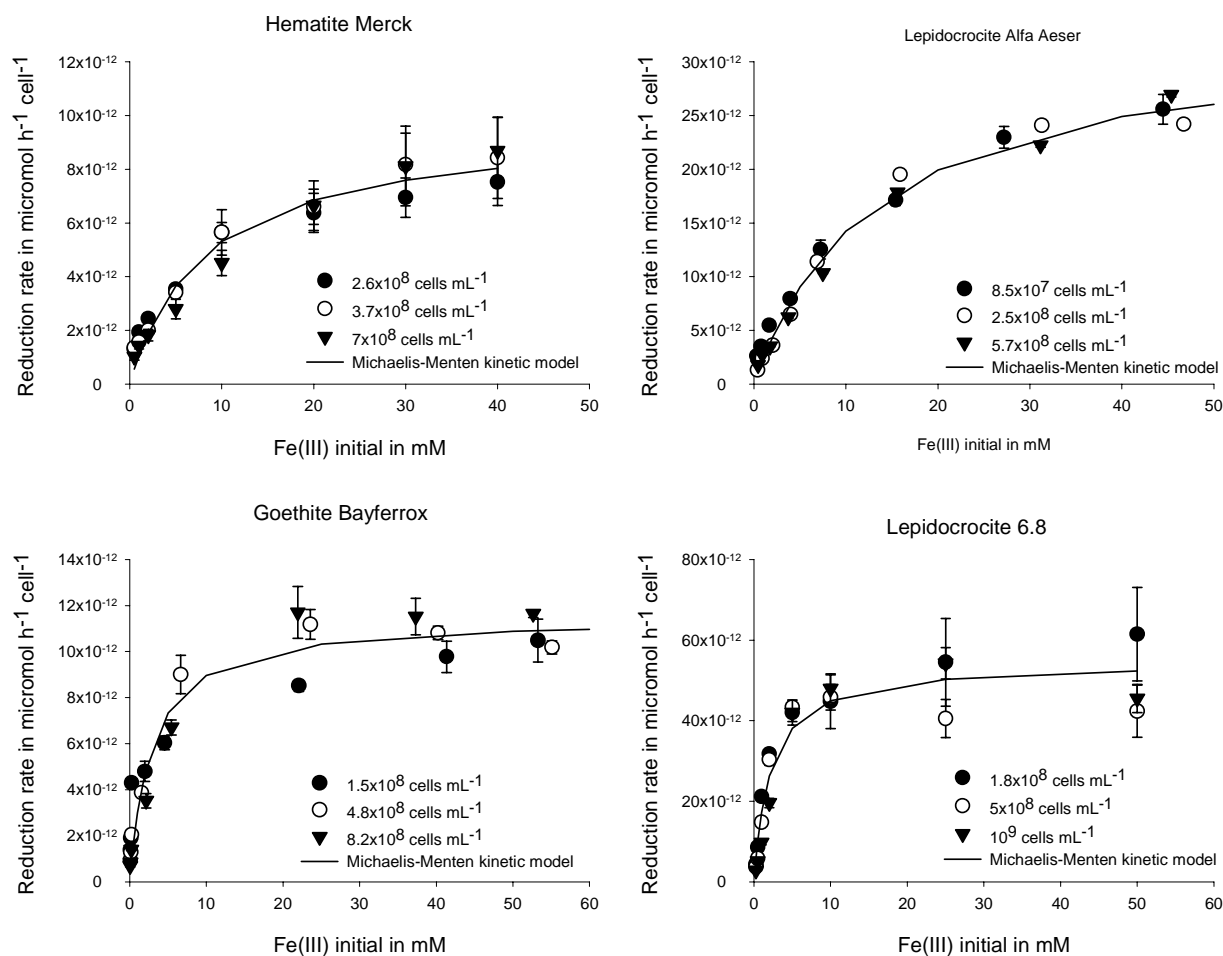


Figure 4.3: Cell-normalized rates of Fe(III) reduction by *S. putrefaciens* as a function of the initial concentrations of Fe(III) substrate. Errors bars for the rates indicate the standard deviations on the slopes of the linear regressions of the total Fe²⁺ concentration *versus* time, for the 24 hours duration of the incubations. The solid lines are the best fits of Equation (4.2) to the data.

4.3.3 Microbial Fe(III) reduction kinetics

Similarly to previous results (Bonneville et al., 2004), the build-up of total Fe²⁺ was quasi-linear over the 24 hours the mineral-bacteria incubations lasted, under all conditions tested (data not shown). Iron reduction rates were calculated by linear least square regression of total Fe²⁺ concentration versus time over the duration of the incubations. The rates exhibited saturation with increasing mineral loading

(Figure 4.3), and were fitted to the Michaelis-Menten rate expression:

$$R = v_{\max} \cdot B \cdot \frac{[\text{Fe(III)}]}{K_m + [\text{Fe(III)}]} \quad (4.2)$$

where v_{\max} is the maximum Fe(III) reduction rate per cell, B is the cell density, K_m is the apparent affinity constant for the Fe(III) solid substrate, and $[\text{Fe(III)}]$ is the initial substrate concentration per unit volume of suspension. The optimized values of the maximum cell-normalized Fe(III) reduction rates for the minerals considered here are listed in Table 4.1, together with values obtained previously (Bonneville et al., 2004).

On a log-log plot, the maximum cell-normalized rates of iron reduction by *S. putrefaciens* and the solubility products of the corresponding Fe(III) oxyhydroxides exhibited a linear relationship (Figure 4.4):

$$\log v_{\max} (\text{mol h}^{-1} \text{ cell}^{-1}) = 0.40 \log^* K_{so} - 16.80 \quad (4.3)$$

($r^2 = 0.90$). A significantly weaker correlation was observed between v_{\max} and the specific surface areas of the Fe(III) solids ($r^2 = 0.54$ on a log-log scale).

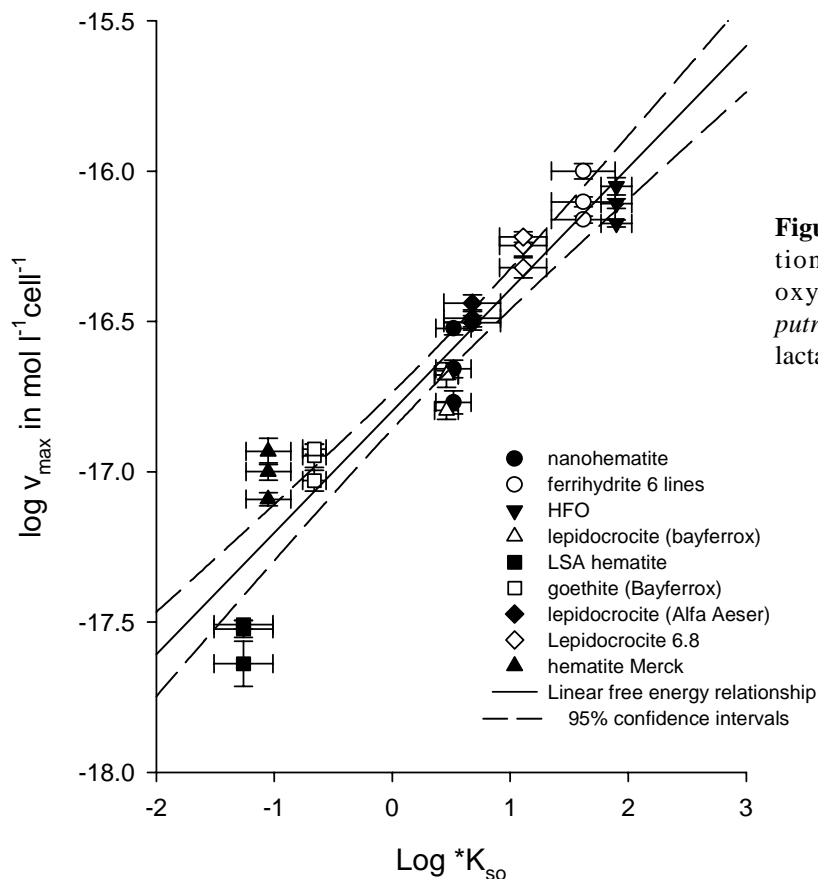


Figure 4.4: Linear Free Energy Relationship (LFER) for Fe(III) oxyhydroxide reduction by *S. putrefaciens* in the presence of excess lactate, at pH 7 and 25°C.

4.4 Discussion

The Linear Free Energy Relationship (LFER) in Figure 4.4 includes a wide range of Fe(III) oxyhydroxides, from soluble, amorphous HFO to insoluble, crystalline minerals, such as goethite and hematite. In itself, the LFER is a purely empirical relationship. Nonetheless, the trend between v_{\max} and mineral solubility implies that, somehow, the iron reducing activity of *S. putrefaciens* is a function of the structure and, hence, the energetics of the mineral Fe(III) substrate. Furthermore, a LFER usually points to a common rate controlling process in a reaction series. In the absence of an added electron shuttle, the reduction of Fe(III) minerals by *S. putrefaciens* requires direct contact of the bacterium with the solid (Arnold et al., 1986; Caccavo and Das, 2002). That is, under the experimental conditions considered, potential reaction mechanisms are restricted to those where electron transfer occurs at the interface between the cell membrane and the mineral surface (Figure 4.5).

A dependence of the iron reduction rate on mineral solubility is expected if the iron reducing factors of the cell membrane (i.e., the “Fe(III) reductases”) transfer electrons exclusively to $\text{Fe}_{(\text{aq})}^{3+}$ dissolving from the mineral surface (reaction path I, II and III, Figure 4.5). A higher concentration of $\text{Fe}_{(\text{aq})}^{3+}$ associated with a more soluble Fe(III) oxyhydroxide would then lead to a higher net reduction rate. However, such a direct mineral solubility control implies a linear dependence of the reduction kinetics on the concentration of $\text{Fe}_{(\text{aq})}^{3+}$ and, therefore, a LFER with a slope approaching one, which is not observed (Equation 4.3). (Note: the slope would be exactly one if the stoichiometric ratio, n , was the same for all mineral phases considered.)

A comparison of the reduction rates of dissolved organic Fe(III) complexes with those of Fe(III) oxyhydroxides further indicates that the origin of the observed LFER is unlikely due to a direct equilibrium control on the $\text{Fe}_{(\text{aq})}^{3+}$ concentration. For example, the equilibrium (as hexaquo ions and hydroxide complexes) concentrations for Fe(III)-NTA and Fe(III)-salicylate are similar to those of LSA hematite and HFO, respectively. The iron reduction rates by *S. putrefaciens* of the organic complexes, however, are at least one order of magnitude higher than the highest rates observed here for HFO (Haas and Dichristina, 2002).

Mechanisms whereby electron transfer (ET) occurs directly from a cell-bound reductase to a Fe(III) center of the solid thus appear more plausible. The reduction kinetics may then be controlled by either the electron transfer (step B, Figure 4.5) or the subsequent release of Fe(II) to solution (step C, Figure 4.5). Rate constants of outer sphere ET between the heme center of cytochrome OmcA, a putative c-type cytochrome responsible for Fe(III) reduction isolated from *S. oneidensis*, and different iron oxyhydroxides are estimated to range between 10^4 and 10^{12} s^{-1} (Neal et al., 2003).

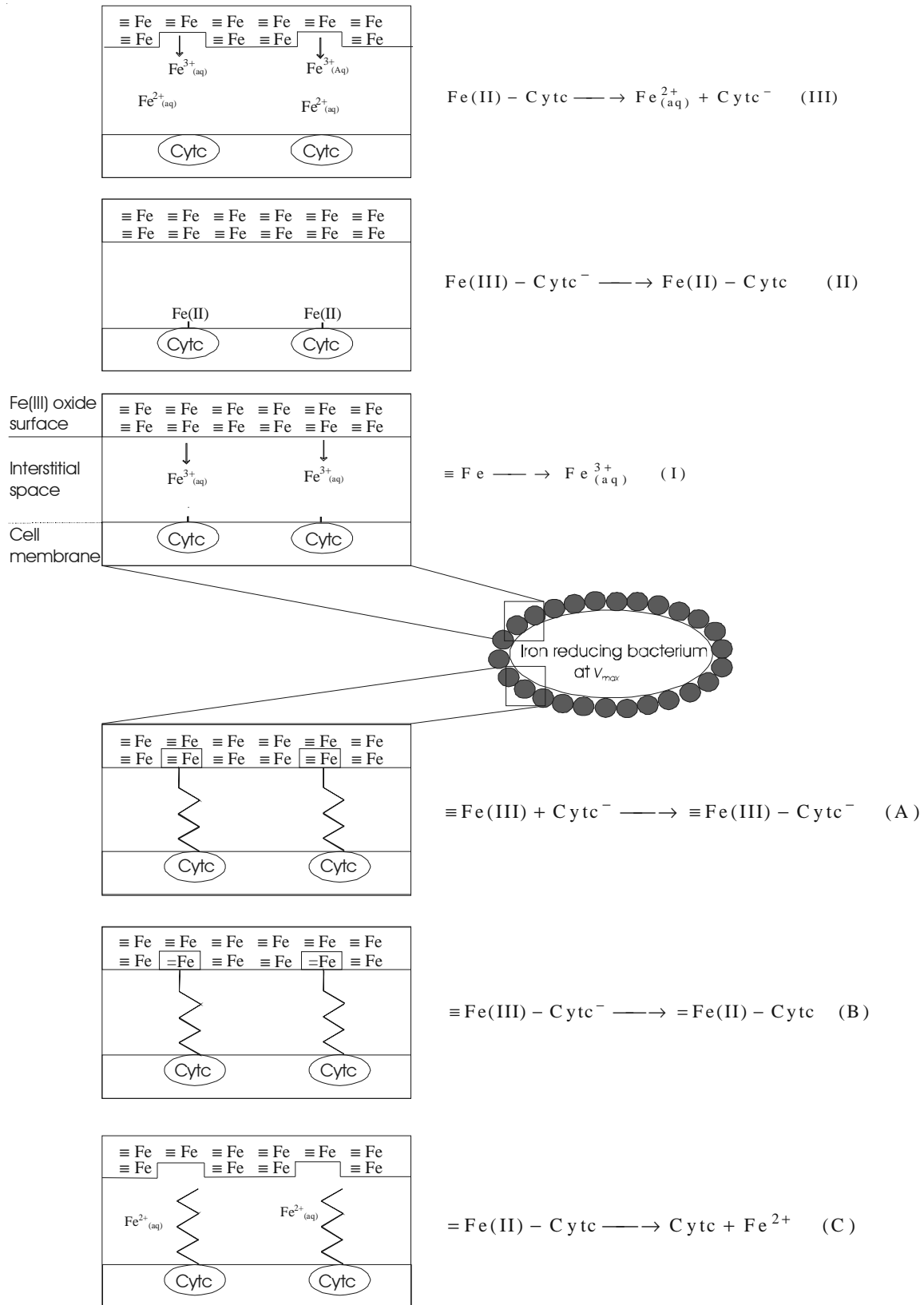


Figure 4.5: Schematic representation of iron reduction pathways in the contact area between the membrane of a *S. putrefaciens* cell and an Fe(III) oxyhydroxide mineral. Pathway I-III requires the non-reductive dissolution of Fe^{3+} prior to electron transfer from a Fe(III) reductase of the cell membrane. Pathway A-C assumes direct electron transfer to a structural Fe(III) center of the mineral. In C, the Fe^{2+} released to solution is shown to correspond to the reduced Fe(III) center. However, as a result electron transport through the lattice, the sites of Fe^{3+} reduction and Fe^{2+} detachment do not necessarily coincide (Rosso et al., 2003).

Combining these rate constants with an estimate of the number of c-type cytochromes at the surface of *S. putrefaciens* (7.5×10^{19} mol cell⁻¹)* yields reduction rates in the range 10^{-11} - 10^{-5} mol h⁻¹ cell⁻¹. Even the lowest estimated ET rates are several orders of magnitude faster than the highest v_{\max} values obtained here, suggesting that ET is not the rate controlling process for the reduction of Fe(III) oxyhydroxides by *S. putrefaciens*. In a similar fashion, it has been shown that outer sphere ET is not limiting the rate of reduction of hematite by hydroquinone (Stack et al., 2004).

Studies on the reductive dissolution kinetics of Fe(III) oxyhydroxides by sulfide (Dos Santos Afonso and Stumm, 1992; Poulton, 2003) and oxalate or ascorbate (Stumm and Sulzberger, 1992; Sulzberger et al., 1989; Suter et al., 1991; Zinder et al., 1986) have concluded that Fe(II) detachment from the mineral surface is the rate limiting step. Differences in abiotic reduction kinetics among solids reflect differences in the surface lattice structure and, hence, the bonding environments of the Fe(II) centers prior to detachment. A similar dependence of the reduction of oxyhydroxides by *S. putrefaciens* on the mineral structure could be at the origin of the observed LFER.

Following Wehrli (1990), the dynamic attachment and detachment of a divalent metal cation Me(II) at the mineral-water interface can be expressed as:

$$-\frac{d[\text{Me(II)}(aq)]}{dt} = K_{os} k_{ads} [\text{Me(II)}(aq)] [\equiv \text{Fe} - \text{OH}] - k_{des} [\equiv \text{Fe} - \text{OMe}^+] \quad (4.4)$$

which, at equilibrium, yields

$$k_{des} = \frac{-K_{os} k_{ads} [\text{Me(II)}(aq)] [\equiv \text{Fe} - \text{OH}]}{[\equiv \text{Fe} - \text{OMe}^+]} \quad (4.5)$$

where $[\text{Me(II)}(aq)]$ is the dissolved concentration of the divalent ion in mol L⁻¹, $[\equiv \text{Fe} - \text{OH}]$ is the concentration of free sorption sites, $[\equiv \text{Fe} - \text{OMe}^+]$ is the concentration of inner-sphere Me(II) complexes at the surface of the Fe(III) oxyhydroxides, K_{os} is the dimensionless outer sphere complex formation constant, k_{ads} is the rate constant of adsorption in L mol⁻¹ h⁻¹, and k_{des} is the rate constant for detachment of Me(II) from the surface in h⁻¹.

To compute values of k_{des} with Equation (4.5), values of K_{os} were derived following the procedure described in Jeon et al. (2004), whereas k_{ads} for Fe²⁺ was estimated to be 3.1×10^5 h⁻¹ based on the LFER between adsorption rate constants and water exchange constants of divalent metals (Hachiya et al., 1984; Wehrli et al., 1990). Surface charges, and the equilibrium concentrations of $[\equiv \text{Fe} - \text{OH}]$ and

* Based on 4.5×10^{-3} μmol c-type cytochrome per mg protein for *S. putrefaciens* grown aerobically (Picardal et al., 1993), plus an average protein content of 56% dry weight and a dry cell mass of 3×10^{-13} g cell⁻¹.

$[\equiv\text{Fe}-\text{OFe}^+]$ were calculated with MINEQL+, using the surface complexation constants for nano hematite, goethite and 6-line ferrihydrite taken from (Liger et al., 1999). The calculations of k_{des} were restricted to these three Fe(III) oxyhydroxides, because the corresponding solids used by the authors of (Liger et al., 1999) in their study of Fe^{2+} adsorption were identical to the ones used here.

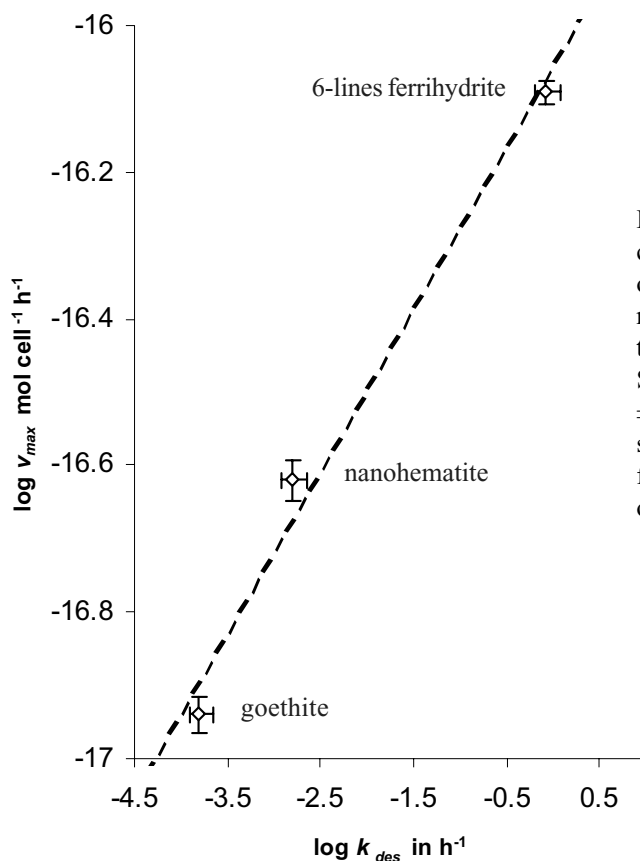


Figure 4.6 Positive correlation between the rate constants of Fe^{2+} detachment from three Fe(III) oxyhydroxide minerals and the corresponding maximum rates of iron reduction by *S. putrefaciens* in the presence of excess lactate, at pH 7 and 25°C. Systematic error on k_{des} values was estimated to be $\pm 30\%$ of the k_{des} values. For v_{max} , errors bars are the standard deviation of the global Michaelis-Menten fit to the 24 experiments for each Fe(III) oxyhydroxides (Bonneville et al., 2004).

The resulting estimates of k_{des} for goethite, nano hematite, and 6 lines ferrihydrite are $1.6 \times 10^{-4} \text{ h}^{-1}$, $1.6 \times 10^{-3} \text{ h}^{-1}$ and $8.5 \times 10^{-1} \text{ h}^{-1}$, respectively. The rate constants for detachment of Fe^{2+} from Fe(III) oxyhydroxide minerals fall in the range reported for other divalent ions, such as Zn^{2+} and Cd^{2+} (Jeon et al., 2004). Furthermore, the order of magnitude variation in k_{des} between the three Fe(III) solids is consistent with the strong dependence on mineralogy of the release rates of labeled ^{55}Fe observed during isotopic exchange between aqueous Fe^{2+} and Fe(III) oxyhydroxides (Pedersen et al., 2005).

The rate constants of Fe^{2+} detachment show a positive correlation with the maximum rates of reduction of the corresponding Fe(III) oxyhydroxides by *S. putrefaciens* (Figure 4.6). This observation, along with the other lines of evidence presented earlier, implies that the LFER linking the microbial reduction kinetics and solubility of Fe(III) oxyhydroxides (Figure 4.4) most likely originates in the rate-limiting role of the detachment of Fe^{2+} from the mineral surface, following electron transfer from the cell to structural Fe(III).

References

- Anderson R. T. and Lovley D. R. (1999) Naphthalene and benzene degradation under Fe(III)-reducing conditions in petroleum-contaminated aquifers. *Biorem. J.* **3**, 121-135.
- Arnold R. G., DiChristina T. J., and Hoffmann M. R. (1986) Bioextraction of iron from iron oxides, pp. 207 pp. W. M. Keck Lab. Environ. Eng., California Inst. Technol., Pasadena, CA, USA.
- Biedermann G. and Chow J. T. (1966) Hydrolysis of metal ions. LVII. Hydrolysis of the Fe(III) ion and the solubility product of the Fe(OH)₂. *Acta Chem. Scand.* **20**, 1376-1388.
- Bonneville S., Van Cappellen P., and Behrends T. (2004) Microbial reduction of iron(III) oxyhydroxides: effects of mineral solubility and availability. *Chem. Geol.* **212**, 255-268.
- Byrne R. H. and Luo Y.-R. (2000) Direct observations of nonintegral hydrous ferric oxide solubility products: $k^*s_0=[Fe^{3+}][H^+]^{-2.86}$. *Geochim. Cosmochim. Acta* **64**, 1873-1877.
- Byrne R. H., Luo Y.-R., and Young R. W. (2000) Iron hydrolysis and solubility revisited: observations and comments on iron hydrolysis characterizations. *Mar. Chem.* **70**, 23-35.
- Caccavo F. J. and Das A. (2002) Adhesion of dissimilatory Fe(III)-reducing bacteria to Fe(III) minerals. *Geomicrobiol. J.* **19**, 161-177.
- Canfield D. E., Thamdrup B., and Hansen J. W. (1993) The anaerobic degradation of organic matter in Danish coastal sediments: iron reduction, manganese reduction, and sulfate reduction. *Geochim. Cosmochim. Acta* **57**, 3867-3883.
- Cornell R. M., Schneider W., and Giovanoli R. (1991) Preparation and characterization of colloidal α -iron oxide hydroxide (FeOOH) with a narrow size distribution. *J. Chem. Soc. Faraday Trans.* **87**, 869-873.
- DiChristina T. J., Arnold R. G., Lidstrom M. E., and Hoffmann M. R. (1988) Dissimilative iron reduction by the marine eubacterium *Alteromonas putrefaciens* strain 200. *Water Sci. Technol.* **20**, 69-79.
- DiChristina T. J., Moore C. M., and Haller C. A. (2002) Dissimilatory Fe(III) and Mn(IV) reduction by *Shewanella putrefaciens* requires ferE, a homolog of the pule (gspE) type II protein secretion gene. *J. Bacteriol.* **184**, 142-151.
- Dos Santos Afonso M. and Stumm W. (1992) Reductive Dissolution of Iron(III) (Hydr)oxides by Hydrogen Sulfide. *Langmuir* **8**, 1671-1675.
- Dousma J. and De Bruyn P. L. (1978) Hydrolysis-precipitation studies of iron solutions. II. Aging studies and the model for precipitation from iron(III) nitrate solutions. *J. Colloid Interface Sci.* **64**, 154-170.
- Fox L. E. (1988) The solubility of colloidal ferric hydroxide and its relevance to iron concentrations in river water. *Geochim. Cosmochim. Acta* **52**, 771-777.
- Fox P. M. and Doner H. E. (2002) Trace element retention and release on minerals and soil in a constructed wetland. *J. Environ. Qual.* **31**, 331-338.
- Fukushima M. and Tatsumi K. (1999) Light acceleration of iron(III) reduction by humic acid in the aqueous solution. *Colloids and Surf. A* **155**, 249-258.
- Haas J. R. and DiChristina T. J. (2002) Effects of Fe(III) Chemical Speciation on Dissimilatory Fe(III) Reduction by *Shewanella putrefaciens*. *Environ. Sci. Technol.* **36**, 373-380.
- Hachiya K., Sasaki M., Ikeda T., Mikami N., and Yasunaga T. (1984) Static and kinetic studies of adsorption-desorption of metal ions on a γ -alumina surface. 2. Kinetic study by means of pressure-jump technique. *J. Phys. Chem.* **88**, 27-31.
- Jakobsen R. and Postma D. (1999) Redox zoning, rates of sulfate reduction and interactions with Fe-reduction and methanogenesis in a shallow sandy aquifer, Romo, Denmark. *Geochim. Cosmochim. Acta* **63**, 137-151.
- Jeon B.-H., Dempsey B. A., Burgos W. D., Royer R. A., and Roden E. E. (2004) Modeling the sorption kinetics of divalent metal ions to hematite. *Water Res.* **38**, 2499-2504.
- Kaplan D. I., Bertsch P. M., and Adriano D. C. (1997) Mineralogical and physicochemical differences between mobile and nonmobile colloidal phases in reconstructed pedons. *Soil Sci. Soc. Am. J.* **61**, 641-649.
- Kuma K., Nakabayashi S., Suzuki Y., and Matsunaga K. (1992) Dissolution rate and solubility of colloidal hydrous ferric oxide in seawater. *Mar. Chem.* **38**, 133-143.
- Larsen O. and Postma D. (2001) Kinetics of reductive bulk dissolution of lepidocrocite, ferrihydrite and goethite. *Geochim. Cosmochim. Acta* **65**, 1367-1379.
- Liger E., Charlet L., and Van Cappellen P. (1999) Surface catalysis of uranium (VI) reduction by iron(II). *Geochim. Cosmochim. Acta* **63**, 2939-2955.
- Lovley D. R. and Phillips E. J. P. (1989) Requirement for a microbial consortium to completely oxidize glucose in iron(III)-reducing sediments. *Appl. Environ. Microbiol.* **55**, 3234-3236.
- Lovley D. R., Phillips E. J. P., and Lonergan D. J. (1991) Enzymic versus nonenzymic mechanisms for iron(III) reduction in aquatic sediments. *Environ. Sci. Technol.* **25**, 1062-1067.

- Luther G. W., III, Giblin A., Howarth R. W., and Ryans R. A. (1982) Pyrite and oxidized iron mineral phases formed from pyrite oxidation in salt marsh and estuarine sediments. *Geochim. Cosmochim. Acta* **46**, 2665-2669.
- Lyngkilde J. and Christensen T. H. (1992) Redox zones of a landfill leachate pollution plume (Vejen, Denmark). *J. Contam. Hydrol.* **10**, 273-289.
- Murphy P. J., Posner A. M., and Quirk J. P. (1976) Characterization of hydrolyzed ferric ion solutions. A comparison of the effects of various anions on the solutions. *J. Colloid Interface Sci.* **56**, 312-319.
- Neal A. L., Rosso K. M., Geesey G. G., Gorby Y. A., and Little B. J. (2003) Surface structure effects on direct reduction of iron oxides by *Shewanella oneidensis*. *Geochim. Cosmochim. Acta* **67**, 4489-4503.
- Pedersen H. D., Postma D., Jakobsen R., and Larsen O. (2005) Fast transformation of iron oxyhydroxides by the catalytic action of aqueous Fe(II). *Geochim. Cosmochim. Acta* **69**, 3967-3977.
- Petruzzelli L., Celi L., and Ajmone-Marsan F. (2005) Effects of soil organic fractions on iron oxide biodissolution under anaerobic conditions. *Soil Sci.* **170**, 102-109.
- Picardal F. W., Arnold R. G., Couch H., Little A. M., and Smith M. E. (1993) Involvement of cytochromes in the anaerobic biotransformation of tetrachloromethane by *Shewanella putrefaciens* 200. *Appl. Environ. Microbiol.* **59**, 3763-3770.
- Poulton S. W. (2003) Sulfide oxidation and iron dissolution kinetics during the reaction of dissolved sulfide with ferrihydrite. *Chem. Geol.* **202**, 79-94.
- Roden E. E. and Edmonds J. W. (1997) Phosphate mobilization in iron-rich anaerobic sediments. Microbial Fe(III) oxide reduction versus iron-sulfide formation. *Arch. Hydrobiol.* **139**, 347-378.
- Roden E. E. and Zachara J. M. (1996) Microbial reduction of crystalline iron(III) oxides: Influence of oxide surface area and potential for cell growth. *Environ. Sci. Technol.* **30**, 1618-28.
- Rosso K. M., Zachara J. M., Fredrickson J. K., Gorby Y. A., and Smith S. C. (2003) Nonlocal bacterial electron transfer to hematite surfaces. *Geochim. Cosmochim. Acta* **67**, 1081-1087.
- Scheidegger A., Borkovec M., and Sticher H. (1993) Coating of silica sand with goethite: preparation and analytical identification. *Geoderma* **58**, 43-65.
- Schwertmann U. and Cornell R. M. (1991) *Iron Oxides in the Laboratory: Preparation and Characterization*. Weinheim.
- Spiro T. G., Allerton S. E., Renner J., Terzis A., Bils R., and Saltman P. (1966) The hydrolytic polymerization of iron(III). *J. Amer. Chem. Soc.* **88**, 2721-2726.
- Stack A. G., Rosso K. M., Smith D. M. A., and Eggleston C. M. (2004) Reaction of hydroquinone with hematite II. Calculated electron-transfer rates and comparison to the reductive dissolution rate. *J. Colloid Interface Sci.* **274**, 442-450.
- Stumm W. and Sulzberger B. (1992) The cycling of iron in natural environments: considerations based on the laboratory studies of heterogeneous redox processes. *Geochim. Cosmochim. Acta* **56**, 3233-3257.
- Sulzberger B., Suter D., Siffert C., Banwart S., and Stumm W. (1989) Dissolution of iron(III) (hydr)oxides in natural waters; laboratory assessment on the kinetics controlled by surface coordination. *Mar. Chem.* **28**, 127-144.
- Suter D., Banwart S., and Stumm W. (1991) Dissolution of hydrous iron(III) oxides by reductive mechanisms. *Langmuir* **7**, 809-813.
- Tipping E., Woof C., and Cooke D. (1981) Iron oxide from a seasonally anoxic lake. *Geochim. Cosmochim. Acta* **45**, 1411-1419.
- Van Breemen N. (1988) Effects of seasonal redox processes involving iron on the chemistry of periodically reduced soils. *NATO ASI Ser., Ser. C* **217**, 797-809.
- van Breukelen B. M., Griffioen J., Roling W. F. M., and van Verseveld H. W. (2004) Reactive transport modeling of biogeochemical processes and carbon isotope geochemistry inside a landfill leachate plume. *J. Contam. Hydrol.* **70**, 249-269.
- Viollier E., Inglett P. W., Hunter K., Roychoudhury A. N., and Van Cappellen P. (2000) The ferrozine method revisited: Fe(II)/Fe(III) determination in natural waters. *Appl. Geochem.* **15**, 785-790.
- Wehrli B., Ibric S., and Stumm W. (1990) Adsorption kinetics of vanadyl(IV) and chromium(III) to aluminum oxide: Evidence for a two-step mechanism. *Colloids Surf.* **51**, 77-88.
- Zinder B., Furrer G., and Stumm W. (1986) The coordination chemistry of weathering: II. Dissolution of iron(III) oxides. *Geochim. Cosmochim. Acta* **50**, 1861-1869.

Chapter V

Thermodynamic constraints on microbial Fe(III) oxyhydroxide reduction

Steeve Bonneville, Thilo Behrends, Ralf Haese and Philippe Van Cappellen.

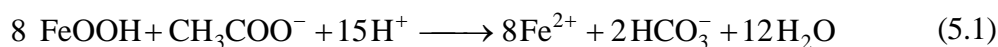
5.1 Introduction

Dissimilatory Fe(III) reduction is an energy yielding pathway of major importance in the biogeochemistry of anaerobic, non-sulfidogenic subsurface environments. The microbiology and environmental significance of microbial Fe(III) oxyhydroxide reduction have been extensively investigated over the last decades (Arnold et al., 1986; Burdige, 1993; Fredrickson and Gorby, 1996; Lovley, 1991; Nealson and Saffarini, 1994; Roden and Wetzal, 2002; Thamdrup, 2000). Solid-phase Fe(III) oxyhydroxides are used as terminal electron acceptors for the oxidation of organic matter and generate soluble Fe²⁺. In addition, microbial iron reduction can have a major impact on the mobility of metals, phosphate, radionuclides and organic contaminants (Behrends and Van Cappellen, 2005; Roden and Edmonds, 1997; Röling et al., 2001; Zachara et al., 2001). As a consequence of the pivotal role of microbial Fe(III) oxyhydroxide reduction in subsurface biogeochemistry, there is great interest in identifying and quantifying the key factors controlling the rate and the extent of dissimilatory Fe(III) reduction.

In the anaerobic food chain, the iron reducing bacteria compete with sulfate reducers and methanogens for electron donors generated by fermentative microorganisms. Building on the concept that competition for a common substrate is regulated by the relative energy yields of the competing metabolic pathways (Winfrey and Zeikus, 1977), Achnich et al. (1995) and Lovley et al. (1994) proposed that, in the presence of bioavailable Fe(III) oxyhydroxides, iron reducers should outcompete sulfate reducers and methanogens. These authors presented evidence that the threshold H₂ concentrations required to sustain metabolic activity increases in the following sequence: Fe(III) reduction < sulfate reduction < methanogenesis.

In contrast to respiratory pathways that rely on dissolved terminal electron acceptors, dissimilatory iron reduction depends on the properties of a solid-state substrate. These properties include, for example, the solubility (Bonneville et al., 2004), specific surface area (Roden and Zachara, 1996), and surface chemical properties. The solubilities of Fe(III) oxyhydroxides in sedimentary environments range over at least 3-4 orders of magnitude (Cornell and Schwertmann, 1996), due to differences in mineralogy, impurity contents, crystal size, and degree of isomorphous substitution. Therefore, the energy yields of dissimilatory iron reduction vary significantly from one Fe(III) oxyhydroxide to another.

For instance, the reduction of goethite coupled to acetate oxidation by *Geobacter metallireducens* (Lovley et al., 1993):



generates the chemical energy required to maintain the metabolism of the organism. In theory, the energetic gain for the bacteria, in other words $-\Delta G_r$ of reaction (5.1), decreases as the aqueous Fe^{2+} activity increases due to iron reducing activity. Liu et al. (2001) calculated that the reduction of goethite by *Shewanella putrefaciens* ceased when the Gibbs free energy of the reaction (ΔG_r) reached -22 kJ mol^{-1} , which is close to the theoretical value of -20 kJ mol^{-1} necessary for a cell to sustain the synthesis of ATP (Schink, 1997). However, other studies do not support such a thermodynamic limitation of Fe(III) oxyhydroxide reduction. For instance, Roden and Urrutia (2002) estimate that $-\Delta G_r$ was still on the order of 40 to 50 kJ mol^{-1} , upon cessation of goethite reduction by *S. alga*.

The objective of this study is to determine whether microbial reduction of colloidal Fe(III) oxyhydroxides is thermodynamically limited. To this end, reduction experiments of nanohematite and 6-lines ferrihydrite coupled to lactate oxidation by *S. putrefaciens* were carried out in a pH-stat reactor, while monitoring the evolution of the aqueous Fe^{2+} activity and pe with time. Combined with previously determined solubility products of the Fe(III) oxyhydroxides (Bonneville et al. 2004), the experimental measurements allow us to calculate the corresponding Gibbs free energies of reaction.

5.2 Materials and Methods

5.2.1 Fe(III) oxyhydroxides

Hematite nanoparticles were prepared by adding 100 mL of a 0.1 M $\text{Fe}(\text{NO}_3)_3$ solution at a flow rate of 3 mL min^{-1} to 1 L of boiling and vigorously stirred demineralized water, according to the method described by Liger et al (1999). After cooling the suspension down to room temperature, the hematite suspension was dialyzed in demineralized water adjusted to pH 4 with 0.5 M HCl, in order to remove the nitrate counter ions from the hematite synthesis. The average grain size of the hematite nanoparticles was 8 nm ($\pm 2 \text{ nm}$), obtained from transmission electron microscopy (TEM) pictures, and the specific surface area $125 \text{ m}^2 \text{ g}^{-1}$. X-ray diffraction and ^{57}Fe Mossbauer spectroscopy analyses revealed a highly crystalline nanohematite, which nevertheless contained minor traces of ferrihydrite (D. Rancourt, University of Ottawa, personal communication).

6-lines ferrihydrite was synthesized by dissolving 20 g of $\text{Fe}(\text{NO}_3)_3$ in 2 L of demineralized water at 75°C under rapid stirring (Schwertmann and Cornell, 1991). The solution was maintained

at 75°C for 10 min and then rapidly cooled by plunging it into ice water. In order to remove the NO_3^- ions, ferrihydrite nanosuspensions were dialyzed in demineralized water adjusted to pH 4, as described above. The X-Ray diffraction pattern exhibited the six broad peaks characteristic of 6-lines ferrihydrite. TEM observations revealed spherical particles of around 8 nm diameter. The specific surface area, measured by BET (N_2), was $175 \text{ m}^2 \text{ g}^{-1}$.

5.2.2 Bacteria

Cultures of *Shewanella putrefaciens* 200R were provided by Dr. T. DiChristina, Georgia Institute of Technology, Atlanta, USA (DiChristina and DeLong, 1994; DiChristina et al., 2002). Cells were kept aerobically on Luria Bertani medium (LB) plates (Tryptone water 15 g L^{-1} , agar 15 g L^{-1} , NaCl 5 g L^{-1} , yeast 5 g L^{-1}) and routinely cultured in liquid Luria Bertani (LB) medium on a rotary shaker (150 rpm) at room temperature. The bacteria were harvested and washed just before being used in the experiments (section 5.2.3), in their late exponential-early stationary growth phase. Cell numbers were determined by epifluorescence microscopy after acridine orange staining (Hobbie et al., 1977): 100 μL of the bacterial suspensions were mixed with 4.4 mL of phosphate buffer solution (8 g L^{-1} NaCl, 2 g L^{-1} KCl, 1.44 g L^{-1} Na_2HPO_4 , 0.24 g L^{-1} KH_2PO_4), 200 μL of a 0.25 g L^{-1} acridine orange solution and 0.5 mL of a 30% formaldehyde solution. After 10 minutes, 100–200 μL of the latter suspension was transferred to a 17 mm diameter filter tower to which 5 mL phosphate buffer solution and 200 μL of acridine orange solution were added in advance. The content of the tower was mixed by swirling and then filtrated through a black $0.2 \mu\text{m}$ polycarbonate filter (Millipore). An epifluorescence microscope equipped with a camera was used to take five pictures of each filter. The counting of the cells was performed automatically using imaging software.

5.2.3 Microbial incubations

Incubations of *S. putrefaciens* and Fe(III) colloids (around 2mM Fe(III) of nanohematite or 6-lines ferrihydrite) were performed in a pH-stat batch reactor (Figure 5.1), in 20 mM NaCl and in the presence of 5 mM lactate as sole electron donor. The reactor consisted of a thermo-stated Teflon vessel containing 250 mL of suspension stirred by a magnetic bar to avoid settling of oxide particles and bacteria. Temperature was kept at 25°C. Argon gas, pre-saturated with water vapor, was continuously bubbled through the solution to keep it free of oxygen. The reaction vessel was placed in a glove box also flushed with argon during the experiments. A pH-stat system (Metrohm automatic titrino plus Xerolit pH electrode) delivered either a 0.01N HCl or 0.01N NaOH solution to maintain pH at $7 \pm$

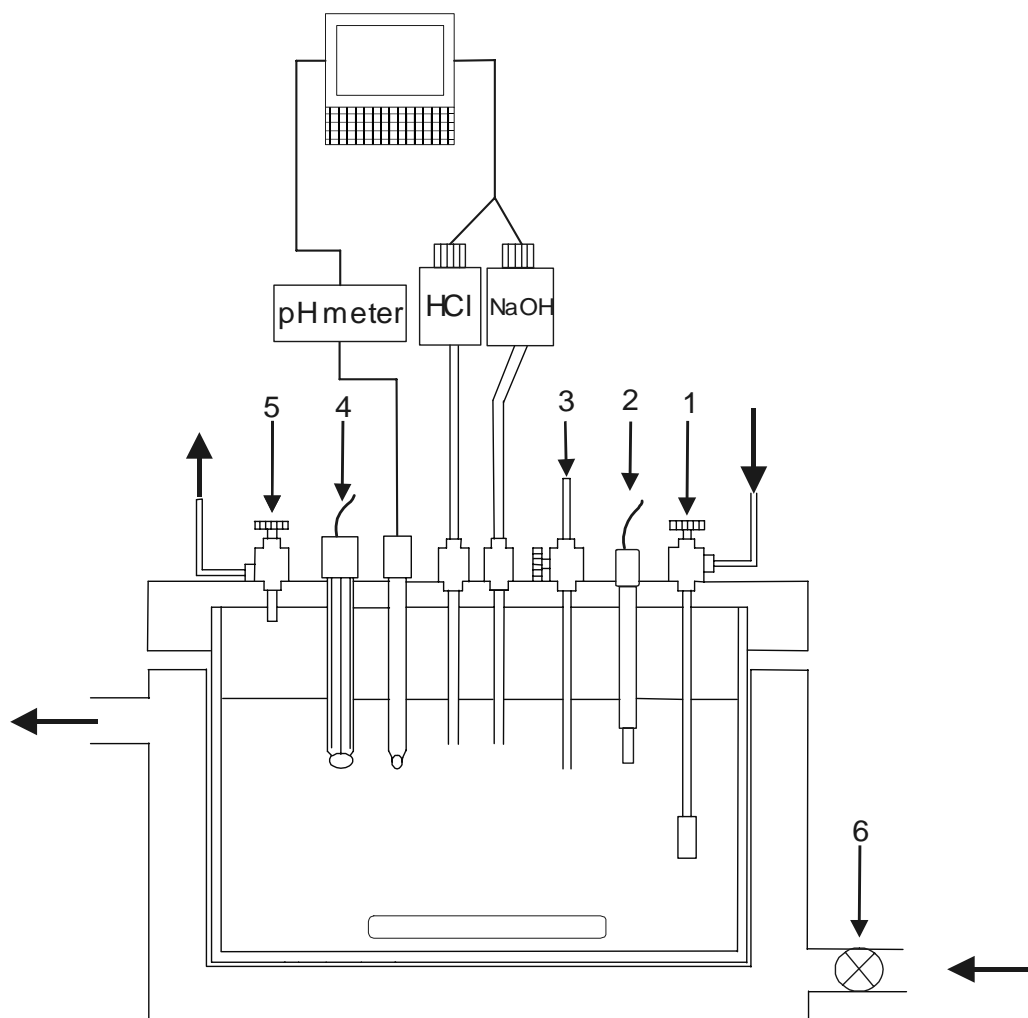


Figure 5.1: Experimental pH stat system used for the incubation experiments with *S. putrefaciens* and 6-lines ferrihydrite or nanohematite. (1) Inlet gas valve; (2) microelectrode for measurements of dissolved Fe^{2+} ; (3) sample extraction valve; (4) redox platinum electrode linked to redox meter; (5) outlet gas valve; (6) pump connected to thermostated water bath.

0.05; the volume of titrant solution added was recorded by a computer. An Ag/AgCl Orion electrode monitored the redox potential. The total Fe^{2+} concentration was measured with the ferrozine method (Viollier et al., 2000) in aliquots of suspension extracted with 0.5 M HCl for 1h. The aqueous Fe^{2+} concentration was measured by voltametry (see next section). The incubations were run until reducing activity stops, up to 300h for 6 lines ferrihydrite and 100h for nanohematite.

An additional microbial reduction experiment was performed with 6-lines ferrihydrite using *S. putrefaciens* cells that had been pre-treated with aqueous Fe^{2+} . The cells were prepared by degassing 250 mL of 20 mM NaCl solution with Ar, then adding cells to a final density of 2×10^8 cells mL^{-1} and degassing further for 20 min. at pH 7. A concentrated anoxic Fe^{2+} solution, adjusted beforehand to pH 7, was added to the cell suspension, to a final concentration of 100 μM . The evolution of the dissolved Fe^{2+} concentration was monitored by voltametry (section 5.2.4) over a period of 2.5 hours. A limited

number of suspension aliquots were sampled for the determination of total Fe²⁺ as described above. The amount of Fe²⁺ sorbed onto the cells was calculated by difference between total and dissolved Fe²⁺ concentrations.

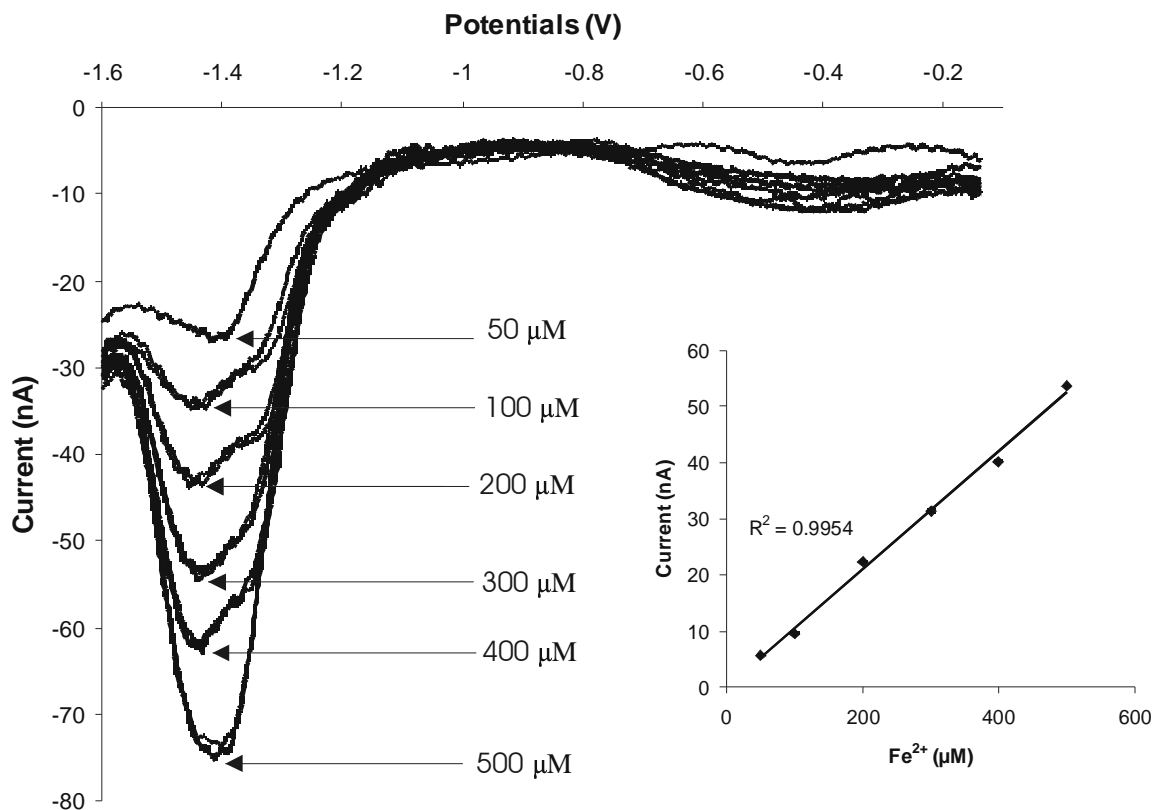
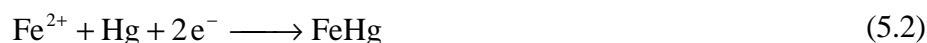


Figure 5.2: Voltammetric scans for 6 different concentrations of dissolved Fe²⁺ from 50 up to 500 μM. The peak at -1.43V is characteristic for dissolved Fe²⁺ and its height can be linearly related with the Fe²⁺ concentration.

5.2.4 Voltammetric measurements of aqueous Fe²⁺

A voltammetric technique was used to monitor the aqueous Fe²⁺ concentration during microbial iron reduction, using a reference, counter and working-electrode. The working microelectrode consisted of a gold wire within an electrochemically inert housing (glass) with, at its tip, a thin film of solid-state amalgamated mercury. The gold wire had a diameter of 100 μm. During a scan over a range of potential (typically from -0.1 to -1.6 V), redox reactions occurring at the electrode tip generate a current. Induced by the changing potential, dissolved species change their oxidation states at different positions in the potential window (Brendel and Luther, 1995). At a potential of -1.43 V, the following reaction occurs at the electrode surface:



The measurement is highly specific for aqueous Fe²⁺ due to the fact that no other reactions occur at this

potential. However, the accumulation of elemental Fe at the surface of the microelectrode may cause a measurement artefact. Therefore, a pre-conditioning step was carried out, by imposing a potential of -1 V for a period of 1 min. As shown in Figure 5.2, the peak heights recorded at -1.43 V during the potential scans exhibited a linear response, for Fe^{2+} concentrations ranging from 50 to $500\ \mu\text{M}$. The Fe^{2+} activities were calculated from the concentrations using the extended Debye-Hückel equation (Stumm and Morgan, 1995).

5.3 Results and Discussion

5.3.1 Microbial Fe(III) oxyhydroxide reduction

The total and dissolved Fe^{2+} concentrations increased near-linearly for about 100 hours during the microbial incubations with 6-lines ferrihydrite and 50 hours for nanohematite. Much higher concentrations were observed for 6-lines ferrihydrite, compared to nanohematite. The ratio between dissolved and total Fe^{2+} remained close to 1 for both solids, indicating that most of the produced Fe^{2+} remained in solution (Figure 5.3). Thus, precipitation of secondary Fe(II) mineral phases or significant adsorption of Fe^{2+} did not occur.

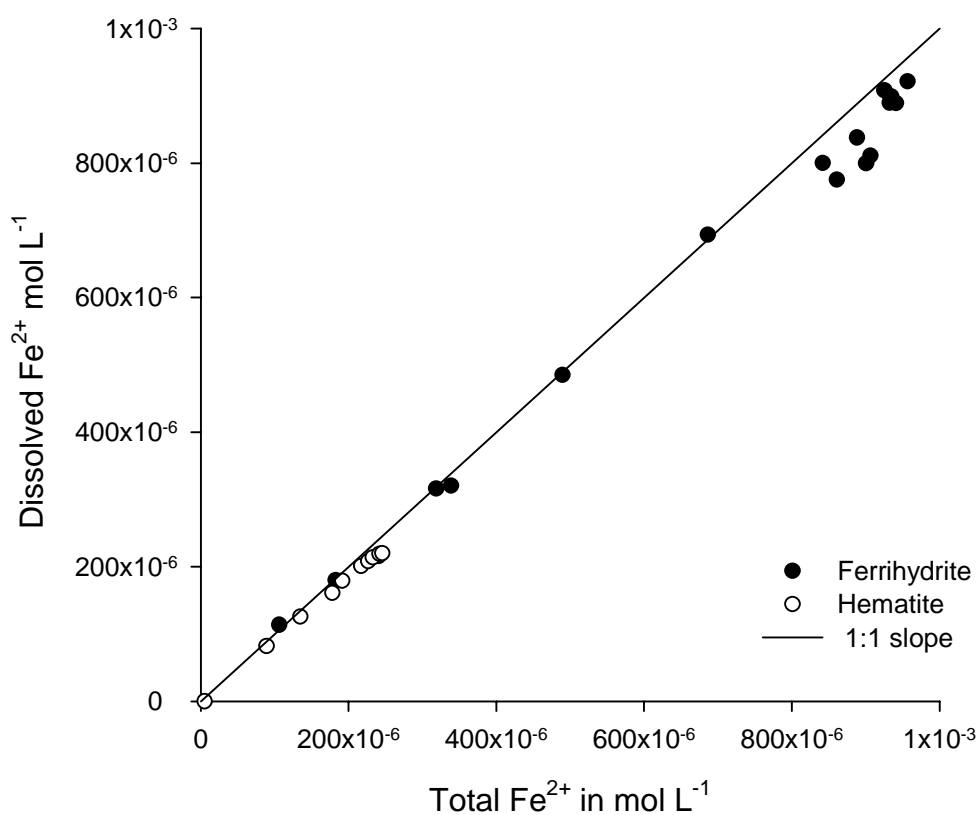
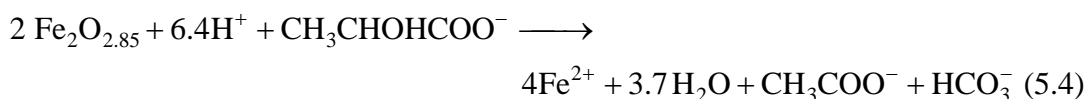
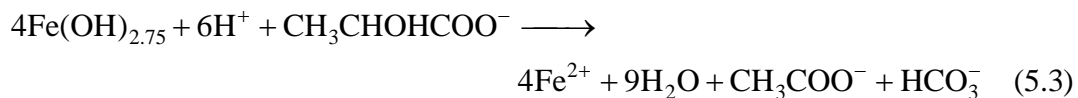


Figure 5.3: Dissolved Fe^{2+} (voltametry) versus total Fe^{2+} (1h 0.5M HCl extraction) concentrations in the microbial incubations of 6-lines ferrihydrite and nanohematite with *S. putrefaciens*.

The reduction of the Fe(III) oxyhydroxides was accompanied by the consumption of protons (equation 5.1). The amount of added H^+ required to keep pH at 7 is plotted against the Fe^{2+} produced in Figure 5.4. The initial slopes between added H^+ and produced Fe^{2+} approached 1.5 and 1.6 for 6-lines ferrihydrite and nanohematite, respectively. These slopes are consistent with the stoichiometries of the reduction reactions of the two oxyhydroxides coupled to the oxidation of lactate to acetate:



In the above reaction formulas, the dissociations of the weak acids and their influence on the proton balance are ignored, by considering only the dominating species at the experimental pH.

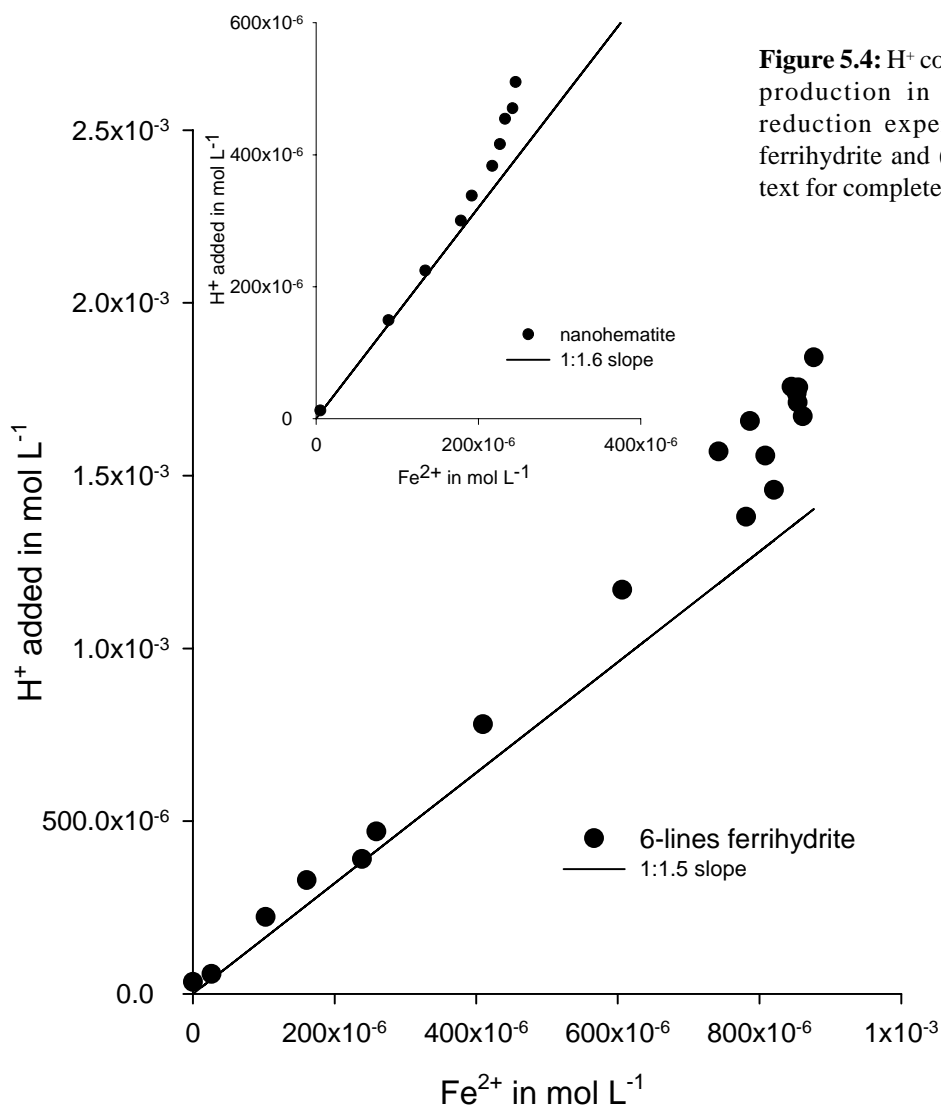


Figure 5.4: H^+ consumption versus Fe^{2+} production in the microbial iron reduction experiments: (a) 6-lines ferrihydrite and (b) nanohematite. See text for complete discussion.

The formulas for 6-lines ferrihydrite and nanohematite in equations (5.3) and (5.4) differ from the ideal stoichiometries of ferrihydrite ($\text{Fe}(\text{OH})_3$) and hematite (Fe_2O_3). The stoichiometries used are based on the pe-pH titrations carried out by Bonneville et al. (2004) on the same solids, which showed non-ideal ratios (i.e. <3) between H^+ consumption and Fe release during dissolution. This feature is systematically observed for synthetic and natural Fe(III) (oxy-)hydroxides. Reported ratios fall mostly in the range between 2 and 2.86 for various Fe(III) oxyhydroxides (Biedermann and Chow, 1966; Byrne and Luo, 2000; Byrne et al., 2000; Dousma and De Bruyn, 1978; Murphy et al., 1976). In the calculations of Gibbs free energies of Fe(III) oxyhydroxide reduction coupled to lactate oxidation, the experimentally-derived solubility products, defined by $^*K_{\text{so}} = a_{\text{Fe}^{3+}} \times a_{\text{H}^+}^{-n}$, with n equal to 2.75 for 6 lines-ferrihydrite and 2.85 for nanohematite, are used below.

5.3.2 Redox measurements and mineral solubilities

Bonneville et al. (2004) used redox potentials measured with a Pt electrode over a range of pH (4-7), at known Fe^{2+} activities, to derive the solubility products of colloidal iron oxyhydroxides. Based on these pe-pH titrations, the following expressions for the equilibrium pe values of 6-lines ferrihydrite and nanohematite were obtained (at 25°C and 1 bar):

$$\text{pe}_{\text{F6L}} = \log(K_{\text{red}} ^* K_{\text{so}}) - 2.75 \text{pH} - \log a_{\text{Fe}^{2+}} \quad (5.5)$$

$$\text{pe}_{\text{NH}} = \log(K_{\text{red}} ^* K_{\text{so}}) - 2.85 \text{pH} - \log a_{\text{Fe}^{2+}} \quad (5.6)$$

where the solubility products of 6-lines ferrihydrite and nanohematite are $\log ^* K_{\text{so}} = 1.62$ and 0.52 , respectively, and the equilibrium constant $\log K_{\text{red}} = 13.05$ corresponds to the reaction:



The pe values calculated with equations (5.5) and (5.6) are compared to the pe measurements during the incubation experiments with nanohematite and 6-line ferrihydrite in Figure 5.5. Note that in the figure the Fe^{2+} activity, derived from the voltametric measurements, is used as a progress variable for the reduction reactions. At the beginning of the experiments, that is when Fe^{2+} activities are low, the measured and calculated pe values deviated significantly from each other. Possibly, the discrepancy was caused by the slow polarization of the redox electrode at low Fe(II) concentrations (Stumm and Morgan, 1995).

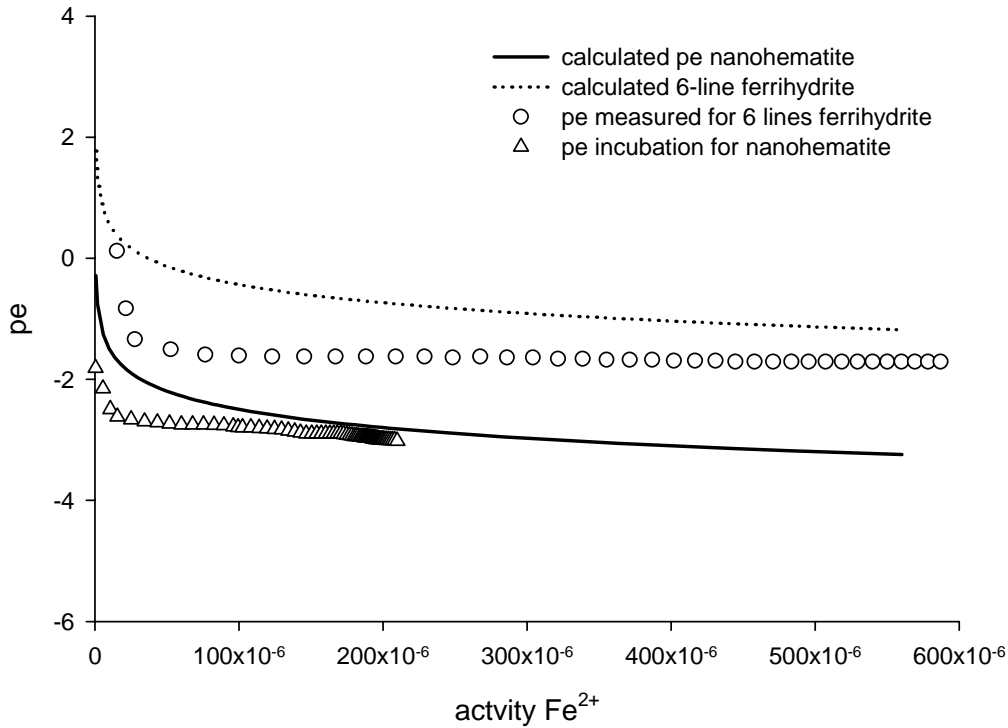


Figure 5.5: pe measured during 6-lines ferrihydrite (open circles) and nano hematite (open triangles) reduction coupled to lactate oxidation and pe calculated from equation (5.5) and (5.6) as a function of Fe^{2+} activity.

However, with increasing Fe^{2+} activity, the measured pe approached the theoretical values. This indicates that the solubilities of 6-lines ferrihydrite and nano hematite at the end of the experiments were similar to those of the initially added materials. Thus, no evidence was found for significant mineral transformation within the time scale of the experiments, as reported in other studies (Hansel et al., 2003; Jolivet et al., 1992; Ona-Nguema et al., 2002; Pedersen et al., 2005).

5.3.3 Thermodynamic control of Fe(III) oxyhydroxide reduction?

The free energies of the oxidation of lactate coupled to the reduction of 6-lines ferrihydrite and hematite are given by:

$$\Delta G_{r(\text{F6L})} = \Delta G_{r(\text{F6L})}^0 + RT \ln \frac{(a_{\text{Fe}^{2+}})^4 (a_{\text{acetate}}) (a_{\text{HCO}_3^-})}{(a_{\text{H}^+})^6 (a_{\text{lactate}})} \quad (5.8)$$

$$\Delta G_{r(\text{NH})} = \Delta G_{r(\text{NH})}^0 + RT \ln \frac{(a_{\text{Fe}^{2+}})^4 (a_{\text{acetate}}) (a_{\text{HCO}_3^-})}{(a_{\text{H}^+})^{6.4} (a_{\text{lactate}})} \quad (5.9)$$

The concentrations of acetate were derived from the total Fe^{2+} concentrations, assuming the reaction stoichiometries in equations (5.3) and (5.4). The concentration of dissolved inorganic carbon was

assumed to be very low at the beginning of the experiments due to the flushing with Ar. The build-up of HCO_3^- was then calculated from the Fe^{2+} production and the stoichiometries in equations (5.3) and (5.4).

The values of ΔG_r calculated with equations 5.8 and 5.9 are shown in Figure 5.6. At the same progress of reaction, the potential energy gain for reducing nanohematite is generally about 40 kJ per mol lactate smaller than for 6-lines ferrihydrite, which reflects the lower solubility of the former solid. The free energies after 100 h, when the rates of Fe(III) reduction approached zero, were about -165 kJ mol⁻¹ and -135 kJ mol⁻¹ for nanohematite and 6-lines ferrihydrite, respectively. That is, the potential free energy yields are significantly higher than the -20 kJ per mol electron acceptor, which is considered as the threshold value for microorganisms to utilize a particular respiratory pathway. Consequently, the termination of dissimilatory iron reduction after about 100 hours for 6-lines ferrihydrite and 50 hours for nanohematite is caused by another reason than insufficient energy generation.

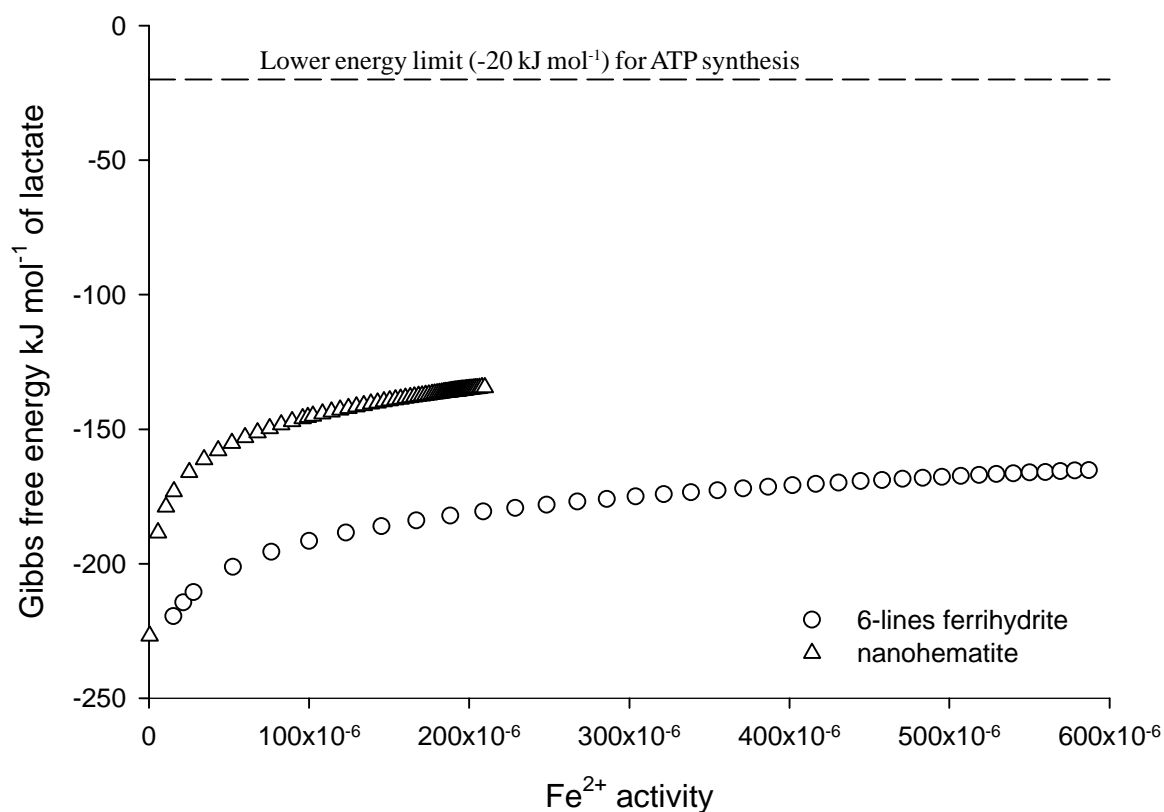


Figure 5.6: Gibbs free energy of reaction, as a function of Fe^{2+} activity for the reduction of 6-lines ferrihydrite and nanohematite reduction coupled to lactate oxidation. See text for complete discussion.

5.3.4 The effect of Fe²⁺ on microbial iron reduction

Roden et al. (2002) reviewed the studies devoted to the effect of Fe²⁺ accumulation on the microbial mediated reduction of iron oxyhydroxides. These authors listed two different mechanisms by which Fe(II) can inhibit microbial Fe(III) oxyhydroxide reduction, at Fe(II) concentrations well below those at which dissimilatory iron reduction becomes thermodynamic unfavourable: (i) adsorption of Fe(II) at the surface of Fe(III) oxyhydroxide, possibly leading to the formation of Fe(II)-bearing surface phases, and (ii) specific inhibition of cellular Fe(III) reductases by Fe²⁺.

The formation of Fe(II) coatings at the surface of Fe(III) oxyhydroxides and its inhibitory effect on microbial Fe(III) reduction has been described in detail (Roden and Urrutia, 2002; Urrutia et al., 1998; Urrutia et al., 1999). In our experiments, however, only a minor fraction of the total Fe²⁺ (<10%) was sorbed (Figure 5.3). Furthermore, the amounts of sorbed Fe²⁺ could at most account for 40-50% of the sorption capacities of 6-lines ferrihydrite and nanohematite estimated from the total concentrations of surface sites (Liger et al., 1999). Therefore, it is unlikely that the adsorption of Fe(II) or the formation of a Fe(II) containing coating on the Fe(III) oxyhydroxide surface caused the cessation of microbial iron reduction in our experiments.

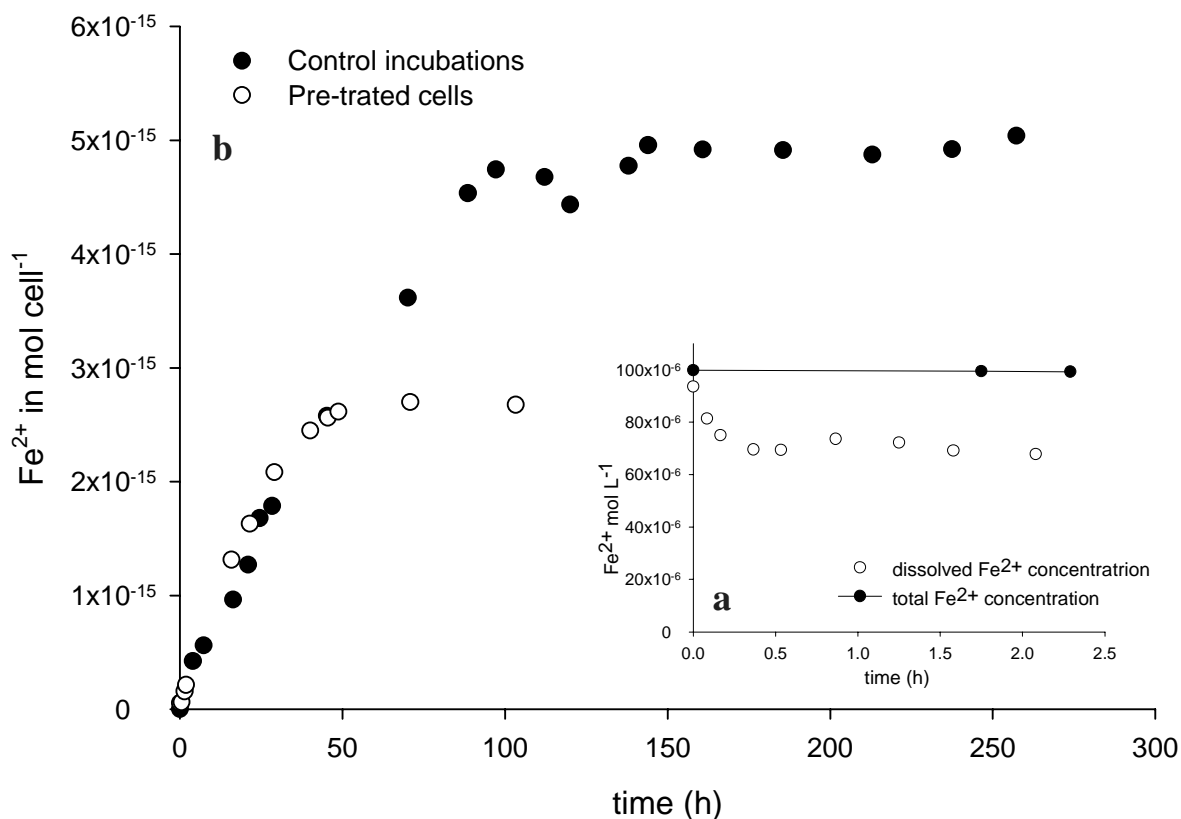


Figure 5.7: (a) Biosorption of Fe²⁺(aq) by *Shewanella putrefaciens*. (b) Reduction of 6-lines ferrihydrite by *Shewanella putrefaciens* cells pre-treated with Fe²⁺(aq) (open symbols) and without Fe²⁺(aq) pre-treatment (full symbols). The Fe²⁺ concentrations level off after about 40h in the pre-treated cell experiment and after 100h for the control experiment.

A possible inhibitory effect of Fe(II) sorbed to the bacteria is assessed by the microbial reduction experiments with cells of *S. putrefaciens* pre-treated with Fe²⁺. Of the initial 100 μM of aqueous Fe²⁺ in the pre-treatment solution, around 34 μM, or 1.5×10^{-16} mol cell⁻¹, was removed onto the bacteria (Figure 5.7a). This amount by far exceeds the abundance of Fe(III) reductase, estimated to be around 7×10^{-19} mol cell⁻¹ (see Chapter III). However, the initial iron reduction rate in the experiments with pre-treated cells did not differ significantly from the reduction rate obtained without Fe²⁺ pre-treatment of the bacteria (Figure 5.7b). This observation could be taken as an indication that Fe²⁺ does not specifically inhibit the activity of the Fe(III) reductases. An effect of cell-bound Fe²⁺ on the efficiency of the Fe(III) reductases, however, may be masked by the fact that the rate-determining step of Fe(III) oxyhydroxide reduction is the detachment of reduced Fe(III) centers from the mineral surface, and not the electron transfer from the cell (see Chapter IV).

Although it did not affect the initial reduction kinetics, the Fe²⁺ pre-treatment caused the reduction of 6-lines ferrihydrite to stop earlier and at lower amounts of reduced Fe(III) than without Fe²⁺ pre-treatment. This suggests that Fe²⁺ exposure had an effect on the ability of *S. putrefaciens* cells to reduce the Fe(III) mineral. Whether the sorbed Fe²⁺ interferes with the functioning of the Fe(III) reductase, or has another toxic effect remains to be clarified. Fe²⁺ toxicity has been reported for *Escherichia coli* and *Rhizobium meliloti* (Botsford, 2000; Kazufumi et al., 1999; Yu et al., 2000) but has not been investigated for *S. putrefaciens*. A toxic effect of Fe(II) is unexpected for a microorganism that has been isolated from environments containing high concentrations of Fe(II). It cannot be excluded that other stress factors during the pre-treatment or during the incubation experiments such as starvation, or limitation by essential elements, had an impact on the vitality of the bacteria. Hence, the effects of Fe(II) on the microbial reduction of Fe(III) oxyhydroxides requires further, more systematic studies on the effect of exposure time and concentration of Fe(II) on the activity of *S. putrefaciens*.

References

- Achtnich C., Bak F., and Conrad R. (1995) Competition for electron donors among nitrate reducers, ferric iron reducers, sulfate reducers, and methanogens in anoxic paddy soil. *Biol. Fertility Soils* **19**, 65-72.
- Arnold R. G., DiChristina T. J., and Hoffmann M. R. (1986) Bioextraction of iron from iron oxides, pp. 207 pp. W. M. Keck Lab. Environ. Eng., California Inst. Technol., Pasadena, CA, USA.
- Behrends T. and Van Cappellen P. (2005) Competition between enzymatic and abiotic reduction of uranium(VI) under iron reducing conditions. *Chem. Geol.* **220**, 315-327.
- Biedermann G. and Chow J. T. (1966) Hydrolysis of metal ions. LVII. Hydrolysis of the Fe(III) ion and the solubility product of the Fe(OH)₂.70Cl_{0.30} in 0.5M (Na⁺)Cl-medium. *Acta Chem. Scand.* **20**, 1376-1388.
- Bonneville S., Van Cappellen P., and Behrends T. (2004) Microbial reduction of iron(III) oxyhydroxides: effects of mineral solubility and availability. *Chem. Geol.* **212**, 255-268.
- Botsford J. L. (2000) Role of EDTA in a simple method for determining toxicity using a bacterial indicator organism. *World J. Microbiol. Biotechnol.* **16**, 353-359.
- Brendel P. J. and Luther G. W., III. (1995) Development of a Gold Amalgam Voltammetric Microelectrode for the Determination of Dissolved Fe, Mn, O₂, and S(-II) in Porewaters of Marine and Freshwater Sediments. *Environ. Sci. Technol.* **29**, 751-761.
- Burdige D. J. (1993) The biogeochemistry of manganese and iron reduction in marine sediments. *Earth Sci. Rev.* **35**, 249-284.
- Byrne R. H. and Luo Y.-R. (2000) Direct observations of nonintegral hydrous ferric oxide solubility products: $k^*s_0=[Fe^{3+}][H^+]-2.86$. *Geochim. Cosmochim. Acta* **64**, 1873-1877.
- Byrne R. H., Luo Y.-R., and Young R. W. (2000) Iron hydrolysis and solubility revisited: observations and comments on iron hydrolysis characterizations. *Mar. Chem.* **70**, 23-35.
- Cornell R. M. and Schwertmann U. (1996) *The Iron Oxides: Structure, Properties, Reactions, Occurrence and Uses*. VCH, 573 pp
- DiChristina T. J. and DeLong E. F. (1994) Isolation of anaerobic respiratory mutants of *Shewanella putrefaciens* and genetic analysis of mutants deficient in anaerobic growth on Fe³⁺. *J. Bacteriol.* **176**, 1468-1474.
- DiChristina T. J., Moore C. M., and Haller C. A. (2002) Dissimilatory Fe(III) and Mn(IV) reduction by *Shewanella putrefaciens* requires ferE, a homolog of the pulE (gspE) type II protein secretion gene. *J. Bacteriol.* **184**, 142-151.
- Dousma J. and De Bruyn P. L. (1978) Hydrolysis-precipitation studies of iron solutions. II. Aging studies and the model for precipitation from iron(III) nitrate solutions. *J. Colloid Interface Sci.* **64**, 154-170.
- Fredrickson J. K. and Gorby Y. A. (1996) Environmental processes mediated by iron-reducing bacteria. *Curr. Opin. Biotechnol.* **7**, 287-294.
- Hansel C. M., Benner S. G., Neiss J., Dohnalkova A., Kukkadapu R. K., and Fendorf M. (2003) Secondary mineralization pathways induced by dissimilatory iron reduction of ferrihydrite under advective flow. *Geochim. Cosmochim. Acta* **67**, 2977-2992.
- Hobbie J. E., Daley R. J., and Jasper S. (1977) Use of nucleopore filters for counting bacteria by fluorescence microscopy. *Appl. Environ. Microbiol.* **33**, 1225-1228.
- Jolivet J. P., Belleville P., Tronc E., and Livage J. (1992) Influence of iron(II) on the formation of the spinel iron oxide in alkaline medium. *Clays Clay Miner.* **40**, 531-539.
- Kazufumi O., Junko U., Aktar A. M., Naoyuki M., and Tetsuya K. (1999) Synergistic effect of lactate and Fe²⁺ on cell killing in *E. coli* and other bacteria. *Res. Comm. Biochem. Cell Molec. Biol.* **3**, 215-222.
- Liger E., Charlet L., and Van Cappellen P. (1999) Surface catalysis of uranium (VI) reduction by iron(II). *Geochim. Cosmochim. Acta* **63**, 2939-2955.
- Liu C., Kota S., Zachara J. M., Fredrickson J. K., and Brinkman C. K. (2001) Kinetic Analysis of the Bacterial Reduction of Goethite. *Environ. Sci. Technol.* **35**, 2482-2490.
- Lovley D. R. (1991) Dissimilatory iron(III) and manganese(IV) reduction. *Microbiol. Rev.* **55**, 259-287.
- Lovley D. R., Chapelle F. H., and Woodward J. C. (1994) Use of Dissolved H₂ Concentrations To Determine Distribution of Microbially Catalyzed Redox Reactions in Anoxic Groundwater. *Environ. Sci. Technol.* **28**, 1205-1210.
- Lovley D. R., Giovannoni S. J., White D. C., Champine J. E., Phillips E. J. P., Gorby Y. A., and Goodwin S. (1993) *Geobacter metallireducens* gen. nov. sp. nov., a microorganism capable of coupling the complete oxidation of organic compounds to the reduction of iron and other metals. *Arch. Microbiol.* **159**, 336-344.
- Murphy P. J., Posner A. M., and Quirk J. P. (1976) Characterization of hydrolyzed ferric ion solutions. A comparison of the effects of various anions on the solutions. *J. Colloid Interface Sci.* **56**, 312-319.

- Nealson K. H. and Saffarini D. (1994) Iron and manganese in anaerobic respiration: environmental significance, physiology, and regulation. *Annual Rev. Microbiol.* **48**, 311-43.
- Ona-Nguema G., Abdelmoula M., Jorand F., Benali O., Gehin A., Block J.-C., and Genin J.-M. R. (2002) Microbial Reduction of Lepidocrocite γ -FeOOH by *Shewanella putrefaciens*; The Formation of Green Rust. *Hyp. Interact.* **139/140**, 231-237.
- Pedersen H. D., Postma D., Jakobsen R., and Larsen O. (2005) Fast transformation of iron oxyhydroxides by the catalytic action of aqueous Fe(II). *Geochim. Cosmochim. Acta* **69**, 3967-3977.
- Roden E. E. and Edmonds J. W. (1997) Phosphate mobilization in iron-rich anaerobic sediments. Microbial Fe(III) oxide reduction versus iron-sulfide formation. *Arch. Hydrobiol.* **139**, 347-378.
- Roden E. E. and Urrutia M. M. (2002) Influence of biogenic Fe(II) on bacterial crystalline Fe(III) oxide reduction. *Geomicrobiology J.* **19**, 209-251.
- Roden E. E. and Wetzel R. G. (2002) Kinetics of microbial Fe(III) oxide reduction in freshwater wetland sediments. *Limnol. Oceanogr.* **47**, 198-211.
- Roden E. E. and Zachara J. M. (1996) Microbial reduction of crystalline iron(III) oxides: Influence of oxide surface area and potential for cell growth. *Environ. Sci. Technol.* **30**, 1618-28.
- Röling W. F. M., van Breukelen B. M., Braster M., Bin L., and van Verseveld H. W. (2001) Relationships between Microbial Community Structure and Hydrochemistry in a Landfill Leachate-Polluted Aquifer. *Appl. Environ. Microbiol.* **67**, 4619-4629.
- Schink B. (1997) Energetics of syntrophic cooperation in methanogenic degradation. *Microbiol. Molec. Biol. Rev.* **61**, 262-280.
- Schwertmann U. and Cornell R. M. (1991) *Iron Oxides in the Laboratory: Preparation and Characterization*. VCH, Weinheim, p. 137
- Stumm W. and Morgan J. J. (1995) *Aquatic Chemistry: Chemical Equilibria and Rates in Natural Waters*. Wiley, p. 1022
- Thamdrup B. (2000) Bacterial manganese and iron reduction in aquatic sediments. *Adv. Microb. Ecol.* **16**, 41-84.
- Urrutia M. M., Roden E. E., Fredrickson J. K., and Zachara J. M. (1998) Microbial and surface chemistry controls on reduction of synthetic Fe(III) oxide minerals by the dissimilatory iron-reducing bacterium *Shewanella alga*. *Geomicrobiol. J.* **15**, 269-291.
- Urrutia M. M., Roden E. E., and Zachara J. M. (1999) Influence of Aqueous and Solid-Phase Fe(II) Complexants on Microbial Reduction of Crystalline Iron(III) Oxides. *Environ. Sci. Technol.* **33**, 4022-4028.
- Viollier E., Inglett P. W., Hunter K., Roychoudhury A. N., and Van Cappellen P. (2000) The ferrozine method revisited: Fe(II)/Fe(III) determination in natural waters. *Appl. Geochem.* **15**, 785-790.
- Winfrey M. R. and Zeikus J. G. (1977) Effect of sulfate on carbon and electron flow during microbial methanogenesis in freshwater sediments. *Appl. Environ. Microbiol.* **33**, 275-281.
- Yu H. Q., Fang H. H. P., and Tay J. H. (2000) Effects of Fe²⁺ on sludge granulation in upflow anaerobic sludge blanket reactors. *Water Sci. Technol.* **41**, 199-205.
- Zachara J. M., Fredrickson J. K., Smith S. C., and Gassman P. L. (2001) Solubilization of Fe(III) oxide-bound trace metals by a dissimilatory Fe(III) reducing bacterium. *Geochim. Cosmochim. Acta* **65**, 75-93

Chapter VI

Summary (English, French, Dutch)

Summary

In many soils, sediments and groundwaters, ferric iron is a major potential electron acceptor for the oxidation of organic matter. In contrast to other terminal electron acceptors, such as nitrate and sulfate, the concentration of aqueous ferric iron, $\text{Fe}^{3+}(\text{aq})$, is limited by the low solubility of Fe(III) oxyhydroxides under the pH conditions typically encountered in subsurface environments. Consequently, iron reducing microorganisms have developed specific strategies to transfer electrons to the structural Fe(III) centers of the solids. It has been proposed that, in some cases, soluble electron shuttles or ligand-bound Fe(III) serve as intermediates between the minerals and the organisms. In other cases, electron transfer occurs only upon direct contact of the microorganisms and the mineral particles. The latter strategy is the one investigated in this study.

The goal of the thesis is to unravel the effects of the physical-chemical properties of Fe(III) oxyhydroxides on dissimilatory iron reduction, particularly focusing on mineral solubility and particle size. The experimental approach adopted is to incubate various Fe(III) oxyhydroxides with the facultative anaerobic, Gram-negative bacterium *Shewanella putrefaciens*, using lactate as sole electron donor. The experiments are carried out in a simplified medium, containing no phosphate or added trace elements, at room temperature and pH 7. The electron donor is present in excess and, therefore, its availability does not affect the rate of iron reduction. The latter is measured by monitoring the build-up of total Fe^{2+} in the reaction system.

In the first part of the study, the rates of iron reduction of different Fe(III) oxyhydroxides are determined as a function of the concentration of solid-phase Fe(III) and the cell density (Chapter II). An important observation is that, for a given Fe(III) oxyhydroxide phase, a unique dependence of the iron reduction rate on the Fe(III) concentration is obtained when normalizing the rates to the number of cells. Furthermore, this dependence can be described by the classic Michaelis-Menten rate equation:

$$R = v_{\max} B \frac{[\text{Fe(III)}]}{K_m^* + [\text{Fe(III)}]} \quad (6.1)$$

where R is the net rate of iron reduction per unit total volume of the bacteria-mineral suspension, v_{\max} is the maximum cell-normalized iron reduction rate (in units of, say, $\mu\text{mol Fe(III)} \text{ h}^{-1} \text{ cell}^{-1}$), B corresponds to the cell density of the suspensions (i.e., the biomass), and K_m^* is a half-saturation constant.

The maximum rate, v_{\max} , is interpreted as the iron reducing activity of a *S. putrefaciens* cell when its membrane-bound Fe(III) reductase sites are fully saturated by the solid-state Fe(III) substrate. The values of v_{\max} vary over 1.5 orders of magnitude, depending on the mineral undergoing reduction. In order to explain this large variation of v_{\max} , the solubilities of the Fe(III) oxyhydroxides are measured using two complementary methods. For fairly soluble, colloidal Fe(III) oxyhydroxides, redox potential measurements are carried out over the pH range 4-7 (Chapter II). For coarser, usually less soluble minerals, a dialysis bag dissolution method is used (Chapter IV). In the latter, the activities of aqueous ferric iron are measured under acid conditions. Both approaches allow us to derive solubility products, $*K_{so}$, that account for the non-ideal stoichiometries of the solids.

The maximum rates of reduction of Fe(III) oxyhydroxides by *S. putrefaciens* and the solubility products exhibit a strong positive correlation, which can be expressed as:

$$\log v_{\max} (\text{mol h}^{-1} \text{ cell}^{-1}) = 0.40 \log *K_{so} - 16.80 \quad (6.2)$$

Equation (6.2) defines a linear free energy relationship (LFER), which relates the iron reducing activity of *S. putrefaciens* to the energetics of the mineral Fe(III) substrate. Although the LFER is an empirical relationship, it hints to a common rate controlling process in the microbial reduction of different Fe(III) oxyhydroxides. In Chapter IV, we show a positive correlation between v_{\max} and the rate constant for detachment of Fe^{2+} from the mineral (k_{des}). The observed LFER thus most likely originates in the rate-limiting role of the detachment of Fe^{2+} from the mineral surface, following electron transfer from a cell membrane-bound reductase site to a structural Fe(III) of an attached oxyhydroxide particle.

For enzymatic reactions in homogeneous solution, the half-saturation constant in the Michaelis-Menten rate equation is a direct measure of the enzyme's affinity to bind chemically to the soluble substrate. The half-saturation constant is uniquely defined in terms of the substrate's bulk dissolved concentration. The reduction of Fe(III) oxyhydroxide mineral particles by *S. putrefaciens* presents a far more complex situation, however. The Fe(III) centers that undergo reduction are located in the contact region between cell and mineral. The direct Fe(III) substrate therefore only represents a fraction of the bulk Fe(III) in the system. This fraction depends not only on the tendency of mineral and bacteria to attach to one another, but also on the particle size of the solid. As a result, K_m^* values expressed in units of bulk concentration of the Fe(III) substrate (e.g., in moles of Fe(III) per unit volume suspension) are conditional, rather than intrinsic, kinetic parameters. For instance, in Chapter II, we show that the K_m^* values depend on the solid-to-cell ratio in the experimental suspensions. Qualitatively, this points to

a crucial role of mineral-bacteria attachment in the reduction process. This role is precisely the topic of Chapter III.

In Chapter III, we first investigate the attachment of nanohematite particles onto *S. putrefaciens* in suspensions of relatively low ionic strength and pH, in order to prevent coagulation of the mineral colloids. Formally, the partitioning of the nanohematite particles follows a Langmuir isotherm. That is, the coverage of the cells by nanohematite can be described using two parameters, the maximum attachment capacity per cell, M_{max} , and an attachment constant, K_p . Next, cells with known amounts of attached nanohematite particles are incubated with lactate under anaerobic conditions. The major finding is that the iron reduction rate correlates linearly with the relative coverage of the cell surfaces by nanohematite particles, hence supporting a direct electron transfer from membrane bound reductases to mineral particles attached to the cells. Using internally consistent parameter values for M_{max} , K_p , and the first-order Fe(III) reduction rate constant, k , a kinetic model for the microbial reduction of Fe(III) oxyhydroxide colloids is developed. The model reproduces the reduction rates of nanohematite, as well as those of other fine-grained Fe(III) oxyhydroxides by *S. putrefaciens*. It explains the observed dependency of the Fe(III) half saturation constant, K_m^* , on the solid-to-cell ratio and, as observed, it predicts that iron reduction rates exhibit saturation with respect to both the cell density and the abundance of the Fe(III) oxyhydroxide substrate.

In addition to cell-mineral attachment and kinetic effects, microbial iron reduction may also be subject to thermodynamic constraints. In particular, the build-up of Fe^{2+} in solution with ongoing Fe(III) oxyhydroxide reduction decreases the Gibbs free energy yield ($-\Delta G_r$) for the microorganisms. In principle, the free energy yield of Fe(III) oxyhydroxide reduction coupled to the oxidation of an organic substrate should exceed 20 kJ mol^{-1} , in order to provide the microorganism with enough energy to synthesize ATP. Thus, under strict thermodynamic control, iron reduction activity should only stop when this lower limit of $-\Delta G_r$ is reached. In Chapter V, we follow the temporal evolution of $-\Delta G_r$ during the microbial oxidation of lactate coupled to 6-lines ferrihydrite and nanohematite reduction. For both solids, iron reduction comes to a halt, even as the calculated thermodynamic energy yields are still favorable ($-\Delta G_r > 20 \text{ kJ mol}^{-1}$). Therefore, cessation of the iron reducing activity of *S. putrefaciens* cannot be attributed solely to a thermodynamic effect of the accumulation of reaction products.

Another possibility is that the build-up of Fe^{2+} during microbial iron somehow poisons the cells. This possibility is further investigated in Chapter V, by pre-treating *S. putrefaciens* cells with Fe^{2+} before starting the iron reduction experiments. The pre-treatments show that the cells readily take up aqueous Fe^{2+} . The initial reduction of 6-lines-ferrihydrite by pre-treated cells proceeds at the same rate

as that in control experiments with cells that were not exposed to Fe^{2+} . However, the Fe(III) reducing activity of the pre-treated cells stops much earlier than in the control experiments. This preliminary observation suggests that accumulation of Fe^{2+} by the cells may interfere with their metabolism and, ultimately, limit the extent of Fe(III) oxyhydroxide reduction. Nonetheless, much more work will be required to fully understand the complex array of physiological and environmental factors that control microbial iron reduction.

Résumé

Dans de nombreux sols, sédiments et aquifères, le fer ferrique est un accepteur d'électron majeur dans le processus d'oxydation de la matière organique. Pourtant, à la différence des autres accepteurs d'électron tels que le nitrate ou le sulfate, la concentration de fer ferrique dissous, $\text{Fe}^{3+}(\text{aq})$, est très faible car limitée par la solubilité réduite des oxyhydroxydes de fer pour les conditions de pH du milieu naturel. En conséquence, les bactéries qui réduisent les oxyhydroxydes de fer ont développé des stratégies spécifiques pour transférer les électrons aux oxyhydroxydes de fer. Par exemple, certains composés et ligands dissous servent d'intermédiaires entre les phases minérales de fer et les bactéries. Les bactéries peuvent aussi être en contact physique direct avec les oxyhydroxydes de fer, c'est l'approche retenue dans cette étude.

Cette thèse souligne le rôle des propriétés physiques et chimiques des oxyhydroxydes de fer dans les cinétiques de réduction microbienne. La solubilité et la taille des particules d'oxyhydroxyde de fer sont plus particulièrement étudiées. Notre approche expérimentale consiste à incuber différents oxyhydroxydes de fer avec *Shewanella putrefaciens*, une bactérie anaérobique facultative, Gram négative. Les incubations sont menées en présence de lactate, en tant que donneur d'électron, dans un milieu simplifié sans phosphate ou métaux traces, à température ambiante et pH 7. La concentration de lactate est toujours en excès par rapport à celle des oxyhydroxydes de fer, pour éviter que la disponibilité du donneur d'électron n'affecte les cinétiques de réduction microbienne. La production de Fe^{2+} dissous, mesurée régulièrement pendant les incubations, sert à définir les cinétiques de réduction des différents oxyhydroxydes de fer.

Les taux de réduction des différents oxyhydroxydes de fer sont définis en fonction de la concentration initiale en Fe(III) et de la densité de bactéries (Chapitre II). Pour une concentration croissante d'oxyhydroxyde de fer, le taux de réduction par bactérie atteint un taux maximum, décrivant une cinétique classique de Michaelis-Menten:

$$R = v_{\max} B \frac{[\text{Fe(III)}]}{K_m^* + [\text{Fe(III)}]} \quad (6.3)$$

Dans l'équation (6.3), R est le taux de réduction par unité de volume de la suspension, v_{\max} est le taux maximum de réduction par bactérie (en $\mu\text{mol Fe(III)} \text{ h}^{-1} \text{ cellule}^{-1}$), B correspond à la densité bactérienne des suspensions (biomasse), et K_m^* est la constante d'affinité.

Le taux maximum de réduction par bactérie, v_{max} , est interprété comme étant l'activité réductrice d'une cellule de *S. putrefaciens* ayant toutes ses Fe(III) réductases saturées par des particules d'oxyhydroxyde de fer. Les valeurs de v_{max} varient fortement selon la minéralogie des oxyhydroxydes de fer dans un intervalle de 1.5 unité logarithmique. Pour les oxyhydroxydes les plus solubles, en général à l'état de suspension colloïdale, la solubilité est déterminée par des titrations pe-pH (entre pH 4 et 7). Pour les phases les moins solubles, les oxyhydroxydes de fer sont placés dans des sacs à dialyse à différents pH acides (pH 1 à 2.5). Les oxyhydroxydes de fer se dissolvent jusqu'à atteindre un équilibre de dissolution, la mesure de l'activité du $Fe^{3+}(aq)$ à l'équilibre permet ensuite de calculer la solubilité. Ces deux méthodes nous ont permis d'établir les produits de solubilité, $*K_{so}$, en tenant compte du caractère non idéal de la stoechiométrie des oxyhydroxydes de fer.

Le taux de réduction maximum pour *S. putrefaciens*, v_{max} , est corrélé avec la solubilité des oxyhydroxydes de fer, selon la relation:

$$\log v_{max} (\text{mol h}^{-1} \text{ cell}^{-1}) = 0.40 \log *K_{so} - 16.80 \quad (6.4)$$

L'équation (6.4) définit une "linear free energy relationship" (LFER), entre l'activité réductrice des bactéries et la stabilité thermodynamique des phases de Fe(III). Bien qu'empirique, cette relation implique l'existence d'une réaction limitante dans le processus de réduction, commune aux différents oxyhydroxydes de fer. Dans le Chapitre IV, nous avons montré que v_{max} est également positivement corrélé avec la constante cinétique de détachement du Fe^{2+} de la surface des oxyhydroxydes de fer. Cette dernière réaction contrôlerait la cinétique de réduction des oxyhydroxydes de fer et expliquerait donc la LFER.

Pour les réactions enzymatiques en milieux homogènes, la constante de Michaelis-Menten (K_m) est une mesure directe de l'affinité d'une enzyme à complexer un substrat donné. Cette constante d'affinité est définie en termes de concentration de substrat. En ce qui concerne la réduction microbienne des oxyhydroxyde de fer, la situation est plus complexe car le substrat de la réaction enzymatique, est un solide. De plus, les Fe(III), susceptible d'être réduit sont localisés à l'interface bactérie-oxyhydroxyde de fer. Ces derniers ne représentent donc qu'une fraction de la concentration totale de Fe(III). De plus, l'interface de contact entre les bactéries et les particules de fer varie en fonction de l'affinité des bactéries pour un oxyhydroxyde de fer donné mais aussi en fonction de la taille et la forme des particules de fer. En conséquence, les valeurs de K_m^* exprimées en concentration de Fe(III) (en moles de Fe(III) par unité de volume de suspension) sont des paramètres cinétiques conditionnels. Par exemple, dans le chapitre II, nous avons démontré que K_m^* varie en fonction du ratio Fe(III) solide/bactéries appliqué

dans les suspensions ce qui souligne le rôle déterminant de l'association oxyhydroxydes de fer-bactéries dans le processus de réduction. Ce dernière thématique est précisément étudiée dans le chapitre III.

Dans le chapitre III, une série d'expériences sur l'association des particules de fer avec les bactéries est menée avec des suspensions de nanohématite et *S. putrefaciens*. Les conditions expérimentales sont fixées de manière à éviter la coagulation des colloïdes de fer: pH 5 et force ionique relativement faible. Les résultats montrent que la partition des particules de fer en présence de bactéries suit un isotherme de Langmuir. Le recouvrement progressif de la surface des bactéries par les particules colloïdales de nanohématite peut ainsi être défini par la capacité maximale d'attachement par bactérie, M_{max} et une constante d'attachement, K_p . Par la suite, des suspensions de bactéries avec des quantités connues de fer associées à leur surface ont été incubées avec du lactate en conditions anaérobiques. La conclusion majeure de ces expériences est que le taux de réduction est proportionnel au recouvrement de la surface de la bactérie par les particules de nanohématite. Ces résultats suggèrent que le transfert d'électron est réalisé directement entre les Fe(III) réductases et les particules de fer associées à la surface bactérienne. A partir d'estimation cohérente des paramètres M_{max} , K_p et k , la constante cinétique de premier ordre de réduction, nous avons développé un modèle cinétique de réduction des oxyhydroxydes de fer par *S. putrefaciens*. Ce modèle reproduit de manière satisfaisante les taux de réduction mesurés avec la nanohématite mais aussi pour d'autres oxyhydroxydes de fer (ferrihydrite, lepidocrocite). De plus, le modèle cinétique permet d'expliquer la dépendance des valeurs de K_m^* vis à vis du ratio Fe(III) solides/densité bactérienne. Enfin, avec le modèle cinétique, nous avons pu montrer qu'une cinétique dite de saturation peut être obtenue avec des concentrations croissantes d'oxyhydroxydes de fer mais aussi en augmentant la densité bactérienne.

Cependant, outre les aspects cinétiques et d'association Fe(III) solide-bactérie, la réduction microbienne des oxyhydroxydes peut aussi être limitée thermodynamiquement. En théorie, la production et l'accumulation en solution de Fe^{2+} due à la réduction des oxyhydroxydes induit une baisse de gain énergétique ($-\Delta G_r$) pour les microorganismes. En principe, le gain d'énergie de la réduction d'oxyhydroxyde de fer couplée à l'oxydation de composés organiques doit excéder 20 kJ mol^{-1} , afin de fournir suffisamment d'énergie aux bactéries pour synthétiser leur ATP. Ainsi, l'activité réductrice des bactéries devrait cesser seulement lorsque ce seuil limite de $-\Delta G_r$ est atteint. Dans le chapitre V, l'évolution du $-\Delta G_r$ est suivie durant l'oxydation de lactate couplée à la réduction de 6-lines ferrihydrite et de nanohématite par des suspensions de *S. putrefaciens*. Néanmoins, pour ces deux phases minérales, l'activité réductrice cesse alors que d'un point de vue thermodynamique, le $-\Delta G_r$ calculé est encore largement favorable ($\Delta G_r > 20 \text{ kJ mol}^{-1}$). Ces résultats montrent que l'arrêt de l'activité réductrice des

suspensions de *S. putrefaciens* n'est pas la conséquence d'une limitation thermodynamique due à l'accumulation des produits de réaction.

Une explication alternative pourrait être que le Fe^{2+} altère d'une certaine manière la viabilité des bactéries. Cette possibilité est étudiée dans le chapitre V en pré-traitant une suspension de *S. putrefaciens* avec du Fe^{2+} avant incubation anaérobie avec des oxyhydroxydes de fer et le lactate. Cette expérience montre que les bactéries adsorbent rapidement le Fe^{2+} (aq), pourtant, la cinétique de réduction des oxyhydroxydes de fer des cellules pré-traitées est très similaire à celle observée lors d'une expérience contrôle avec des bactéries non traitées préalablement avec du Fe^{2+} . Néanmoins, l'activité réductrice des bactéries pré-traitées cesse nettement plus tôt que dans l'expérience contrôle. Ces résultats préliminaires montrent que l'accumulation de Fe^{2+} pourrait altérer le métabolisme des bactéries et donc finalement limiter leur activité de réduction des oxyhydroxydes de fer. Cependant un travail exhaustif et systématique devrait être poursuivi afin de comprendre complètement la complexité des facteurs physiologiques et environnementaux qui contrôlent la réduction microbienne des oxyhydroxydes de fer.

Samenvatting

In veel bodems, sedimenten en grondwater is driewaardig ijzer een belangrijke elektronenacceptor voor de oxidatie van organisch materiaal. In tegenstelling tot andere terminale elektronenacceptoren, zoals nitraat en sulfaat, wordt de concentratie van opgelost driewaardig ijzer, $\text{Fe}^{3+}(\text{aq})$, beperkt door de lage oplosbaarheid van Fe(III) oxyhydroxiden onder de pH condities die gebruikelijk zijn in de ondergrond. Als gevolg daarvan hebben ijzerreducerende micro-organismen specifieke strategieën ontwikkeld voor de overdracht van elektronen naar de structurele Fe(III) centra van de vaste fase. In sommige gevallen kunnen de oplosbare elektron shuttles of ligand-gebonden Fe(III) een intermediaire rol spelen tussen de mineralen en de organismen. In andere gevallen vindt elektronenoverdracht alleen plaats in direct contact met de micro-organismen en de mineraal deeltjes. Deze laatste mogelijkheid is onderzocht in deze studie.

Het doel van dit proefschrift is om de effecten van de fysico-chemische eigenschappen van de Fe(III) oxyhydroxiden op dissimilaire ijzerreductie te ontrafelen, met de nadruk op de oplosbaarheid van mineralen en deeltjes grootte. De experimentele benadering is om verschillende Fe(III) oxyhydroxyden te bedekken met de facultatieve anaërobe, Gram-negatieve bacterie *Shewanella putrefaciens*, waarbij lactaat de enige elektronendonor is. De experimenten zijn uitgevoerd in een vereenvoudigd medium, zonder fosfaat of andere toegevoegde elementen, bij kamer temperatuur en pH 7. De elektronendonor is in overvloed aanwezig zodat deze altijd beschikbaar is en de snelheid van ijzerreductie niet beïnvloed wordt. Dit laatste wordt gemeten via het monitoren van het totale Fe^{2+} gehalte dat opgebouwd is in het reactie systeem.

In het eerste deel van de studie worden de ijzerreductie snelheden van verschillende Fe(III) oxyhydroxyden bepaald als functie van de concentratie van vaste fase Fe(III) en de celdichtheid (hoofdstuk II). Een belangrijke observatie is dat, voor een gegeven Fe(III) oxyhydroxyde fase, de ijzerreductie snelheid op een unieke manier afhankelijk is van de Fe(III) concentratie na het normaliseren van de snelheden tot het aantal cellen.

Deze afhankelijkheid kan beschreven worden door de klassieke Michaelis-Menten snelheidsformule:

$$R = v_{\max} B \frac{[\text{Fe(III)}]}{K_m^* + [\text{Fe(III)}]} \quad (6.5)$$

waarbij R de netto snelheid is van ijzerreductie per eenheid totaal volume van de bacterie-mineraal suspensie, v_{\max} de maximale cel-genormaliseerde ijzerreductie snelheid (in eenheden van $\mu\text{mol Fe(III)}$)

uur⁻¹ cel⁻¹), B de celdichtheid van de suspensies (i.e., de biomassa), en K_m^* een constante voor halve verzadiging. De maximale snelheid, v_{\max} , is geïnterpreteerd als de ijzerreducerende activiteit van een *S. putrefaciens* cel wanneer haar membraan-gebonden Fe(III) reductase sites volledig verzadigd zijn door het vaste Fe(III) substraat. De waarden van v_{\max} variëren over een grootte-orde van 1,5, afhankelijk van het mineraal dat reductie ondergaat. Om deze grote variatie van v_{\max} uit te leggen, worden de oplosbaarheden van de Fe(III) oxyhydroxiden gemeten aan de hand van twee complementaire methodes.

Voor redelijk oplosbare, colloïdale Fe(III) oxyhydroxides, worden de redox potentiaal metingen uitgevoerd over de pH range 4-7 (hoofdstuk II). Voor grovere, gewoonlijk minder oplosbare mineralen, wordt een dialyse-membraan methode gebruikt (hoofdstuk IV). Bij deze methode worden de activiteiten gemeten onder zure condities. Met beide benaderingen kunnen we oplosbaarheidsproducten, $*K_{so}$, afleiden die rekening houden met de niet-ideale stoichiometrieën in van de vaste stoffen.

De maximale snelheden van de reductie van Fe(III) oxyhydroxides door *S. putrefaciens* en de oplosbaarheidsproducten vertonen een sterke positieve correlatie, die kan uitgedrukt worden als:

$$\log v_{\max} \left(\text{mol uur}^{-1} \text{ cel}^{-1} \right) = 0.40 \log *K_{so} - 16.80 \quad (6.6)$$

Vergelijking (2) definieert een lineaire vrije energie relatie (LFER), die de ijzerreducerende activiteit van *S. putrefaciens* relateert met de thermodynamica van het minerale Fe(III) substraat. Hoewel de LFER een empirische relatie is, lijkt het een beperkende reactie te zijn die gemeenschappelijk is voor de microbiële reductie van verschillende Fe(III) oxyhydroxydes. In hoofdstuk 4, tonen we een positieve correlatie tussen v_{\max} en de snelheidsconstante voor de dissociatie van Fe²⁺ van het mineraal (k_{des}). De geobserveerde LFER is dus hoogstwaarschijnlijk het gevolg van de reactie-beperkende rol van de dissociatie van Fe²⁺ van het mineraal oppervlak, volgend na de elektronentransfer van een celmembraan-gebonden reductase site naar structureel Fe(III) van een gebonden oxyhydroxide deeltje.

Voor enzymatische reacties in homogene oplossingen, is de halve verzadigingsconstante in de Michaelis-Menten vergelijking een directe maat voor de neiging van het enzym om zich chemisch te binden aan het oplosbare substraat. De halve verzadigingsconstante is uniek gedefinieerd in termen van de bulk opgeloste concentratie van het substraat. De reductie van Fe(III) oxyhydroxide deeltjes door *S. putrefaciens* vertoont nochtans een veel complexere situatie. De Fe(III) centra die reductie ondergaan zijn gelokaliseerd in de contactzone tussen de cel en het mineraal. Het directe Fe(III) substraat vertegenwoordigt daarom slechts een fractie van het bulk Fe(III) in het systeem. Deze fractie hangt niet enkel af van de neiging van mineraal en bacterie om zich aan elkaar te hechten maar ook van de

deeltjesgrootte van de vaste stof. Dit resulteert in K_m^* waarden die conditioneel zijn, eerder dan intrinsiek, wanneer ze uitgedrukt worden in eenheden van bulk concentratie van het Fe(III) substraat (bijvoorbeeld in mol Fe(III) per eenheid volume suspensie). Bijvoorbeeld in hoofdstuk II, tonen we aan dat de K_m^* waarden afhankelijk zijn van de vaste stof-tot-cel ratio in experimentele oplossingen. Kwalitatief duidt dit op een cruciale rol in de mineraal-bacterie hechting in het reductie proces. Deze rol is het onderwerp van hoofdstuk III.

In hoofdstuk III onderzoeken we eerst de hechting van nanohematiet deeltjes aan *S. putrefaciens* in oplossingen van relatief lage ionsterkte en pH om te voorkomen dat de minerale colloïden coaguleren. Formeel volgt de partitionering van nanohematiet een Langmuir isotherm. Dat betekent dat de bedekking van de cellen door nanohematiet beschreven kan worden door 2 parameters, namelijk de maximale hechtingscapaciteit per cel, M_{max} , en een aanhechtingconstante, K_p . Vervolgens werden cellen met bekende concentraties aangehecht nanohematiet deeltjes geïncubeerd met lactaat onder anaërobe omstandigheden. De belangrijkste vinding is dat de ijzerreductie lineair correleert met de relatieve bedekking van cel oppervlaktes door nanohematiet deeltjes, en dus de directe elektronenoverdracht van membraan gebonden reductases naar minerale deeltjes ondersteunen. Door het gebruik van intern consistente parameterwaardes voor M_{max} , K_p , en de eerste orde Fe(III) reductie snelheidsconstante, k , werd een kinetisch model voor de microbiële reductie van Fe(III) oxyhydroxide colloïden ontwikkeld. Het model reproduceert de reductiesnelheden van nanohematiet alsmede die van andere fijnkorrelige Fe(III) oxyhydroxides door *S. putrefaciens*. Het verklaart de geobserveerde afhankelijkheid van de Fe(III) half verzadigingsconstante, K_m^* , op de solid-to-cell ratio en, zoals geobserveerd, het voorspelt dat ijzerreductie snelheden verzadiging vertonen met betrekking tot zowel de celdichtheid als de hoeveelheid Fe(III) oxyhydroxide substraat.

Naast de cel-mineraal aanhechting en de kinetische effecten, kan ijzerreductie ook onderworpen zijn aan thermodynamische randvoorwaarden. In het bijzonder, de opbouw van Fe^{2+} in de oplossing met voortschrijdende Fe(III) oxyhydroxide reductie doet de Gibbs vrije energie opbrengst ($-\Delta G_r$) voor micro-organismen afnemen. In principe zou de vrije energie opbrengst van Fe(III) oxyhydroxide reductie die gekoppeld is aan de oxidatie van een organisch substraat hoger moeten zijn dan 20 kJ mol^{-1} , om een micro-organisme van energie te kunnen voorzien en ATP aan te maken. Dus, onder strikt thermodynamische controle, zou ijzerreductie alleen stoppen wanneer de ondergrens van $-\Delta G_r$ bereikt wordt. In hoofdstuk V volgen we de tijdsontwikkeling van de $-\Delta G_r$ tijdens de microbiële oxidatie van lactaat gekoppeld aan 6-lijns ferrihydriet en nanohematiet reductie. Voor beide stoffen stopt de ijzerreductie zelfs als de berekende thermodynamische energie opbrengst nog steeds gunstig is ($-\Delta G_r$

$>20 \text{ kJ mol}^{-1}$). Vandaar dat het stoppen van ijzerreductie door *S. putrefaciens* niet alleen kan worden toegeschreven aan een thermodynamisch effect van de ophoping van reactie producten.

Een andere mogelijkheid is dat de opbouw van Fe^{2+} tijdens de microbiële ijzerreductie de cel vergiftigt. Deze mogelijkheid is verder onderzocht in hoofdstuk V door cellen van *S. putrefaciens* voor te behandelen met Fe^{2+} voor het starten van ijzerreductie experimenten. De voorbehandeling laat zien dat de cellen oplosbaar Fe^{2+} opnemen. De initiële reductie van 6-lijns ferrihydriet door voorbehandelde cellen gaat met dezelfde snelheid als in controle experimenten met cellen die niet waren blootgesteld aan Fe^{2+} . Echter, de Fe(III) reducerende activiteit van voorbehandelde cellen stopt eerder dan in de controle experimenten. Deze voorlopige observatie suggereert dat de ophoping van Fe^{2+} door de cellen hun metabolisme kan verstoren en, uiteindelijk de duur van de Fe(III) oxyhydroxide reductie. Desondanks, veel werk is nog steeds nodig om het complexe geheel van fysiologische en omgevingsfactoren te begrijpen die de microbiële ijzerreductie bepalen.

Dankwoord (Acknowledgements)

I know very well that this is the part of my thesis that everybody will read for sure! There is only one name on the cover of the thesis, but it does not mean that I did it alone. So along those lines, I will try my best not to forget any of the people who helped me during my dutch years....

First, I would like to thank my supervisors:

-Philippe Van Cappellen, thanks for believing that a french biologist could write a PhD in Geochemistry...in english. This work is the illustration that this bet, even though difficult and uncertain, was after all possible!

-Thilo Behrends, your contribution to this thesis can be summarized in one sentence: you taught me the experimental side of Geochemistry day after day! Thanks, Thilo, for your patience in answering to the few thousand questions I asked you along those years.

To both of you, I would like to say that your presence, guidance, ideas and stimulation have been invaluable and showed me what scientific research means!

The members of my reading committee, E. Roden, O. Pokrovsky, W. Röling, J. Middelburg and G. de Lange are thanked for carefully reading the thesis. I am grateful to W. Röling and Bin Lin (Vrije Universiteit) for their enthusiastic collaboration in the TRIAS project. I appreciated also the advises and feedbacks of the the scientific committee of the TRIAS project, T. Bosma, J. Griffioen, T. Keijzer, J. Olie, H. Passier, H. Rogaar and H. van Verseveld. I would like to thank Tom DiChristina for providing the culture of *Shewanella putrefaciens* and D. Rancourt for the Mossbauer analysis of the Fe(III) oxyhydroxides.

Along those years, I enjoyed very much the collaboration, talks, exchange of ideas, dinners, coffee, cigarettes...with the members of the Geochemistry Department:

-Je voudrais commencer avec une mention particuliere pour Christelle Hyacinthe, avec qui j'ai partagé les frustrations et les doutes mais aussi les bons jours, les idées, les expériences qui font partie du quotidien de la condition de Ph.D student....merci pour tout! j'espere sous peu avoir le plaisir de pouvoir t'appeller Dr Hyacinthe et de voir ta petite famille.

-To Peter Kleingeld and Ralf Haese who helped me for the experimental set-up and learned to use the microelectrode.

-To Anniet Laverman and Simon Vriend for their help in writing the dutch summary of this thesis at the last moment.

-To all my colleagues and ex-colleagues at the Geochemistry Department, I would like to express my grateful thanks for your encouragements and your presence whenever needed!

I discovered soon after the beginning of the Ph.D that there is life after the work in the lab and that Utrecht is a very enjoyable place to live...I could write another 100 pages about those last five years in Utrecht, full of anecdotes...so I want to thanks all my friends in Utrecht who shared with me the daily life but also my nightlife...all the diners, parties, talks, laughs, supports...your presence and your enthusiasm made from those years an unforgettable life experience.

A mes parents et ma famille, merci pour toujours avoir été à mes cotés en toutes circonstances tout au long de ces années. Cette thèse, je la dois largement aux qualités et principes que vous m'avez transmis...merci!

Enfin, je voudrais adresser un grand merci à Siska qui a aussi contribué au résumé en néerlandais et qui, surtout, m'a supporté, encouragé, reconforté, stimulé, écouté (beaucoup) dans la dernière ligne droite de la thèse...j'espère pouvoir t'offrir autant que tu m'as donné quand tu finiras la tienne!

Steeve Bonneville

Curriculum vitae

Steeve Bonneville was born the 4th May 1974 in Fecamp, France. After his graduation from the Guy de Maupassant high-school (Fecamp) in 1993, he joined the University du Havre (Normandy). He obtained his bachelor's degree of biology in 1997. After a trainingship at the Department of Geology at the University of Rouen, he graduated in 1999 from a master's degree equivalent (DEA) in Hydrology and Aquatic Sciences from the University of Montpellier. In the framework of the TRIAS project "Redox reactivity and bioavailability of iron oxyhydroxydes in the subsurface", he joined the Earth Sciences-Geochemistry Department (Faculty of Geosciences-Utrecht University) in January 2001, where he performed his PhD under the supervision of Prof. Dr. Philippe Van Cappellen and Dr. Thilo Behrends. He will defend his PhD thesis on December the 19th 2005 at Utrecht University.